



# Deconstruction of tropospheric chemical reactivity using aircraft measurements: the ATom data

Michael J. Prather<sup>1</sup>, Hao Guo<sup>1,2</sup>, and Xin Zhu<sup>1</sup>

<sup>1</sup>Department of Earth System Science, University of California at Irvine, Irvine, CA 92697-3100, USA

5 <sup>2</sup>State Key Laboratory of Organic Geochemistry, Guangzhou Institute of Geochemistry, Chinese Academy of Sciences, Tianhe, Guangzhou 510640, China

*Correspondence to:* Michael J. Prather (mprather@uci.edu)

**Abstract.** The NASA Atmospheric Tomography (ATom) Mission completed four seasonal deployments (August 2016, February 2017, October 2017, May 2018), each with regular 0.2-12 km profiling through transecting the remote Pacific and Atlantic Ocean basins. Additional data are acquired also for the Southern Ocean and Arctic basin, as well as two flights over Antarctica. ATom in situ measurements provide a near-complete chemical characterization of the ~140,000 10-second (80 m by 2 km) air parcels measured along the flight path. This paper presents the Modeling Data Stream (MDS), a continuous gap-filled record of the 10-s parcels containing the chemical species needed to initialize a gas-phase chemistry model for the budgets of tropospheric ozone and methane. Global 3D models have been used to calculate the Reactivity Data Stream (RDS), which is comprised of the chemical reactivities (production and loss) for methane, ozone, and carbon monoxide, through 24-hour integration of the 10-s parcels. These parcels accurately sample tropospheric heterogeneity and allow us to partially deconstruct the spatial scales and variability that defines tropospheric chemistry from composition to reactions. This paper provides a first look and analysis of the up-to-date MDS and RDS data including all four deployments (Prather et al., 2023, doi: 10.7280/D1B12H).

10  
15  
20  
25  
30

ATom's regular profiling of the ocean basins allows for weighted averages to build probability densities for key species and reactivities presented here. These statistics provide climatological metrics for global chemistry models, for example, the large-scale pattern of ozone and methane loss in the lower troposphere, and the more sporadic hot spots of ozone production in the upper troposphere. The profiling curtains of reactivity also identify meteorologically variable and hence deployment-specific hot spots of photochemical activity. Added calculations of the sensitivities of the production and loss terms relative to each species emphasize the few dominant species that control the ozone and methane budgets, and whose statistical patterns should be key model-measurement metrics. From the sensitivities, we also derive linearized lifetimes of ozone and methane on a parcel-by-parcel basis and average over the basins, providing an observational basis for these previously model-only diagnostics. We had found that most model differences in the ozone and methane budgets are caused by the models calculating different climatologies for the key species such as O<sub>3</sub>, CO, H<sub>2</sub>O, NO<sub>x</sub>, CH<sub>4</sub> plus T, and thus these ATom measurements provide a substantial contribution to the understanding of model differences and even identifying model errors in global tropospheric chemistry.

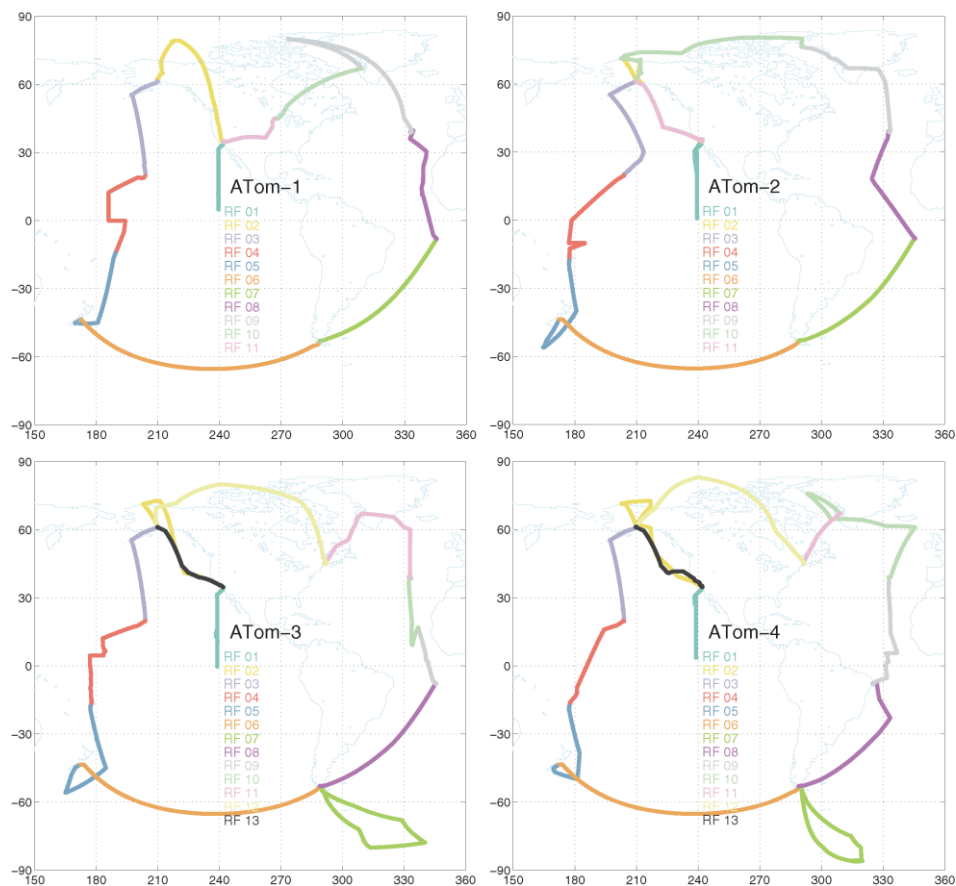


## 1 Introduction

35 The environmental damage caused by chemically reactive greenhouse gases and most air pollutants is controlled by a  
balance between their sources and sinks, with atmospheric photochemistry as the major sink. The net chemical loss is  
comprised of a highly heterogeneous mixture of air parcels, each with its own mix of species, and each with its own  
chemical production and/or loss rates that are designated here as reactivities: P-O<sub>3</sub>, L-O<sub>3</sub>, L-CH<sub>4</sub>, and L-CO (see Prather et  
al., 2017; 2018, hence P2017 and P2018). A reactivity is calculated as the 24-hour integration of a reaction rate, or the sum  
of several reaction rates, that describe budgets of species in units of ppb (10<sup>-9</sup> mole fraction) per day. In this paper we  
40 continue our efforts to deconstruct global tropospheric chemistry, examining its finest scales, reconstructing and parsing the  
O<sub>3</sub> and CH<sub>4</sub> budgets over the remote ocean basins as sampled by the NASA Atmospheric Tomography (ATom) Mission.

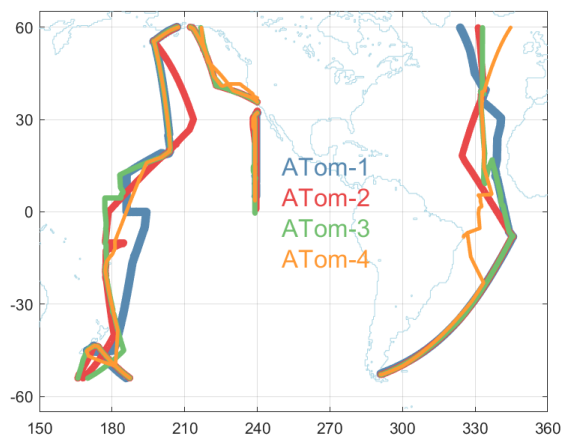
ATom provided intensive, chemically comprehensive measurement of air parcels (typically 10 s averages, equivalent to 2  
km along flight by 80 m in the vertical) and extensive four-season semi-global 0-12 km profiling through the remote  
troposphere (Wofsy et al., 2021; Thompson et al., 2021). Recent publications have identified new scientific opportunities  
45 coming from the ATom observation, with topics including scales of variability (Schill et al., 2020; Allen et al., 2022), global  
CO forecasting (Strode et al., 2018), and OH oxidative capacity (Wolfe et al., 2019; Brune et al., 2020; Travis et al., 2020;  
Anderson et al., 2021), as well as aerosol distribution, formation, and precursors (Brock et al., 2021; Williamson et al., 2021;  
Veres et al., 2020). Guo et al. (2023; hence G2023) calculated the reactivities for all 10 s air parcels from the first  
deployment ATom-1 (29 July – 23 August 2016) and compared their statistics with six global chemistry model's sample day  
50 in mid-August. Note that the first published version (Guo et al., 2021) has been withdrawn due to some errors in the  
reactivities and is corrected with G2023.

Here we report reactivities for all four seasonal deployments (ATom-1234, see Fig. 1) and examine how their statistical  
patterns change with season. We extend the analysis of Pacific and Atlantic basins (Fig. 2) to the Southern Ocean and Polar  
regions, with a first look at Antarctic tropospheric chemistry. We present sensitivity analyses to identify which of the  
55 ATom-measured species drives the reactivities and are thus critical for the chemistry-climate models (CCMs) to simulate  
accurately. We show how the sensitivity analyses on each parcel can be used to estimate the true lifetime of tropospheric O<sub>3</sub>  
and the CH<sub>4</sub> chemical feedback. Overall, we hope to use the 10 s parcel statistics (>140,000 parcels in ATom) to build  
performance metrics for CCMs.



60

**Figure 1.** Map of ATom1234 flights, noting Research Flight number for each deployment. The flight sequence is counter clockwise starting at Palmdale CA. The first research flight of each deployment is the transect from CA nearly to the Equator along 121°W. The dates of each deployment are: ATom-1, 29 Jul – 23 Aug 2016; ATom-2, 26 Jan – 21 Feb 2017; ATom-3, 28 Sep – 27 Oct 2017; ATom-4, 24 Apr – 21 May 2018.



65

**Figure 2.** Map of the portion of ATom1234 flights included in the Pacific and Atlantic basin analysis. Flight tracks are plotted in successively thinner lines to see the overlap. These flights comprise 91,912 parcels out of the total of 146,494.



## 2 Methods, measurements, and outline

### 70 2.1 Reactivities

Our interests in the reactivity of air parcels or model grid cells began with P2017, continuing with P2018 and G2023. We focused on the budgets of O<sub>3</sub> and CH<sub>4</sub>, and now add CO. Reactivities are defined by a few key reaction rates:

Loss of CH<sub>4</sub> (L-CH<sub>4</sub>),



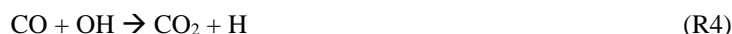
### 75 Production of O<sub>3</sub> (P-O<sub>3</sub>),



Loss of O<sub>3</sub> (L-O<sub>3</sub>),



Loss of CO (L-CO).



### 85 In addition, we include statistics on two key photolysis rates that drive the chemistry:

Photolysis of O<sub>3</sub> yielding O(<sup>1</sup>D) (j-O<sub>3</sub>D).



Photolysis of NO<sub>2</sub> (j-NO<sub>2</sub>).



### 90 These rates are readily diagnosed in most CCMs. We found that the net P-O<sub>3</sub> minus L-O<sub>3</sub> describes the 24 h O<sub>3</sub> tendencies over the ocean basins, but not exactly as expected, and particularly not in highly polluted regions (G2023). Reaction 2c is important in tropospheric budget of O<sub>3</sub> only above ATom flight levels (12 km, Prather, 2009). In terms of the overall CO budget, we lack the chemical production of CO from CH<sub>4</sub> and other volatile organic compounds.

We focus on the Pacific and Atlantic oceanic flights of ATom, which we constrain to be 53°S to 60°N (see the map of included flights in Fig. 2), because these two ocean basins dominate the loss of CH<sub>4</sub> and O<sub>3</sub> and are a large part of the production of O<sub>3</sub> in most CCMs (P2017). The tropics clearly dominate the chemical budgets and we single out the three ATom-measured regions: Central Pacific (30°S-30°N, about the Dateline), Eastern Pacific (0°-30°N, ~121°W, the first flight of each deployment, to/from Palmdale), Tropical Atlantic (30°S-30°N). The Southern Ocean (66°S-55°S, the Christ Church



100 to Punta Arenas flight) and two polar regions (Arctic,  $>66^{\circ}\text{N}$ ; Antarctic,  $<66^{\circ}\text{S}$ ) are also examined separately. Only over-ocean data is analyzed here except for the two polar regions.

## 2.2 Protocols

105 The ATom observations used for the reactivity calculations here are taken from the Modeling Data Stream MDS-2b, described in G2023 and available at Prather et al. (2023). When completing this analysis, it was found that the method of gap-filling for NO<sub>x</sub> did not take advantage of all the observations (i.e., flight segments where NO was measured but NO<sub>2</sub> was not). Thus, the updated NO<sub>x</sub> gap-filling MDS-3 was developed.

110 The Reactivity Data Stream (RDS) reports the reactivities listed above plus the net 24-hour change in O<sub>3</sub> for each 145,388 parcels, land or ocean. (Research flight number 11 of Atom-4 was a ferry flight from Greenland to Maine without profiling for which many instruments were shut down, and thus the 1,106 parcels have NaN values for MDS and RDS.) Reactivity calculations here use the UCIZ model and the RDS\* protocol described in G2023. UCIZ is the updated UCI chemistry-transport model (CTM version q7.4) by Xin Zhu that is adapted to calculating ATom air parcels. RDS\* protocol allows the PAN and HNO<sub>4</sub> species to thermally decay for 24 hours before use. The overall ATom protocol for CTM/CCMs averages five days separated by five days centered on each deployments' central month (ATom-1, August; ATom-2, February; ATom-3, October; ATom-4, May) to average over the cloud fields (see P2017; P2018).

115 The ATom RDS protocol for CTM/CCMs is to locate the nearest model grid cell and then place the ATom air parcel in that cell (along with all the other parcels in their own cells) and then integrate for 24 hours (usually starting at 0000 UTC). The problem is that many 10 s parcels may lie in the same grid cell. We use the following nested search algorithm to locate an unoccupied cell nearby: (1<sup>st</sup>) search E-W from -8 to +8 longitude-shifted cells; (2<sup>nd</sup>) search up-down in pressure by -2 to +2 levels; (3<sup>rd</sup>) search N-S by -2 to +2 latitude-shifted cells. With our 1.1-degree CTM, we are always able to find an empty cell, however, the latitude, longitude, and pressure of the grid cell may differ from the ATom-measured value. Figure 3 shows the ATom value (MDS, x-axis) versus the CTM grid-cell value (RDS, y-axis) for the 32,383 parcels of ATom-1. The mean errors in placement are very small, and even the root-mean square error is modest ( $\pm 1.7^{\circ}$  latitude,  $\pm 5.7^{\circ}$  longitude,  $\pm 15.3$  hPa).

125 The CTM/CCM is run 24 hours without advection, convection or other mixing, without wet scavenging or dry deposition or emissions. These requirements are critical because otherwise the air parcel's evolution would depend on the composition of neighboring cells, which are unknown from the ATom measurements. The key model-dependent quantities that control the reactivities are the photolysis rates, which depend on clouds and overhead column ozone. Figure 4 compares the j-values and reactivities for the ATom-1 parcels calculated for day numbers 213 (1 Aug) and 223 (11 Aug). The j-values have the largest scatter, and that drives a reduced level of scatter in reactivities. The j-NO<sub>2</sub> value is not much affected by overhead ozone column and so we conclude the scatter in j-values and reactivities is driven primarily by the time varying cloud fields. (The UCI CTM uses 3-hour averaged cloud fields.) The O<sub>3</sub> tendency (dO<sub>3</sub>/dt) has less scatter than any of the four reactivities (P-O<sub>3</sub>, L-O<sub>3</sub>, L-CH<sub>4</sub>, L-CO) because the production and loss co-vary with clouds and their net difference has less scatter.

135 We expect the abundance of the reactive species to evolve over the 24-hour period of the reactivity calculation, and this is documented in Fig. 5. Species with no sources, because emissions are shut off, decrease over the 24 hour (CO, C<sub>2</sub>H<sub>6</sub>, alkane, alkene). NO<sub>x</sub> systematically decreases because there are no direct emissions and HNO<sub>3</sub> is a major sink. HOOH systematically increases because wet scavenging is turned off. O<sub>3</sub> and PAN show plus-minus scatter. HNO<sub>3</sub> increases at values less than 2 ppb, but decreases at the highest values ( $\sim 3$  ppb). In terms of the calculation of ATom reactivities, the

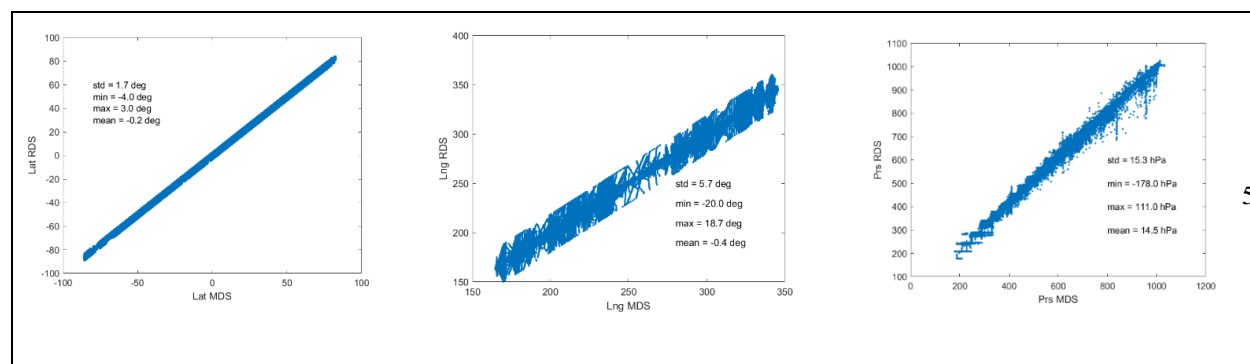


140 scatter is not worrisome, but the systematic shifts in HOOH and NO<sub>x</sub> are a concern. The P2017 experiments showed that  
averaged over an ocean basin, the reactivities with all processes running for 24 hours versus the ATom protocol were  
similar. A protocol that slowly removed HOOH and added NO<sub>x</sub> is tempting but would require some arbitrary  
parameterizations.

### 2.3 Outline

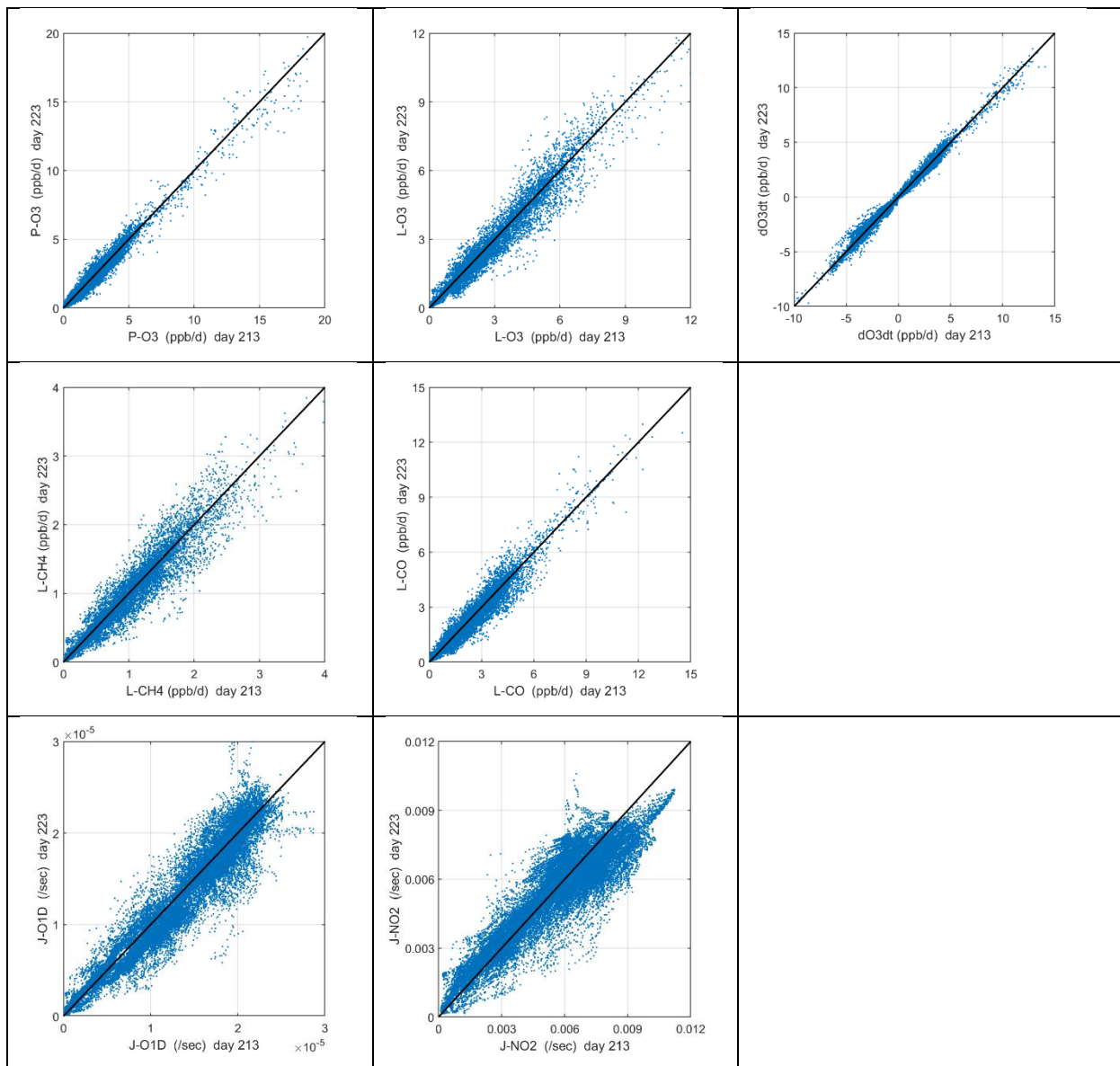
145 Latitude-by-altitude curtain plots of the reactivities along flight tracks are presented in Section 3, along with reactivity  
statistics of the means and extremes, altitude mean profiles, and probability densities. In Section 4, we analyze the  
sensitivities of the reactivities to each of the observed species for ATom-1. These sensitivities identify those critical species  
where a model bias will introduce large errors in the O<sub>3</sub> and CH<sub>4</sub> budgets. In Section 5, we examine the impacts of MDS-3  
on these analyses, and we introduce probability densities for some critical species as a possible model metric. In Section 6  
we show how the ATom parcel reactivities and sensitivities can be used to derive chemical feedbacks, such as the lifetime  
for O<sub>3</sub> perturbations and the CH<sub>4</sub> lifetime feedback factor. Section 7 concludes this analysis.

150



160 **Figure 3.** Comparison of the model grid cell value for pressure, latitude, and longitude used in the RDS calculation with those from the  
32,383 10 s ATom-1 parcels (MDS). In each figure the standard deviation, minimum error, maximum error and mean error are shown.  
Values are specific to the UCI CTM with a T159L57 grid. These displacement errors occur because several 10 s parcels often occur within  
one CTM cell and must be shifted to nearby vacant cells.

165



170 **Figure 4.** Reactivities (ppb/d) and J-values (/sec) calculated for all 32,383 ATom-1 10 s parcels using two different days with different cloud fields and ozone columns. The net integrated ozone change over the day, dO<sub>3</sub>/dt (ppb/d), is also shown. Day 213 = August 1 and day 223 = August 11. Mean reactivity statistics here are calculated as the mean of five days (August 1, 6, 11, 16, 21), while sensitivity analyses used only day 223.

175

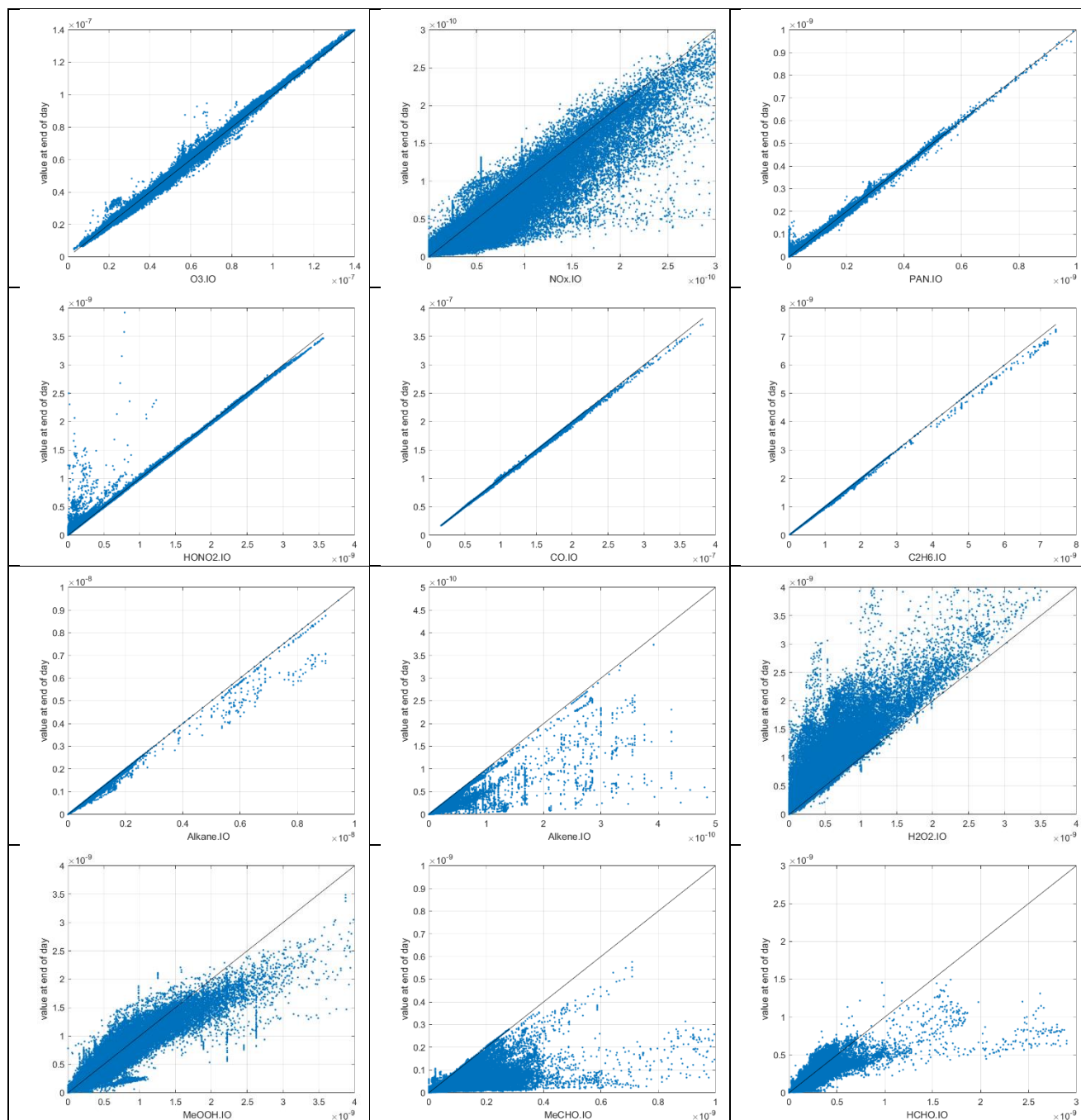


**Figure 5.** The input/output values of reactive species showing the 24-hour change from the ATom-1 MDS input value (x-axis) to the final value (y-axis) calculated following the ATom protocol in the UCI CTM. First row: O<sub>3</sub>, NO<sub>x</sub>, PAN. Second row: HONO<sub>2</sub>, CO, C<sub>2</sub>H<sub>6</sub>. Third row: Alkane (C<sub>3+</sub>), Alkene (C<sub>2</sub>H<sub>4</sub>), H<sub>2</sub>O<sub>2</sub>. Fourth row: CH<sub>3</sub>OOH (MeOOH), CH<sub>3</sub>CHO (MeCHO), HCHO.

180





### 3 Variation of photochemical reactivities across the four ATom deployments

#### 3.1 Reactivity statistics – means and extremes

185 We developed statistics that identify extremes (i.e., photochemical hot spots) and characterize the heterogeneous mix of air  
parcels. Table 1 presents the means and medians of each of the four reactivities (P-O<sub>3</sub>, L-O<sub>3</sub>, L-CH<sub>4</sub>, L-CO) and two j-  
values (j-O<sub>1</sub>D, j-NO<sub>2</sub>) for each of the eight regions (Pacific, Atlantic, Central Tropical Pacific, Eastern Tropical Pacific,  
Tropical Atlantic, Southern Ocean, Arctic, Antarctic) and four deployments (ATom-1234: in August, February, October,  
May respectively). Each 10 s parcel is weighted to give equal sampling by mass from 0-12 km for each 10° latitude bin or a  
single latitude bin for polar latitudes. The extreme statistics look at the top 50%, 10%, and 3% of the weighted parcels,  
190 giving the mean reactivity in those ranges as well as the fraction of total weighted reactivity in those upper ranges.

Starting with the Pacific and Atlantic basins, we see that the average photolysis rates (j-O<sub>1</sub>D, j-NO<sub>2</sub>, Table 1ef) have little  
seasonality (variation across deployments), and further, have a flat distribution with median greater than mean. For P-O<sub>3</sub>  
(Table 1a) the Atlantic mean is slightly larger (10-20 %) than the Pacific except for ATom-2. The medians are always  
smaller than the mean. The reactivity of the top 10% is about 2.5 times that of the mean, indicating a distribution peaked to  
195 photochemical hot spots. For L-O<sub>3</sub> (Table 1b) the Atlantic mean is much larger (30-50 %) than the Pacific, and the extreme  
statistics are similar. What is unusual is that ATom-1 has the lowest mean P-O<sub>3</sub> in both Pacific and Atlantic, while it has a  
high or the highest L-O<sub>3</sub>. Thus, ATom-1 has a distinctly different mix of species than ATom-234. A clear seasonality is  
seen for L-O<sub>3</sub> with ATom-2 (February) having the lowest reactivities, presumably due to the reduced activity of northern  
mid-latitude continental pollution in winter. L-CO (Table 1d) shows similar patterns as L-O<sub>3</sub> (lowest in ATom-2 Pacific,  
200 highest in ATom-1 Atlantic), while that of L-CH<sub>4</sub> (Table 1c) is more uniform across deployments. This feature can be seen  
in the curtain and mean profile plots where L-CH<sub>4</sub> is restricted to the lower troposphere due to the high temperature  
sensitivity of rate coefficient for reaction (1).

The Arctic region is highly seasonal, and photochemistry mostly shuts down in ATom-2 and -3 (Feb and Oct) but it is quite  
reactive in ATom-1 and -4 (Aug and May). This is seen clearly in the j-values (Table 1ef), particularly j-O<sub>1</sub>D, which is the  
205 primary source of OH. The Arctic reactivities in ATom-1 and -4 are about 2/3 of the mean Pacific and Atlantic values year  
round, with the exception of L-CH<sub>4</sub> which is extremely repressed due to the colder Arctic temperatures in all seasons. The  
extreme statistics in the Arctic are similar to the Pacific and Atlantic except for P-O<sub>3</sub> in ATom-234 which is dominated by  
hot parcels. Note that we have excluded the stratospheric parcels in these statistics (see Supplement of G2023).

The Southern Ocean has high reactivities for ATom-2 and -3 as expected for austral summer. L-O<sub>3</sub> and L-CO are about half  
210 the reactivity of the Arctic for the complementary seasons, but P-O<sub>3</sub> and L-CH<sub>4</sub> are more similar to the Arctic. Clearly, the  
chemical mixture of these two regions is different. The extreme statistics for the S. Ocean are similar to the Arctic.

The Antarctic flights of ATom were a target of opportunity for ATom-3 and -4. ATom-4 (May) was too dark to have  
significant reactivity (extremely low j-values, Table 1ef). ATom-3 Antarctica has distinctly lower reactivities than ATom-3  
S. Ocean except for P-O<sub>3</sub> which is surprisingly comparable.

215



**Table 1. Statistics on Reactivities and J-values by basin and deployment**

P-O3	reactivity	deployment	avg R (ppb/d)	mdn R (ppb/d)	avg R (ppb/d) in			fraction of total R in		
					top50	top10	top03	top50	top10	top03
Pacific	P-O3	ATom1	1.11	0.94	1.76	3.03	4.25	80%	27%	12%
Pacific	P-O3	ATom2	1.42	1.38	2.10	3.09	3.75	74%	22%	8%
Pacific	P-O3	ATom3	1.57	1.40	2.38	4.10	6.17	76%	26%	12%
Pacific	P-O3	ATom4	1.37	1.31	2.08	3.07	3.73	76%	22%	8%
Atlantic	P-O3	ATom1	1.25	1.10	2.07	3.38	4.21	83%	27%	10%
Atlantic	P-O3	ATom2	1.44	1.30	2.16	3.21	3.74	75%	22%	8%
Atlantic	P-O3	ATom3	1.84	1.70	2.65	3.94	4.73	72%	22%	8%
Atlantic	P-O3	ATom4	1.60	1.43	2.42	3.99	5.53	76%	25%	10%
C.Pacific	P-O3	ATom1	1.23	1.14	1.78	2.74	3.52	73%	22%	9%
C.Pacific	P-O3	ATom2	1.69	1.67	2.24	2.99	3.56	66%	18%	7%
C.Pacific	P-O3	ATom3	2.02	1.80	2.88	4.89	7.72	71%	24%	12%
C.Pacific	P-O3	ATom4	1.72	1.66	2.32	3.17	3.63	68%	19%	6%
E.Pacific	P-O3	ATom1	1.88	1.71	2.61	4.17	5.57	70%	22%	9%
E.Pacific	P-O3	ATom2	1.98	1.89	2.54	3.36	3.71	64%	17%	6%
E.Pacific	P-O3	ATom3	1.89	1.80	2.26	3.00	3.57	60%	16%	6%
E.Pacific	P-O3	ATom4	2.11	2.14	2.68	3.55	4.28	64%	17%	6%
T.Atlantic	P-O3	ATom1	1.47	1.35	2.24	3.57	4.33	76%	24%	9%
T.Atlantic	P-O3	ATom2	1.72	1.60	2.37	3.30	3.80	69%	19%	7%
T.Atlantic	P-O3	ATom3	2.28	2.18	3.00	4.13	4.80	66%	18%	6%
T.Atlantic	P-O3	ATom4	1.96	1.73	2.75	4.53	6.02	70%	23%	10%
Arctic	P-O3	ATom1	0.76	0.52	1.26	2.58	3.44	83%	34%	14%
Arctic	P-O3	ATom2	0.03	0.02	0.06	0.11	0.14	93%	37%	14%
Arctic	P-O3	ATom3	0.15	0.07	0.27	0.62	0.86	91%	41%	17%
Arctic	P-O3	ATom4	1.01	0.89	1.40	2.05	2.27	70%	21%	7%
S.Ocean	P-O3	ATom1	0.12	0.11	0.18	0.28	0.34	72%	22%	8%
S.Ocean	P-O3	ATom2	0.98	0.90	1.39	2.00	2.50	71%	21%	8%
S.Ocean	P-O3	ATom3	0.54	0.48	0.79	1.18	1.42	73%	22%	8%
S.Ocean	P-O3	ATom4	0.11	0.08	0.18	0.34	0.44	81%	32%	12%
Antarctic	P-O3	ATom3	0.53	0.49	0.71	0.98	1.12	68%	19%	7%
Antarctic	P-O3	ATom4	0.00	0.00	0.01	0.02	0.04	99%	72%	38%

220

L-O3	reactivity	deployment	avg R (ppb/d)	mdn R (ppb/d)	avg R (ppb/d) in			fraction of total R in		
					top50	top10	top03	top50	top10	top03
Pacific	L-O3	ATom1	1.42	1.02	2.42	4.53	6.44	85%	32%	14%
Pacific	L-O3	ATom2	1.05	0.94	1.65	2.44	2.84	78%	23%	8%
Pacific	L-O3	ATom3	1.42	1.23	2.20	3.65	5.20	77%	26%	11%
Pacific	L-O3	ATom4	1.43	1.01	2.41	4.57	5.59	84%	32%	12%



Atlantic	L-O3	ATom1	2.12	1.18	3.73	6.12	7.37	88%	29%	11%
Atlantic	L-O3	ATom2	1.61	0.99	2.77	5.51	7.84	86%	34%	15%
Atlantic	L-O3	ATom3	1.84	1.27	3.04	6.10	9.06	83%	33%	15%
Atlantic	L-O3	ATom4	1.68	1.19	2.84	4.94	6.74	85%	30%	12%
C.Pacific	L-O3	ATom1	1.31	1.13	2.09	2.97	3.44	80%	23%	9%
C.Pacific	L-O3	ATom2	1.31	1.38	1.94	2.53	2.86	74%	19%	7%
C.Pacific	L-O3	ATom3	1.74	1.58	2.57	4.18	6.28	74%	24%	11%
C.Pacific	L-O3	ATom4	1.54	1.25	2.43	4.83	5.73	79%	32%	11%
E.Pacific	L-O3	ATom1	3.03	2.71	4.61	6.97	7.87	76%	23%	8%
E.Pacific	L-O3	ATom2	1.19	1.02	1.81	3.00	3.47	76%	26%	9%
E.Pacific	L-O3	ATom3	1.53	1.39	2.34	3.24	3.89	77%	21%	8%
E.Pacific	L-O3	ATom4	2.23	1.88	3.49	5.33	5.99	79%	24%	9%
T.Atlantic	L-O3	ATom1	2.59	1.89	4.36	6.60	7.85	84%	26%	10%
T.Atlantic	L-O3	ATom2	2.17	1.79	3.53	6.58	8.80	81%	30%	13%
T.Atlantic	L-O3	ATom3	2.47	1.90	3.97	7.29	10.20	81%	30%	13%
T.Atlantic	L-O3	ATom4	1.93	1.38	3.17	5.57	7.71	82%	29%	12%
Arctic	L-O3	ATom1	0.80	0.70	1.10	1.71	2.13	69%	22%	8%
Arctic	L-O3	ATom2	0.04	0.04	0.06	0.09	0.10	76%	22%	8%
Arctic	L-O3	ATom3	0.11	0.10	0.16	0.24	0.29	73%	22%	8%
Arctic	L-O3	ATom4	1.08	1.09	1.42	1.75	1.94	65%	16%	6%
S.Ocean	L-O3	ATom1	0.07	0.06	0.09	0.13	0.16	66%	21%	8%
S.Ocean	L-O3	ATom2	0.44	0.41	0.60	0.80	0.88	69%	19%	6%
S.Ocean	L-O3	ATom3	0.52	0.42	0.79	1.42	1.69	75%	27%	10%
S.Ocean	L-O3	ATom4	0.07	0.07	0.10	0.14	0.16	68%	19%	7%
Antarctic	L-O3	ATom3	0.25	0.25	0.33	0.43	0.48	65%	17%	6%
Antarctic	L-O3	ATom4	0.01	0.01	0.02	0.04	0.07	89%	35%	17%

L-CH4	react- ivity	deploy- ment	avg R (ppb/d)	mdn R (ppb/d)	avg R (ppb/d) in			fraction of total R in		
					top50	top10	top03	top50	top10	top03
Pacific	L-CH4	ATom1	0.63	0.50	1.05	1.71	2.12	84%	27%	10%
Pacific	L-CH4	ATom2	0.58	0.46	0.95	1.40	1.56	83%	24%	8%
Pacific	L-CH4	ATom3	0.63	0.51	1.00	1.58	1.98	79%	25%	10%
Pacific	L-CH4	ATom4	0.58	0.44	0.96	1.50	1.81	83%	26%	9%
Atlantic	L-CH4	ATom1	0.69	0.48	1.18	1.74	1.99	85%	25%	9%
Atlantic	L-CH4	ATom2	0.61	0.45	1.00	1.56	1.69	83%	26%	8%
Atlantic	L-CH4	ATom3	0.68	0.53	1.10	1.83	2.23	82%	27%	10%
Atlantic	L-CH4	ATom4	0.67	0.54	1.09	1.69	2.00	81%	25%	9%
C.Pacific	L-CH4	ATom1	0.71	0.62	1.10	1.56	1.77	78%	22%	8%
C.Pacific	L-CH4	ATom2	0.75	0.69	1.15	1.47	1.62	77%	20%	7%
C.Pacific	L-CH4	ATom3	0.85	0.85	1.26	1.74	2.28	74%	21%	8%
C.Pacific	L-CH4	ATom4	0.76	0.78	1.14	1.56	1.82	75%	21%	7%



E.Pacific	L-CH4	ATom1	1.18	1.19	1.70	2.26	2.52	72%	19%	7%
E.Pacific	L-CH4	ATom2	0.65	0.59	0.95	1.30	1.41	73%	20%	7%
E.Pacific	L-CH4	ATom3	0.74	0.65	1.07	1.36	1.48	73%	19%	6%
E.Pacific	L-CH4	ATom4	0.94	0.95	1.40	1.97	2.20	75%	21%	7%
T.Atlantic	L-CH4	ATom1	0.82	0.68	1.29	1.74	1.98	79%	22%	7%
T.Atlantic	L-CH4	ATom2	0.75	0.72	1.18	1.62	1.72	78%	22%	7%
T.Atlantic	L-CH4	ATom3	0.89	0.80	1.39	2.00	2.40	78%	22%	8%
T.Atlantic	L-CH4	ATom4	0.84	0.74	1.29	1.82	2.09	77%	22%	8%
Arctic	L-CH4	ATom1	0.21	0.17	0.29	0.46	0.56	72%	23%	8%
Arctic	L-CH4	ATom2	0.01	0.01	0.01	0.01	0.02	81%	25%	10%
Arctic	L-CH4	ATom3	0.02	0.02	0.04	0.07	0.10	81%	29%	13%
Arctic	L-CH4	ATom4	0.22	0.20	0.31	0.41	0.47	69%	18%	7%
S.Ocean	L-CH4	ATom1	0.02	0.02	0.04	0.06	0.07	70%	23%	9%
S.Ocean	L-CH4	ATom2	0.28	0.24	0.43	0.59	0.66	76%	21%	7%
S.Ocean	L-CH4	ATom3	0.18	0.15	0.29	0.52	0.65	78%	29%	11%
S.Ocean	L-CH4	ATom4	0.03	0.02	0.04	0.06	0.07	72%	22%	8%
Antarctic	L-CH4	ATom3	0.10	0.09	0.14	0.20	0.22	70%	21%	7%
Antarctic	L-CH4	ATom4	0.00	0.00	0.00	0.01	0.01	91%	38%	14%
<b>L-CO</b>	reactivity	deployment	avg R (ppb/d)	mdn R (ppb/d)	avg R (ppb/d) in			fraction of total R in		
					top50	top10	top03	top50	top10	top03
Pacific	L-CO	ATom1	1.30	1.08	2.01	3.36	4.29	78%	26%	10%
Pacific	L-CO	ATom2	1.15	1.15	1.61	2.17	2.56	70%	19%	7%
Pacific	L-CO	ATom3	1.49	1.34	2.10	3.23	4.56	70%	22%	9%
Pacific	L-CO	ATom4	1.49	1.25	2.35	4.08	4.92	79%	27%	10%
Atlantic	L-CO	ATom1	2.11	1.76	3.50	5.98	7.83	83%	28%	11%
Atlantic	L-CO	ATom2	1.76	1.26	2.84	5.95	8.76	81%	34%	15%
Atlantic	L-CO	ATom3	1.94	1.49	2.92	5.71	8.87	75%	30%	14%
Atlantic	L-CO	ATom4	1.80	1.52	2.83	4.92	7.42	79%	27%	13%
C.Pacific	L-CO	ATom1	1.21	1.07	1.66	2.30	2.62	69%	19%	7%
C.Pacific	L-CO	ATom2	1.42	1.43	1.78	2.26	2.57	63%	16%	6%
C.Pacific	L-CO	ATom3	1.76	1.64	2.36	3.69	5.55	67%	21%	10%
C.Pacific	L-CO	ATom4	1.59	1.35	2.28	4.10	4.91	72%	26%	9%
E.Pacific	L-CO	ATom1	2.45	2.37	3.31	4.58	5.17	68%	19%	7%
E.Pacific	L-CO	ATom2	1.53	1.39	1.96	2.85	3.34	64%	19%	7%
E.Pacific	L-CO	ATom3	1.71	1.68	2.20	2.82	3.25	64%	17%	6%
E.Pacific	L-CO	ATom4	2.40	2.18	3.26	4.70	5.65	68%	20%	8%
T.Atlantic	L-CO	ATom1	2.67	2.19	4.14	6.74	8.54	77%	25%	10%
T.Atlantic	L-CO	ATom2	2.41	1.86	3.70	7.22	10.05	77%	30%	13%
T.Atlantic	L-CO	ATom3	2.55	1.98	3.70	6.99	10.24	73%	28%	12%
T.Atlantic	L-CO	ATom4	2.12	1.67	3.14	5.81	8.69	74%	28%	13%



Arctic	L-CO	ATom1	1.03	0.93	1.44	2.28	2.86	70%	22%	9%
Arctic	L-CO	ATom2	0.05	0.04	0.07	0.11	0.12	81%	24%	8%
Arctic	L-CO	ATom3	0.14	0.11	0.22	0.41	0.53	81%	29%	12%
Arctic	L-CO	ATom4	1.33	1.30	1.56	1.91	2.10	59%	15%	5%
S.Ocean	L-CO	ATom1	0.10	0.09	0.13	0.19	0.23	67%	20%	7%
S.Ocean	L-CO	ATom2	0.62	0.60	0.82	1.05	1.22	66%	17%	6%
S.Ocean	L-CO	ATom3	0.64	0.57	0.85	1.33	1.50	67%	21%	7%
S.Ocean	L-CO	ATom4	0.08	0.07	0.12	0.21	0.27	73%	27%	10%
Antarctic	L-CO	ATom3	0.45	0.44	0.55	0.69	0.76	61%	15%	5%
Antarctic	L-CO	ATom4	0.01	0.00	0.01	0.02	0.03	90%	38%	16%

225

j-O1D	j-value	deploy- ment	avg J 1e-5 /s	mdn J 1e-5 /s	avg J (1e-5 /s) in			fraction of total J in		
					top50	top10	top03	top50	top10	top03
Pacific	j-O1D	ATom1	1.30	1.44	1.89	2.24	2.34	73%	17%	5%
Pacific	j-O1D	ATom2	1.31	1.28	1.94	2.64	2.81	74%	20%	7%
Pacific	j-O1D	ATom3	1.28	1.21	1.86	2.44	2.61	73%	19%	6%
Pacific	j-O1D	ATom4	1.24	1.33	1.85	2.26	2.39	75%	18%	6%
Atlantic	j-O1D	ATom1	1.25	1.46	1.82	2.15	2.27	73%	17%	6%
Atlantic	j-O1D	ATom2	1.25	1.29	1.79	2.29	2.42	72%	18%	6%
Atlantic	j-O1D	ATom3	1.21	1.19	1.74	2.28	2.38	72%	19%	6%
Atlantic	j-O1D	ATom4	1.18	1.33	1.73	2.05	2.15	74%	17%	6%
C.Pacific	j-O1D	ATom1	1.67	1.77	2.08	2.30	2.41	62%	14%	4%
C.Pacific	j-O1D	ATom2	1.76	1.79	2.26	2.74	2.86	64%	16%	5%
C.Pacific	j-O1D	ATom3	1.72	1.68	2.17	2.54	2.68	63%	15%	5%
C.Pacific	j-O1D	ATom4	1.57	1.68	2.02	2.25	2.33	65%	14%	5%
E.Pacific	j-O1D	ATom1	1.86	1.92	2.14	2.33	2.38	57%	13%	4%
E.Pacific	j-O1D	ATom2	1.44	1.48	1.79	2.10	2.18	62%	15%	5%
E.Pacific	j-O1D	ATom3	1.66	1.64	2.01	2.26	2.36	61%	14%	4%
E.Pacific	j-O1D	ATom4	1.95	2.05	2.27	2.46	2.54	58%	13%	4%
T.Atlantic	j-O1D	ATom1	1.55	1.71	1.95	2.21	2.31	63%	14%	5%
T.Atlantic	j-O1D	ATom2	1.61	1.63	1.99	2.36	2.45	62%	15%	5%
T.Atlantic	j-O1D	ATom3	1.58	1.55	1.97	2.33	2.40	63%	15%	5%
T.Atlantic	j-O1D	ATom4	1.46	1.55	1.88	2.10	2.18	65%	15%	5%
Arctic	j-O1D	ATom1	0.51	0.51	0.67	0.80	0.85	65%	16%	5%
Arctic	j-O1D	ATom2	0.01	0.01	0.02	0.02	0.02	79%	23%	8%
Arctic	j-O1D	ATom3	0.04	0.03	0.06	0.09	0.11	82%	26%	9%
Arctic	j-O1D	ATom4	0.73	0.71	0.83	0.96	1.02	58%	13%	4%
S.Ocean	j-O1D	ATom1	0.07	0.06	0.09	0.13	0.14	68%	19%	6%
S.Ocean	j-O1D	ATom2	1.26	1.32	1.68	2.04	2.14	67%	16%	5%
S.Ocean	j-O1D	ATom3	0.79	0.75	1.04	1.32	1.43	66%	17%	6%
S.Ocean	j-O1D	ATom4	0.03	0.03	0.05	0.07	0.08	71%	22%	7%



Antarctic	j-O1D	ATom3	0.50	0.43	0.66	0.90	0.98	66%	18%	6%
Antarctic	j-O1D	ATom4	0.00	0.00	0.01	0.01	0.01	99%	45%	16%
<b>j-NO2</b>	<b>j-value</b>	<b>deploy-</b>	<b>avg J</b>	<b>mdn J</b>	<b>avg J (1e-2 /s) in</b>			<b>fraction of total J in</b>		
		<b>ment</b>	<b>/s</b>	<b>/s</b>	<b>top50</b>	<b>top10</b>	<b>top03</b>	<b>top50</b>	<b>top10</b>	<b>top03</b>
Pacific	j-NO2	ATom1	0.48	0.52	0.61	0.71	0.75	64%	15%	5%
Pacific	j-NO2	ATom2	0.50	0.53	0.62	0.72	0.76	63%	15%	5%
Pacific	j-NO2	ATom3	0.49	0.53	0.60	0.67	0.70	61%	14%	4%
Pacific	j-NO2	ATom4	0.47	0.50	0.62	0.73	0.78	66%	15%	5%
Atlantic	j-NO2	ATom1	0.48	0.52	0.61	0.70	0.74	64%	15%	5%
Atlantic	j-NO2	ATom2	0.50	0.54	0.62	0.70	0.75	62%	14%	5%
Atlantic	j-NO2	ATom3	0.49	0.52	0.61	0.69	0.73	62%	14%	5%
Atlantic	j-NO2	ATom4	0.47	0.49	0.60	0.70	0.74	64%	15%	5%
C.Pacific	j-NO2	ATom1	0.50	0.53	0.59	0.65	0.68	59%	13%	4%
C.Pacific	j-NO2	ATom2	0.53	0.55	0.62	0.71	0.74	59%	13%	4%
C.Pacific	j-NO2	ATom3	0.52	0.55	0.60	0.67	0.70	58%	13%	4%
C.Pacific	j-NO2	ATom4	0.49	0.52	0.59	0.65	0.67	60%	13%	4%
E.Pacific	j-NO2	ATom1	0.56	0.60	0.65	0.70	0.73	58%	13%	4%
E.Pacific	j-NO2	ATom2	0.51	0.54	0.59	0.63	0.66	58%	12%	4%
E.Pacific	j-NO2	ATom3	0.53	0.56	0.61	0.69	0.72	57%	13%	4%
E.Pacific	j-NO2	ATom4	0.58	0.63	0.68	0.72	0.75	58%	13%	4%
T.Atlantic	j-NO2	ATom1	0.51	0.55	0.61	0.67	0.70	59%	13%	4%
T.Atlantic	j-NO2	ATom2	0.54	0.56	0.61	0.67	0.69	57%	13%	4%
T.Atlantic	j-NO2	ATom3	0.53	0.56	0.62	0.68	0.72	59%	13%	4%
T.Atlantic	j-NO2	ATom4	0.49	0.51	0.58	0.65	0.67	59%	13%	4%
Arctic	j-NO2	ATom1	0.57	0.63	0.71	0.80	0.84	62%	14%	4%
Arctic	j-NO2	ATom2	0.05	0.03	0.08	0.12	0.12	83%	26%	8%
Arctic	j-NO2	ATom3	0.11	0.09	0.18	0.27	0.29	79%	24%	8%
Arctic	j-NO2	ATom4	0.80	0.80	0.90	1.02	1.05	56%	13%	4%
S.Ocean	j-NO2	ATom1	0.13	0.13	0.19	0.24	0.27	71%	19%	6%
S.Ocean	j-NO2	ATom2	0.61	0.68	0.73	0.79	0.82	60%	13%	4%
S.Ocean	j-NO2	ATom3	0.49	0.53	0.60	0.66	0.68	60%	14%	4%
S.Ocean	j-NO2	ATom4	0.09	0.08	0.14	0.21	0.24	75%	23%	8%
Antarctic	j-NO2	ATom3	0.49	0.48	0.56	0.64	0.68	58%	13%	4%
Antarctic	j-NO2	ATom4	0.01	0.00	0.02	0.04	0.06	99%	48%	22%

230 Table notes: The primary ocean basins (Pacific & Atlantic) use the over-ocean flight data from 53°S to 60°N, see Figure 2. The tropical ocean sections are Central Pacific (30°S-30°N, near Dateline), Eastern Pacific (0°-30°N, ~121°W), and Tropical Atlantic (30°S-30°N). All 10 s data are weighted inversely by frequency of occurrence in 10° latitude by 100 hPa bins and by



cosine(latitude). For the high-latitude sections – Arctic (66°N-90°N), Southern Ocean (66°S-55°S), and Antarctica (90°S-66°S) – parcels are weighted only by frequency of occurrence in 100 hPa bins.

235

### 3.2 Curtain plots

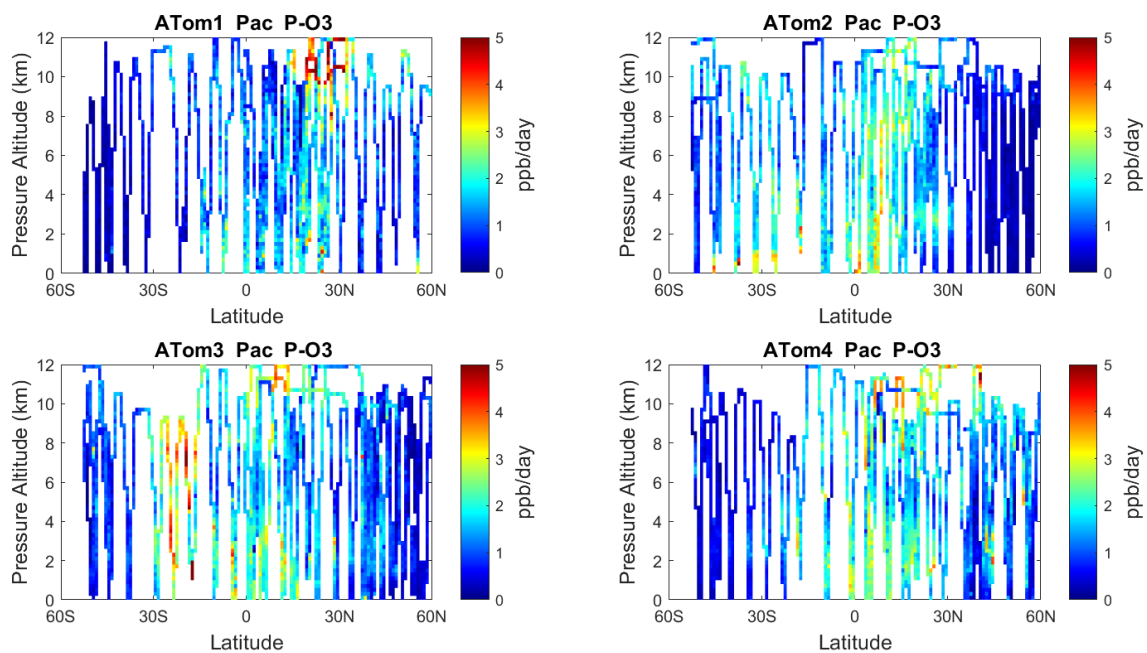
The spatial structures and variability of P-O3 as sampled by the four ATom transects over the Pacific Ocean are presented as 2D latitude-height curtain plots in Fig. 6. The full set of plots covering all four reactivities and also the Atlantic Ocean are shown sequentially in Fig. 6-13. For these curtain plots, the 10 s reactivities (2 km by 80 m thick parcels) are averaged and plotted in 1° latitude by 200 m thick cells. For both Atlantic and Pacific basins, the reactivities (L-O3, L-CH4, L-CO) generally follow the sun with more southerly hot parcels in ATom-23 (Feb, Oct) and northerly hot parcels in ATom-14 (Aug, May). The P-O3 hot spots have no simple seasonality, being dominated by middle- to upper-tropospheric regions with high NOx presumably from the outflow of deep convection from the nearby continents.

Because the E. Pacific flights (~121°W) are clearly influenced by continental outflow from Northern and Central America, we separate them from the C. Pacific in our examination of the tropical oceans (see Fig. 2). Curtain plots of the four reactivities for ATom-1234 in the C. Pacific are shown in Fig. 14-17; in the E. Pacific, in Fig. 18-21; and in the T. Atlantic, in Fig. 22-25. In terms of P-O3, the C. Pacific shows a few hot spots, but generally no large regions > 3 ppb/d. The T. Atlantic shows extensive regions in the middle-to-upper troposphere with P-O3 > 3 ppb/d; and these look like continental outflow with both NOx and HOx sources. The E. Pacific shows extensive 1-2 km thick, 10° latitude layers of mostly above 8 km. In the E. Pacific these P-O3 layers are clearly separated from the moderately high (ATom-23) to extremely high (ATom-14) L-O3 > 5 ppb/d layers below 8 km. The large L-O3 (and also L-CH4 and L-CO) layers contain highly reactive HOx-VOC chemistry but little NOx, and these are associated with continental outflow, see discussion in G2023. The T. Atlantic, in contrast with the C. Pacific, shows large 20-30° wide tropical regions below 8 km with L-O3 > 4 ppb/d, L-CH4 > 1.5 ppb/d and L-CO > 4 ppb/d. These regions follow the sun, northward in ATom-14 and southward in ATom-23. For L-O3 and L-CO, the T. Atlantic has 50% greater loss than the C. Pacific.

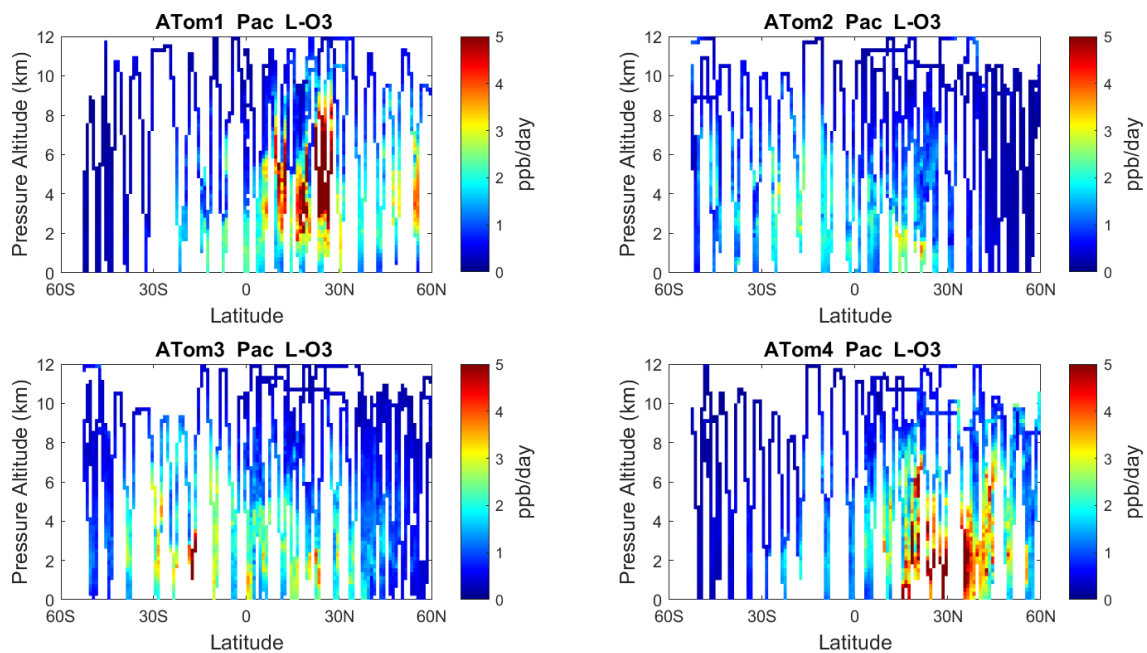
Overall, these figures (Fig. 6-25) show the dominance of the tropics (30°S - 30°N) for photochemical reactivity over the oceans. Only the northern mid-latitudes (30°N - 60°N) contribute almost a fifth tropics-like reactive region in summer (ATom-14), especially in the Atlantic.

Curtain profiles for the Arctic are presented only for ATom-1 (Fig. 26) and ATom-4 (Fig. 27) when there was enough sunlight to generate non-negligible reactivities. The very low reactivity statistics for ATom-23 Arctic are seen in Table 1. Stratospheric air parcels are excluded in these Arctic statistics. Reactivities appear moderately high, but the color scale is 3 times smaller than in Figures 6-25. Similar to the ocean basins, in the Arctic much of the P-O3 occurs above 8 km, and losses (L-O3, L-CH4, L-CO) occurs between 1 and 6 km. Curiously, there is a region of high L-CO above 10 km in the region of high P-O3. Notably, that rate (R4) is not sensitive to cold temperatures. Only one of the two Antarctic flights had enough sunlight to produce much reactivity (ATom-3, Fig. 28). Like the Arctic, P-O3 is concentrated in the upper troposphere, while L-O3 and L-CH4 are in the lower. Note that the color scale is 6-to-12 times smaller than in Fig. 6-25.

265



270 **Figure 6.** 2D curtain plots (altitude-latitude profiling) of P-O3 (ppb/day) in Pacific basin (53°S-60°N) for Atom-1234. In all these curtain plots, ATom 10s parcel data are weighted by cosine (latitude) and sampling frequency, and then they are averaged into 1° latitude and 200 m altitude bins.



275 **Figure 7.** Curtain plots of L-O3 (ppb/day) in Pacific basin (53°S-60°N) for Atom-1234. See Fig. 6



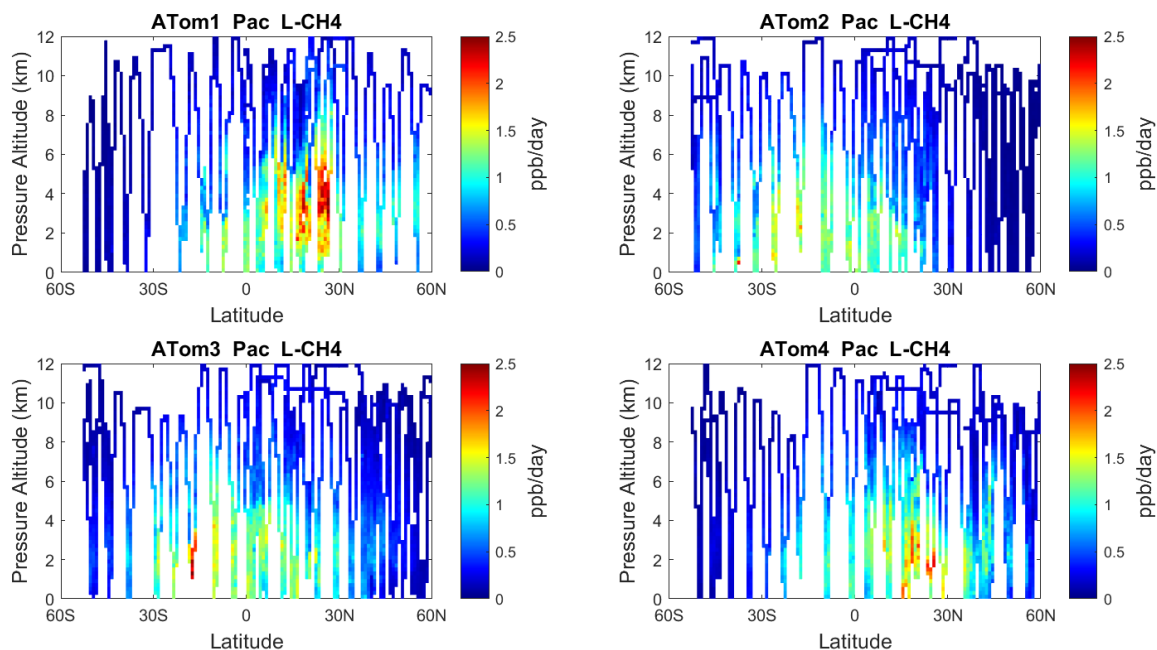


Figure 8. Curtain plots of L-CH<sub>4</sub> (ppb/day) in Pacific basin (53°S-60°N) for Atom-1234. See Fig. 6

280

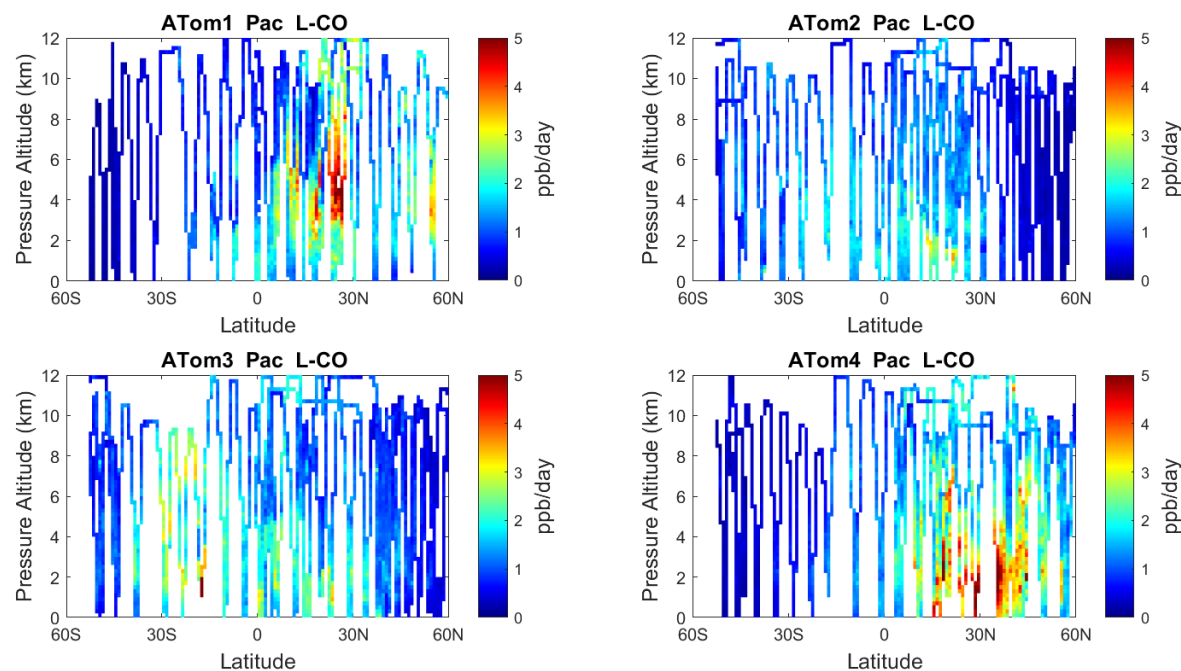
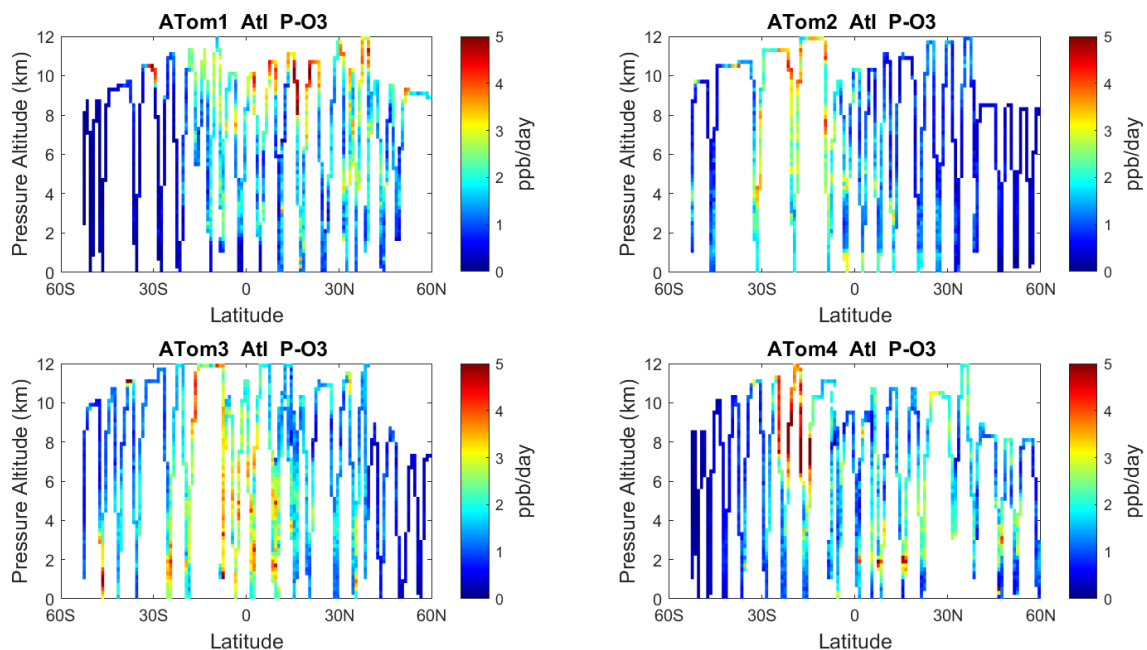
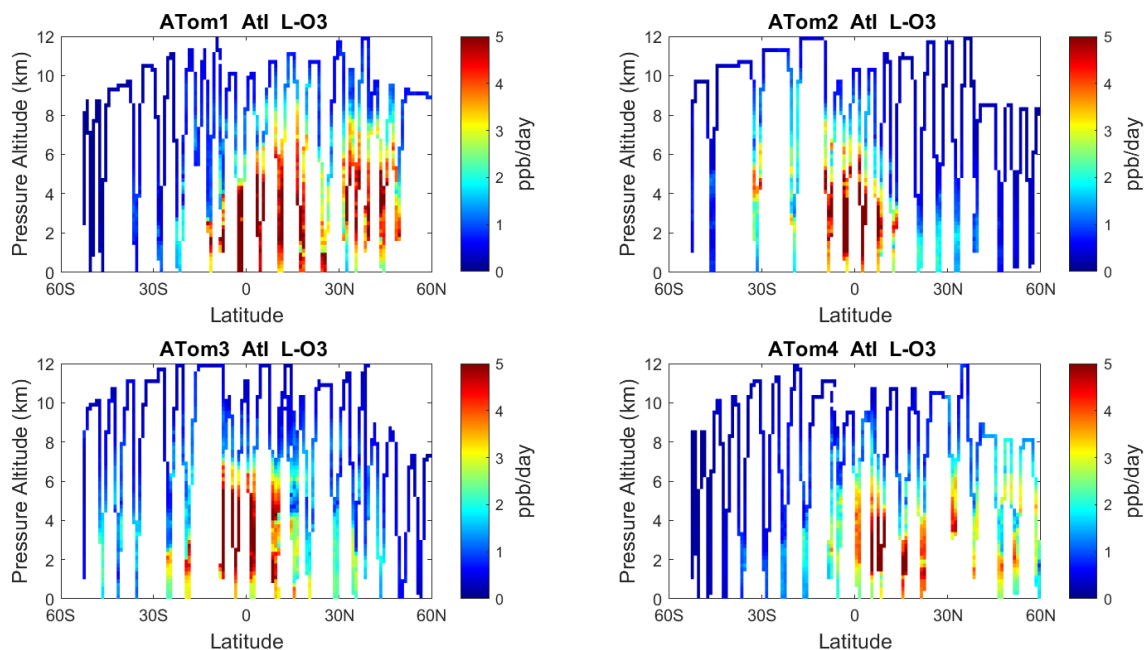


Figure 9. Curtain plots of L-CO (ppb/day) in Pacific basin (53°S-60°N) for Atom-1234. See Fig. 6



285

**Figure 10.** Curtain plots of P-O3 (ppb/day) in Atlantic basin (53°S-60°N) for Atom-1234. See Fig. 6.



290

**Figure 11.** Curtain plots of L-O3 (ppb/day) in Atlantic basin (53°S-60°N) for Atom-1234. See Fig. 6.

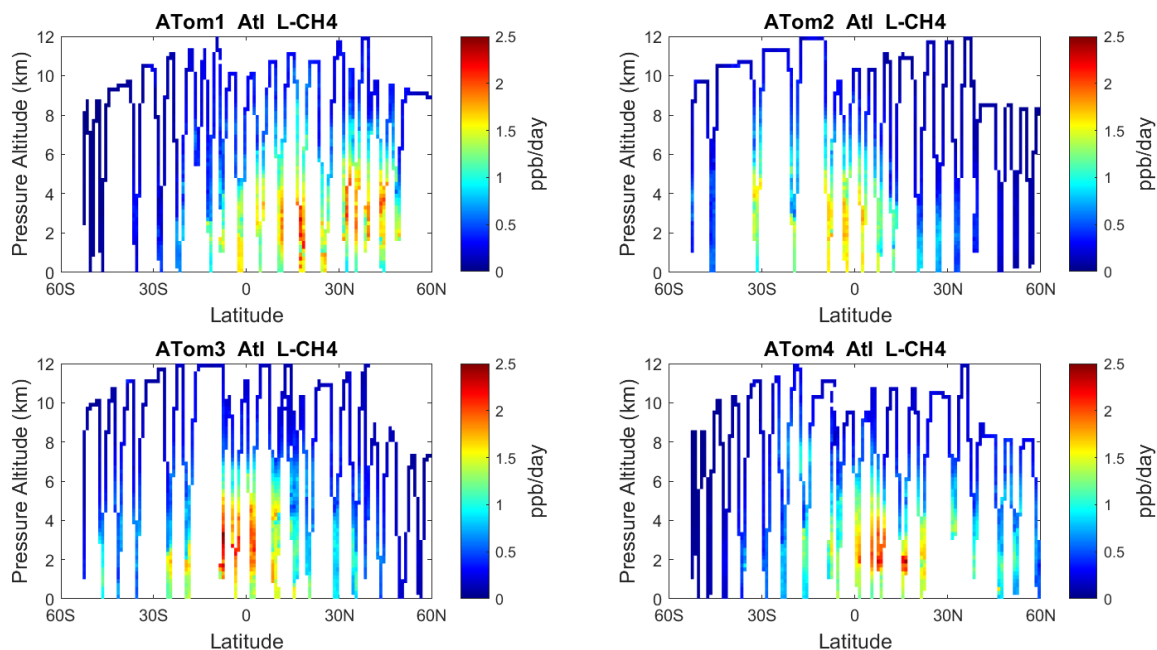


Figure 12. Curtain plots of L-CH<sub>4</sub> (ppb/day) in Atlantic basin (53°S-60°N) for Atom-1234. See Fig. 6.

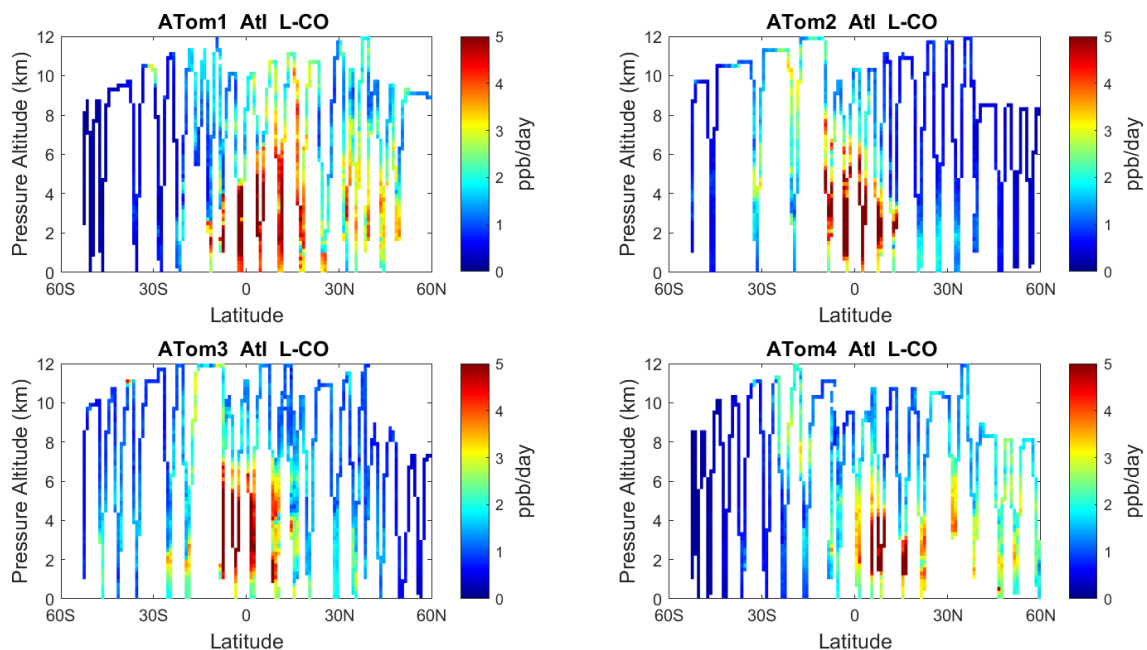
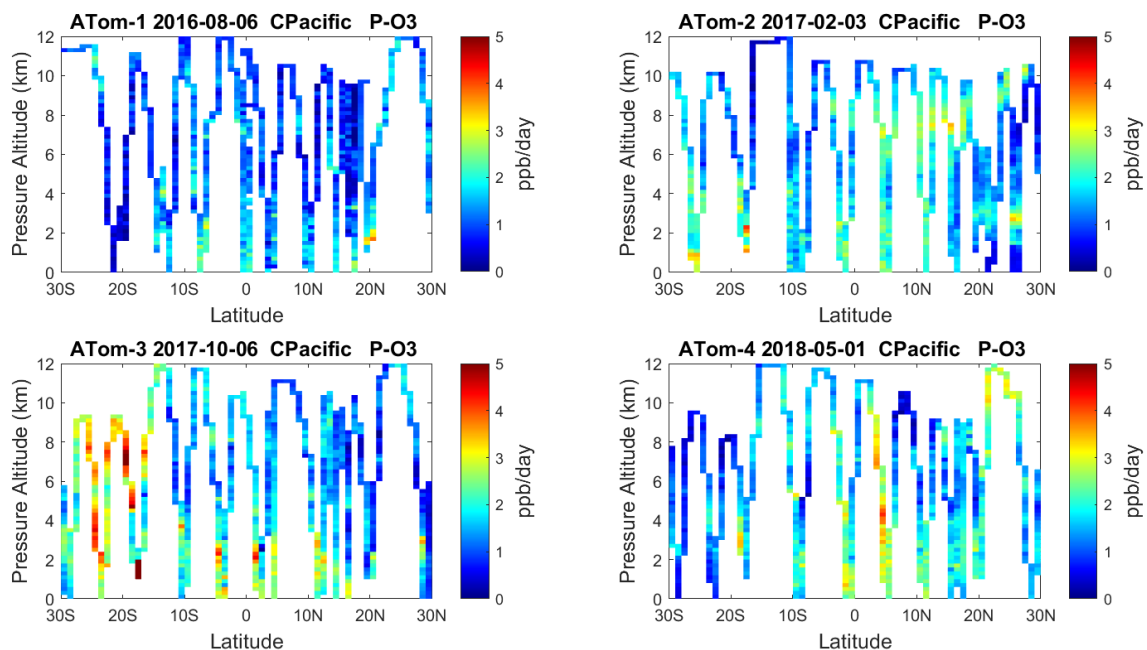
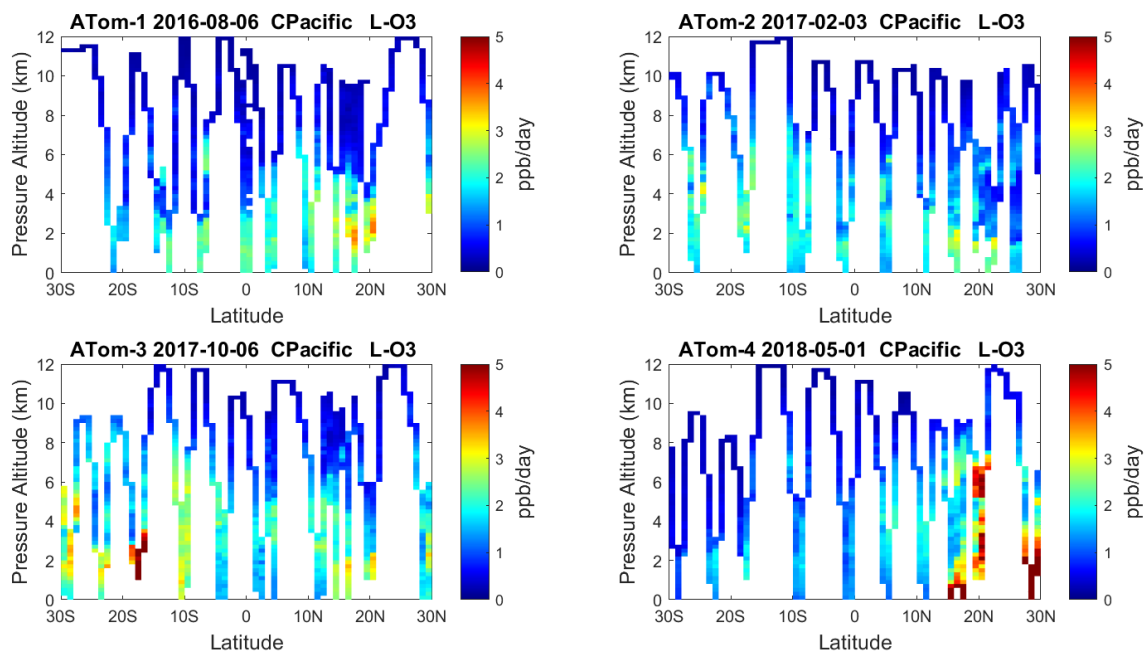


Figure 13. Curtain plots of L-CO (ppb/day) in Atlantic basin (53°S-60°N) for Atom-1234. See Fig. 6.



300 **Figure 14.** Curtain plots of P-O3 (ppb/day) in the tropical Central Pacific (30°S-30°N) for ATom-1234. See Fig. 6. The date of the flight crossing the equatorial Pacific for each deployment are given.



305 **Figure 15.** Curtain plots of L-O3 (ppb/day) in the tropical Central Pacific (30°S-30°N) for ATom-1234. See Fig. 6.

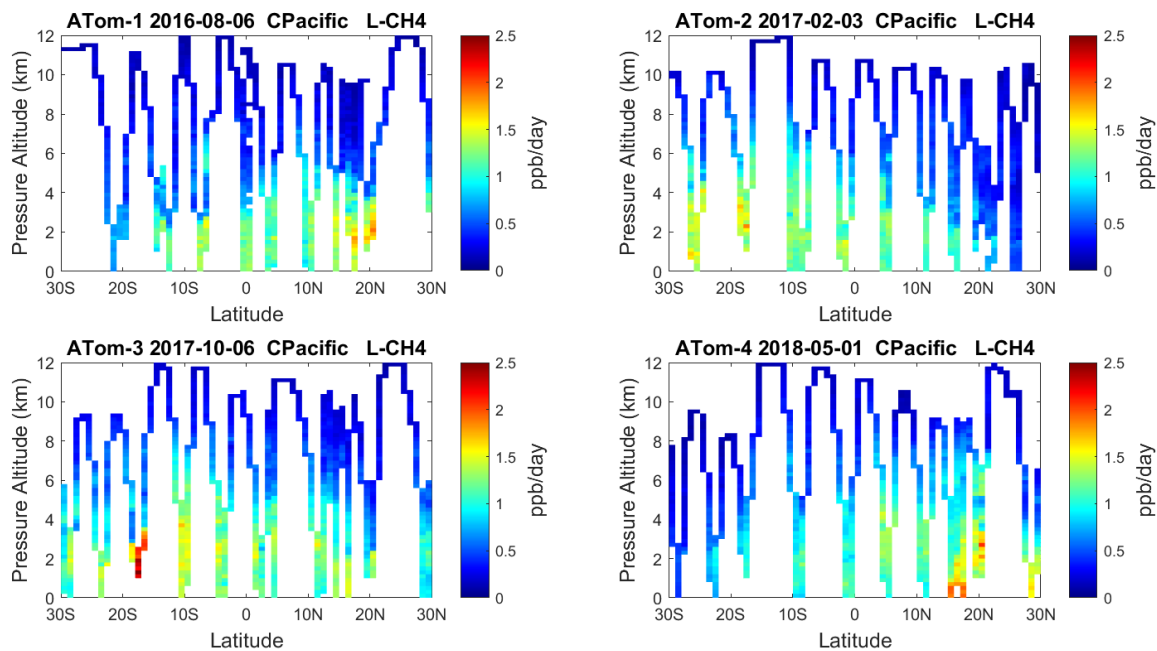
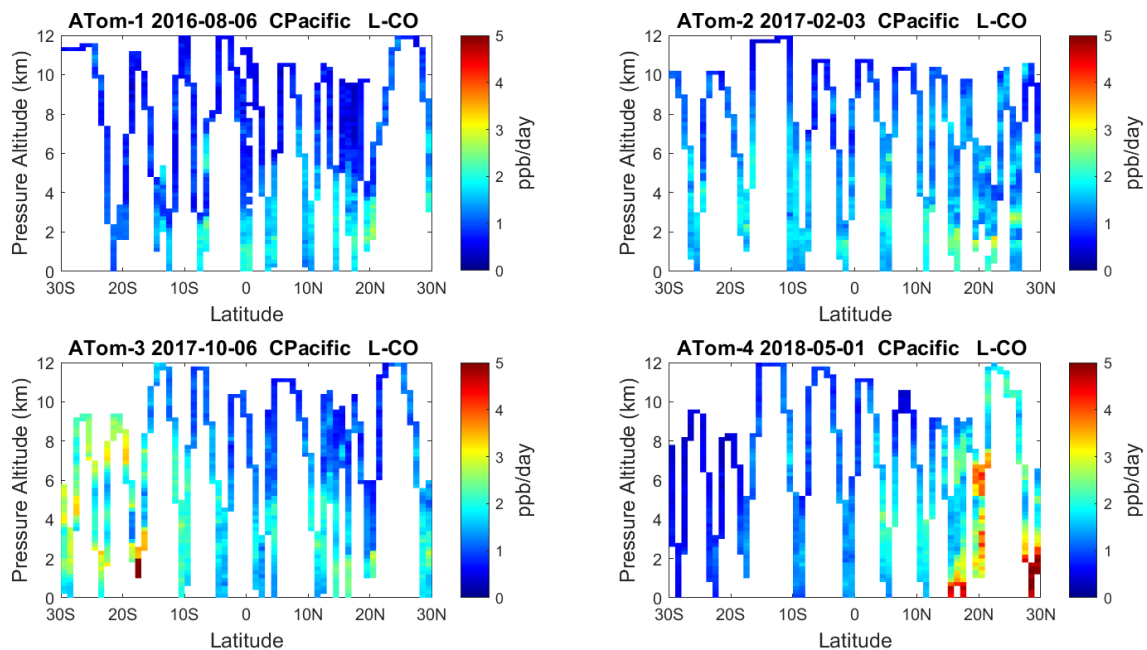
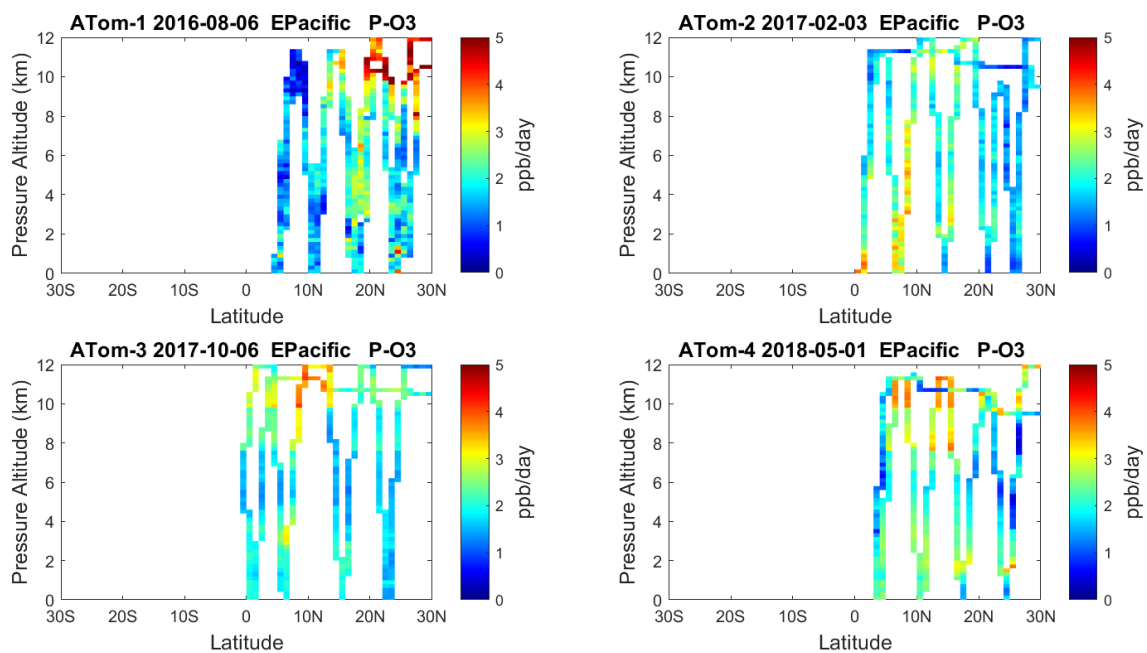


Figure 16. Curtain plots of L-CH4 (ppb/day) in the tropical Central Pacific (30°S-30°N) for ATom-1234. See Fig. 6.



310 Figure 17. Curtain plots of L-CO (ppb/day) in the tropical Central Pacific (30°S-30°N) for ATom-1234. See Fig. 6.



**Figure 18.** Curtain plots of P-O3 (ppb/day) in the tropical Eastern Pacific (0°-30°N) for ATom-1234. See Fig. 6.

315

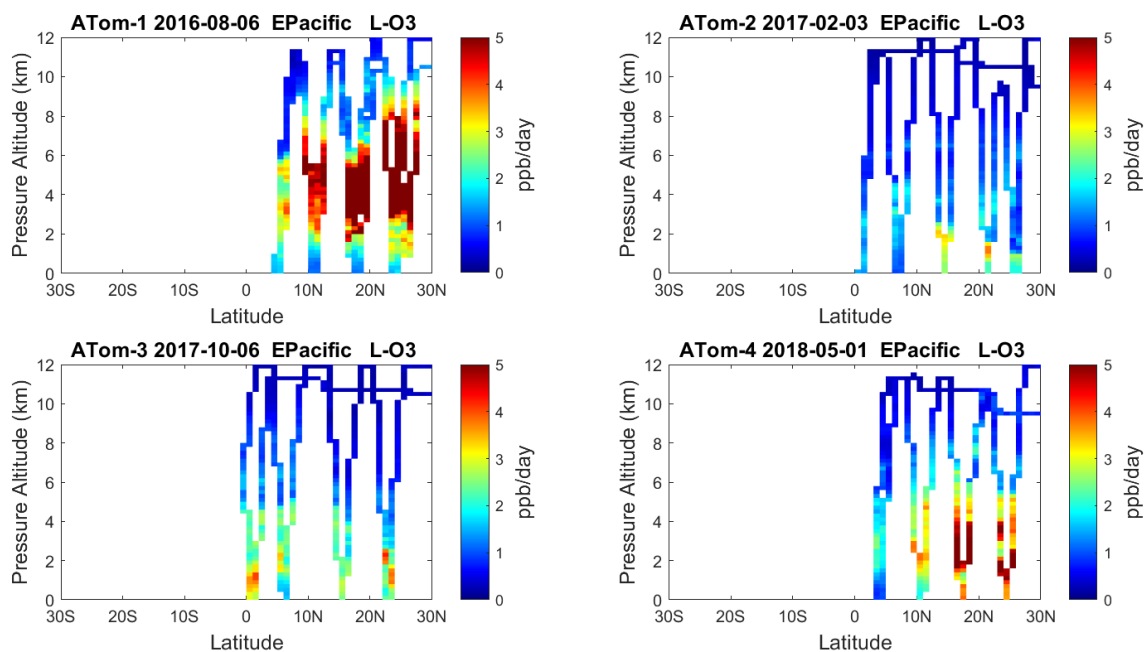
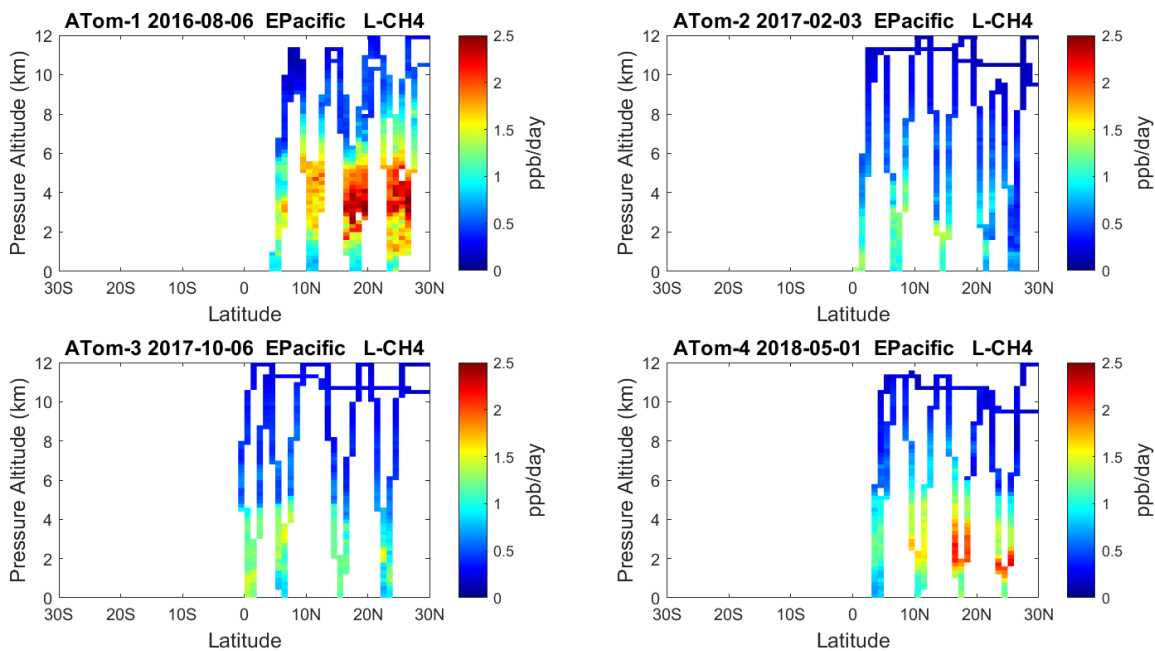
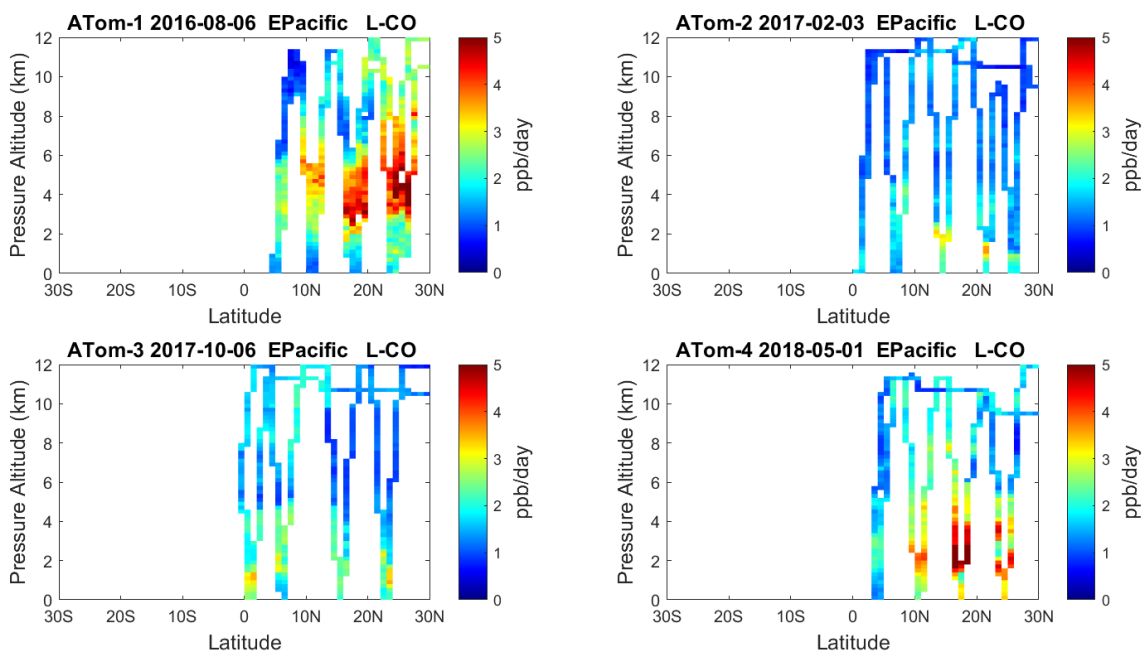


**Figure 19.** Curtain plots of L-O3 (ppb/day) in the tropical Eastern Pacific (0°-30°N) for ATom-1234. See Fig. 6.



320

**Figure 20.** Curtain plots of L-CH4 (ppb/day) in the tropical Eastern Pacific (0°-30°N) for ATom-1234. See Fig. 6.



325

**Figure 21.** Curtain plots of L-CO (ppb/day) in the tropical Eastern Pacific (0°-30°N) for ATom-1234. See Fig. 6.

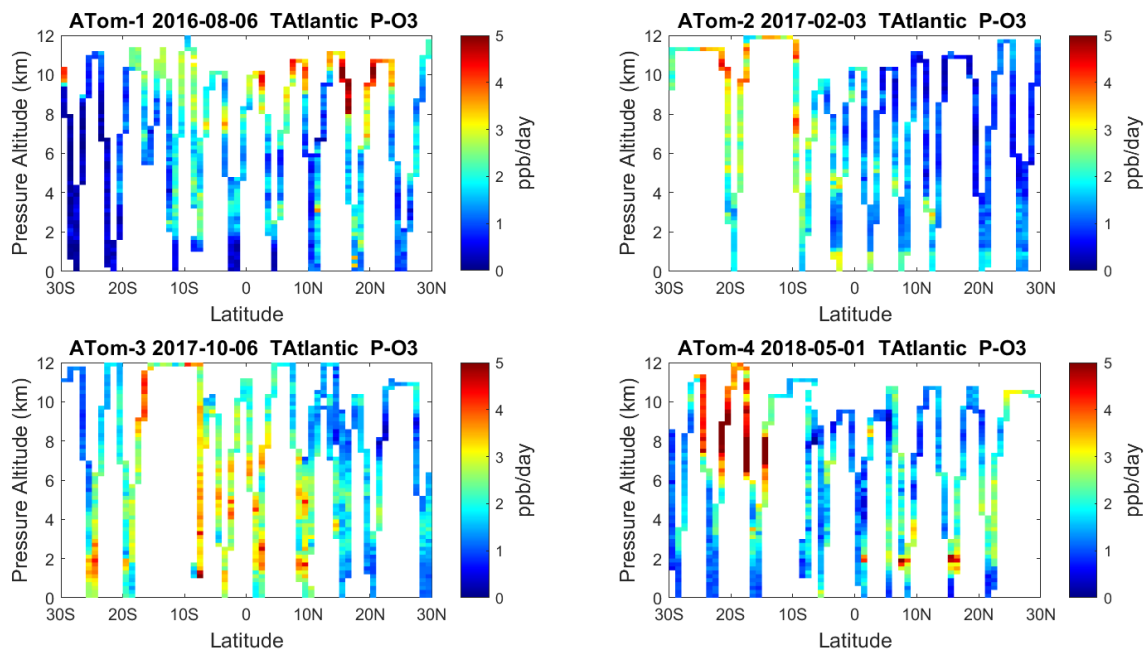
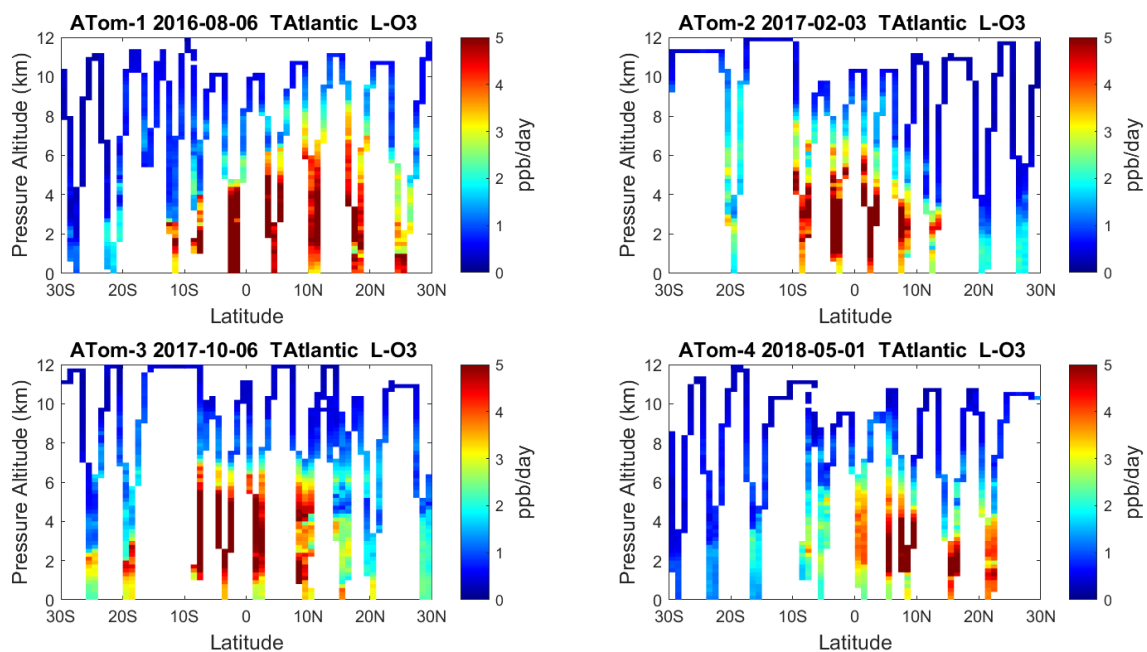


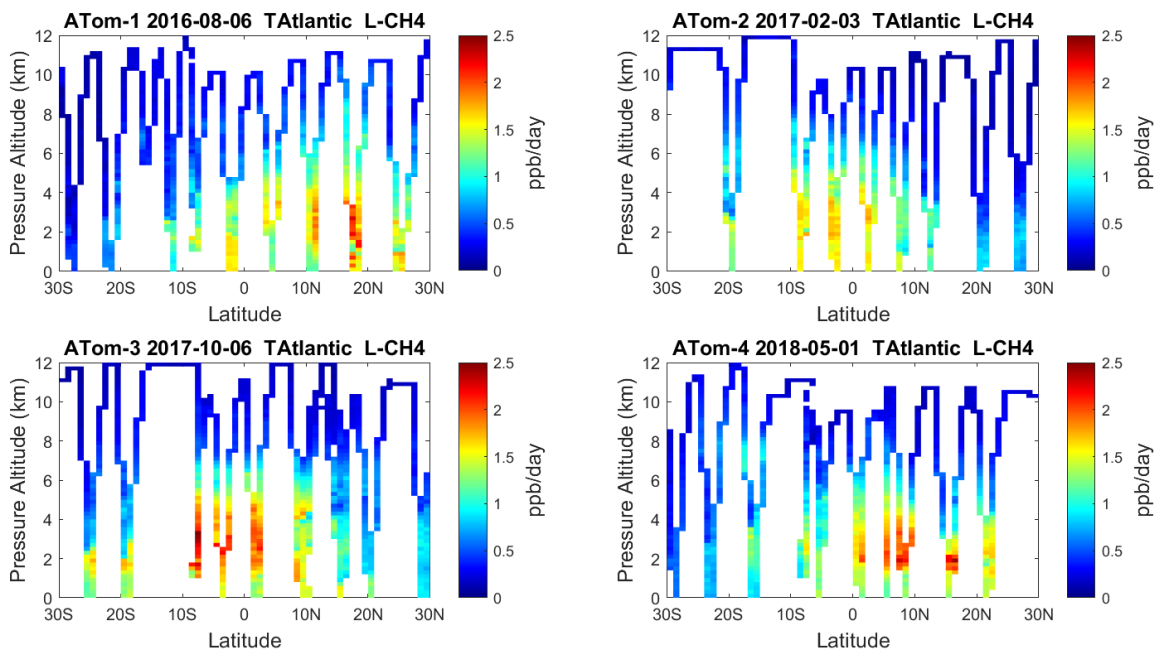
**Figure 22.** Curtain plots of P-O3 (ppb/day) in the tropical Atlantic (30°S-30°N) for ATom-1234. See Fig. 6.



330

**Figure 23.** Curtain plots of L-O3 (ppb/day) in the tropical Atlantic (30°S-30°N) for ATom-1234. See Fig. 6.





335 **Figure 24.** Curtain plots of L-CH<sub>4</sub> (ppb/day) in the tropical Atlantic (30°S-30°N) for ATom-1234. See Fig. 6.

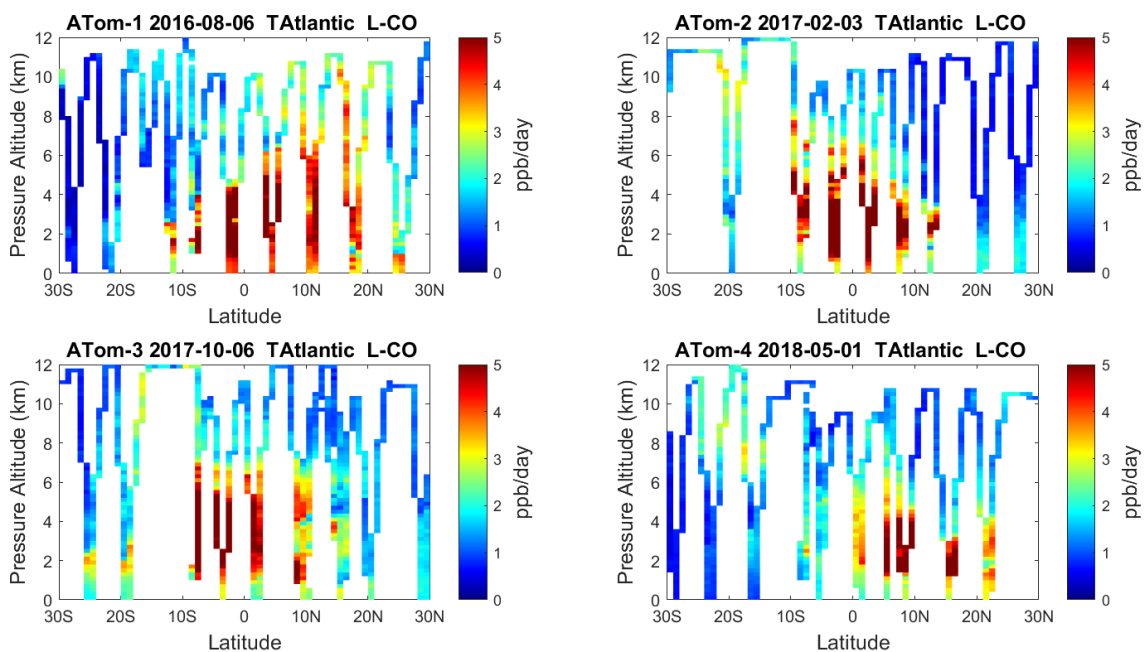
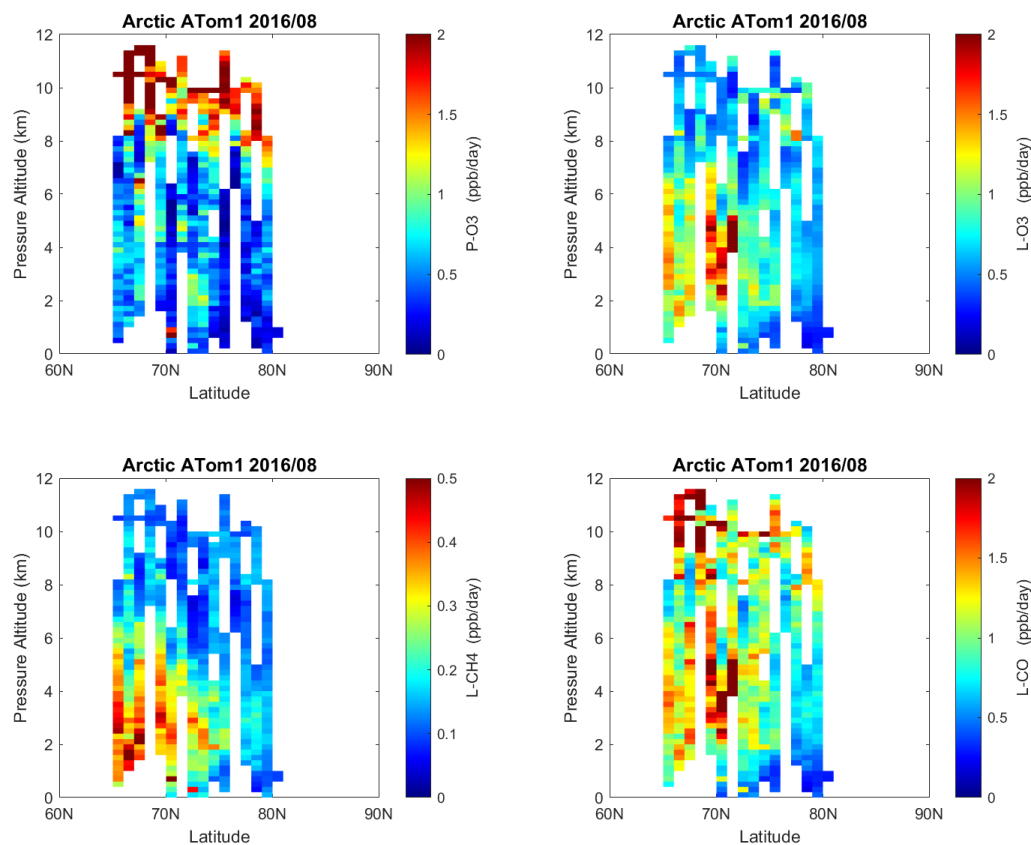
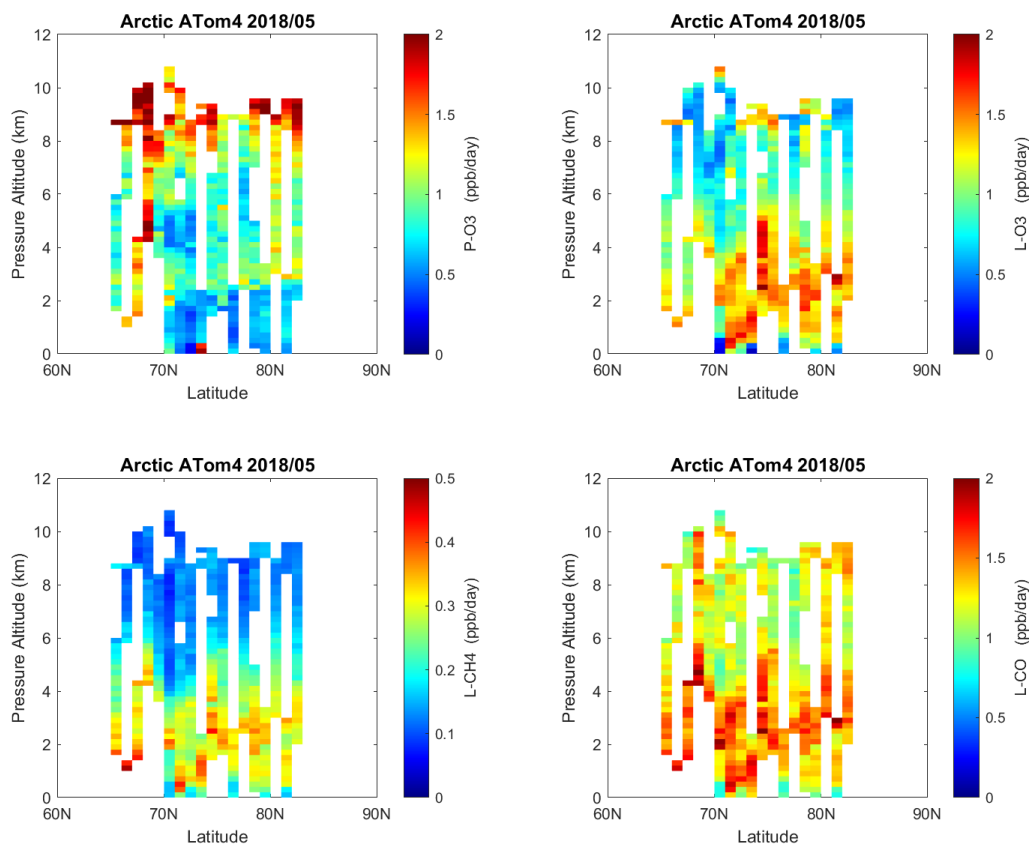


**Figure 25.** Curtain plots of L-CO (ppb/day) in the tropical Atlantic (30°S-30°N) for ATom-1234. See Fig. 6.

340



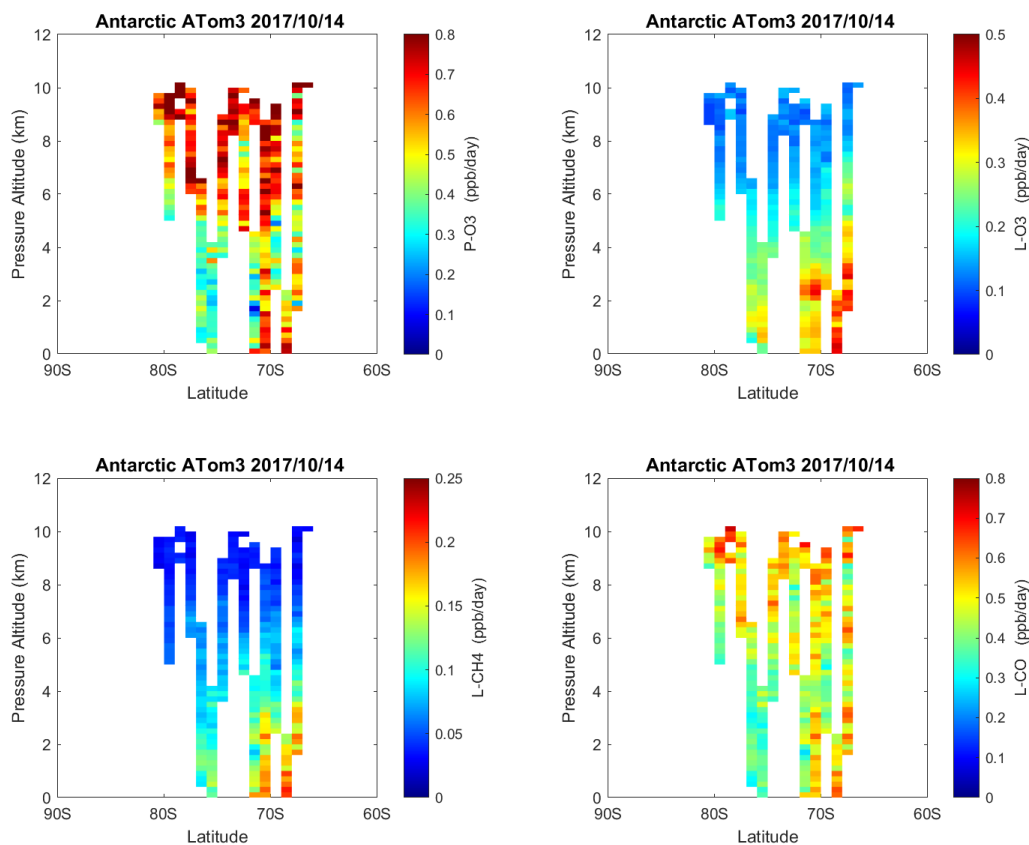
345 **Figure 26.** Curtain plots of the 4 reactivities (P-O3, L-O3, L-CH4, L-CO ppb/day) over the Arctic for ATom-1. Note the color bars have a much smaller range than in the Pacific and Atlantic basin plots. Troposphere-only parcels are shown, with stratosphere defined as ( $H_2O < 30$  ppm) and ( $O_3 > 80$  ppb) and ( $CO < 120$  ppb). See Fig. 6.



350

**Figure 27.** Curtain plots of the 4 reactivities (P-O3, L-O3, L-CH4, L-CO ppb/day) over the Arctic on ATom-4. Troposphere-only parcels, see Fig. 6 & 26.

355



360 **Figure 28.** Curtain plots of the 4 reactivities (P-O3, L-O3, L-CH4, L-CO, ppb/day) over Antarctica on ATom-3. Note the color bars have a smaller range than in the Pacific and Atlantic and Arctic basin plots. Troposphere-only parcels. See Fig. 6 & 26.



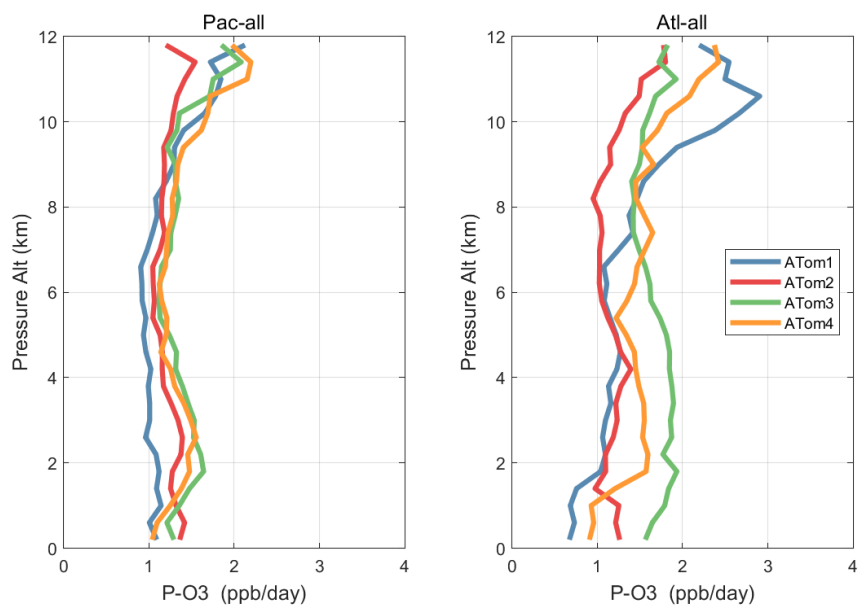
### 3.3 Mean altitude profiles

365 Altitude profiles of the weighted mean P-O<sub>3</sub> for the three tropical basins and 4 deployments are compared in Fig. 29. For  
other reactivities, see Fig. 30-32. These profiles highlight the consistency in basin averages across the four ATom  
deployments with some exceptions. In the Pacific, the P-O<sub>3</sub> profiles are similar, but ATom-1 is systematically less below 6  
km. Although the hot spots of P-O<sub>3</sub> are dominated by the higher altitudes, the mean profile shows only a modest increase  
above 10 km. In the Atlantic, ATom-3 has much greater P-O<sub>3</sub> below 6 km, but above 8 km, all deployments show a wide  
370 range of mean values, with ATom-1 exceeding 2.5 ppb/d above 10 km. For L-O<sub>3</sub> and L-CH<sub>4</sub>, the spread is much larger with  
ATom-1 largest in both Pacific and Atlantic. For L-CO, the variation is different still, with a relatively large spread, e.g., in  
the Pacific, ATom-4 is 50-100% larger than ATom-2.

Mean reactivity profiles for the three tropical basins are shown in Fig. 33-36. Here the C. Pacific shows small variability  
across deployments (except for P-O<sub>3</sub> minimum in ATom-1) while the E. Pacific shows little range in P-O<sub>3</sub> but very large L-  
375 O<sub>3</sub>, L-CH<sub>4</sub> and L-CO below 8 km for ATom-14. The end of the biomass burning season in Central America (15°N-20°N) is  
probably the cause of the peak L-O<sub>3</sub> below 6 km in ATom-4 (May); while the start of the North American Monsoon season  
is probably the cause of the extensive highly reactive deep-convection layer (2-10 km) in ATom-1 (August). With this high  
level of variability, it will be important to re-examine the time period of the ATom flights with a chemistry-transport model  
to assess the spatio-temporal scales and origins of these events.

380 In the Arctic (Fig. 37), ATom-14 show similar profiles but with different shapes for each reactivity; while ATom-23 have  
negligible reactivities as expected from the limited sunlight. P-O<sub>3</sub> peaks at 8-12 km with values from 1-2 ppb/day; while L-  
O<sub>3</sub> and L-CH<sub>4</sub> peak around 2-4 km. As in the curtain plots, L-CO peaks with L-O<sub>3</sub> in the lower troposphere and also with  
P-O<sub>3</sub> in the upper. The reactivities in the Arctic, even in summer are less than the average over the Pacific and Atlantic  
oceans and thus have little impact on the global O<sub>3</sub> or CH<sub>4</sub> budgets.

385 In the Antarctic (Fig. 38), reactivities are much less than the Arctic and only reported for ATom-3; however, due to the  
limited sampling of the Antarctic, this may underestimate its role in the global or even regional budgets. The S. Ocean  
reactivity profiles (Fig. 39) can be directly compared with the Arctic (Fig. 37) since both use the same axes scale. For L-  
CH<sub>4</sub>, they are almost identical (S. Ocean ATom-23 with Arctic ATom-14), and the differences in L-CO are simply  
attributable to the smaller CO abundance in the southern hemisphere. The O<sub>3</sub> reactivities are much less in the S. Ocean,  
390 however, and there is no peak in P-O<sub>3</sub> (1-2 ppb/d) above 8 km as found in the Arctic. The Arctic clearly has much  
greater pollution in the upper troposphere, including possibly aviation NO<sub>x</sub> sources.



395 **Figure 29.** Mean altitude profile of P-O3 (ppb/day) over the Pacific and Atlantic basins (53°S-60°N) for ATom-1234.

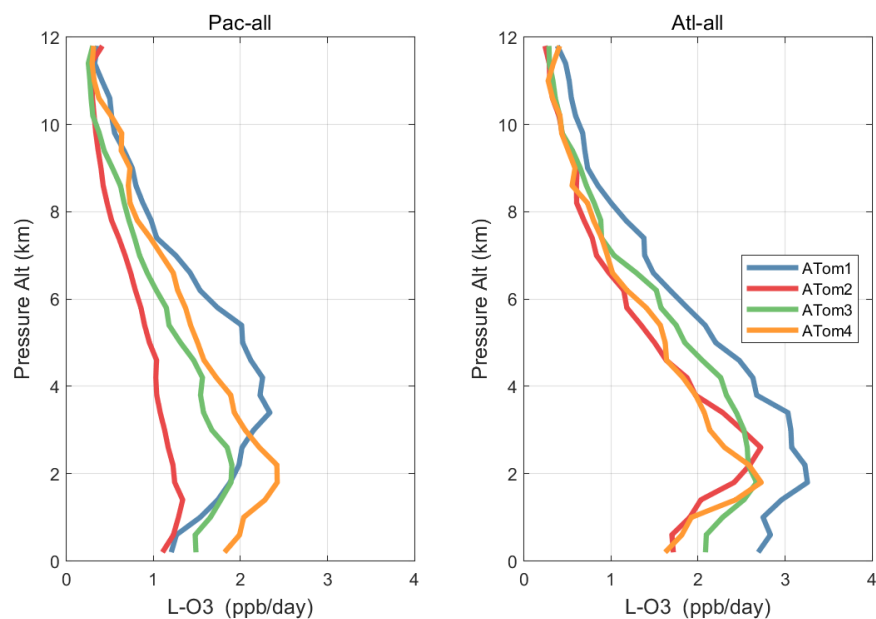
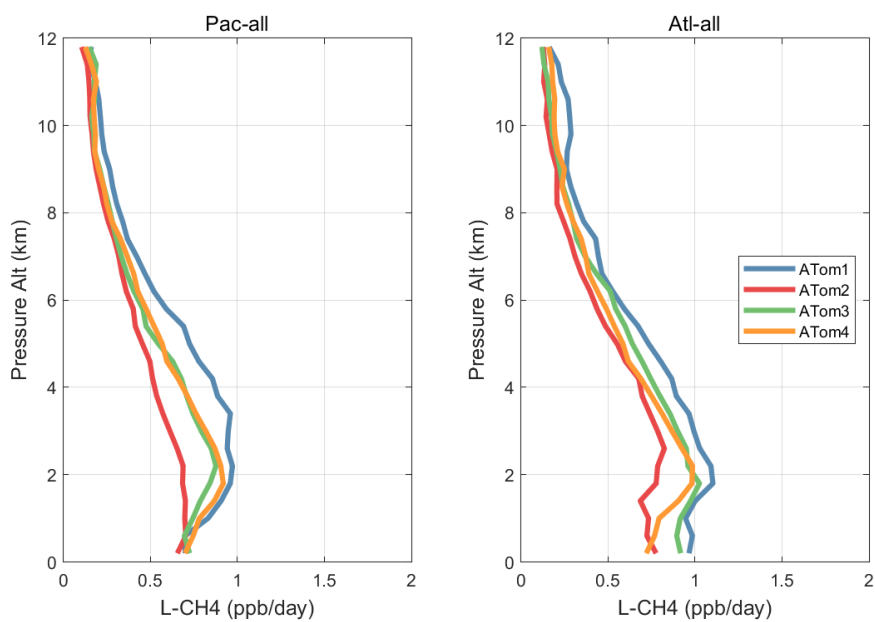
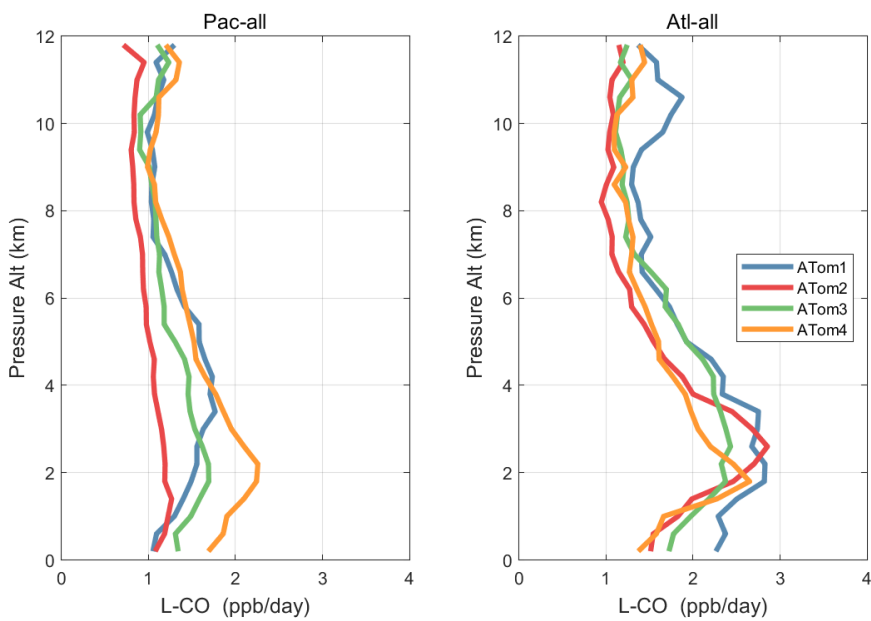


**Figure 30.** Mean altitude profile of L-O3 (ppb/day) over the Pacific and Atlantic basins (53°S-60°N) for ATom-1234.



400 **Figure 31.** Mean altitude profile of L-CH<sub>4</sub> (ppb/day) over the Pacific and Atlantic basins (53°S-60°N) for ATom-1234.



405 **Figure 32.** Mean altitude profile of L-CO (ppb/day) over the Pacific and Atlantic basins (53°S-60°N) for ATom-1234.

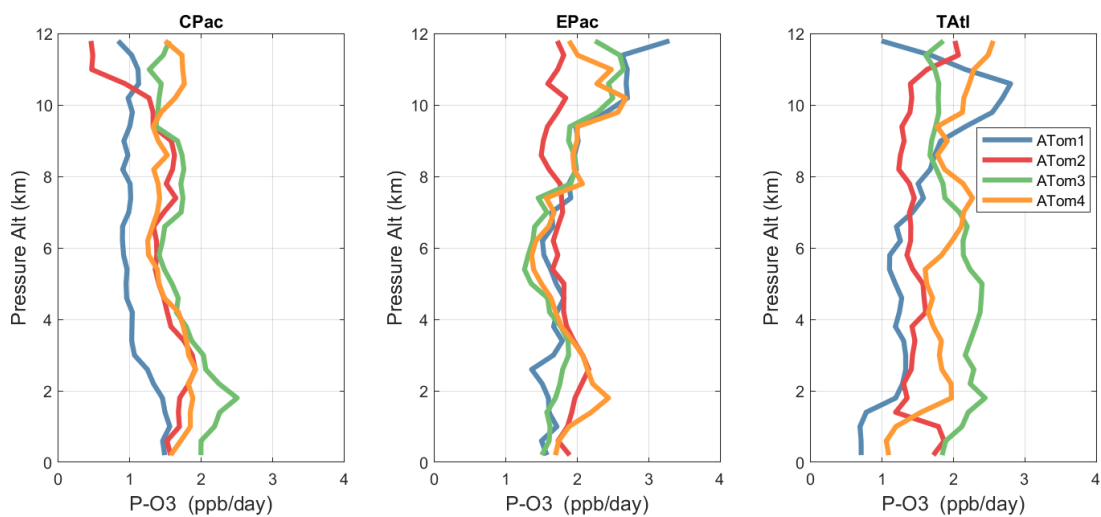


**Figure 33.** Mean altitude profile of P-O3 (ppb/day) over the 3 tropical basins for ATom-1234.

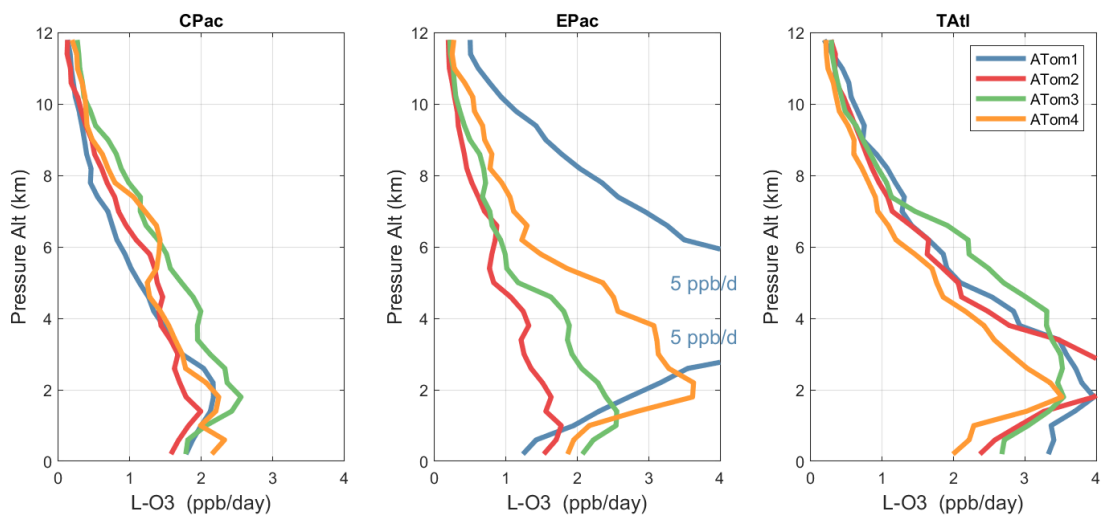


**Figure 34.** Mean altitude profile of L-O3 (ppb/day) over the 3 tropical basins for ATom-1234.



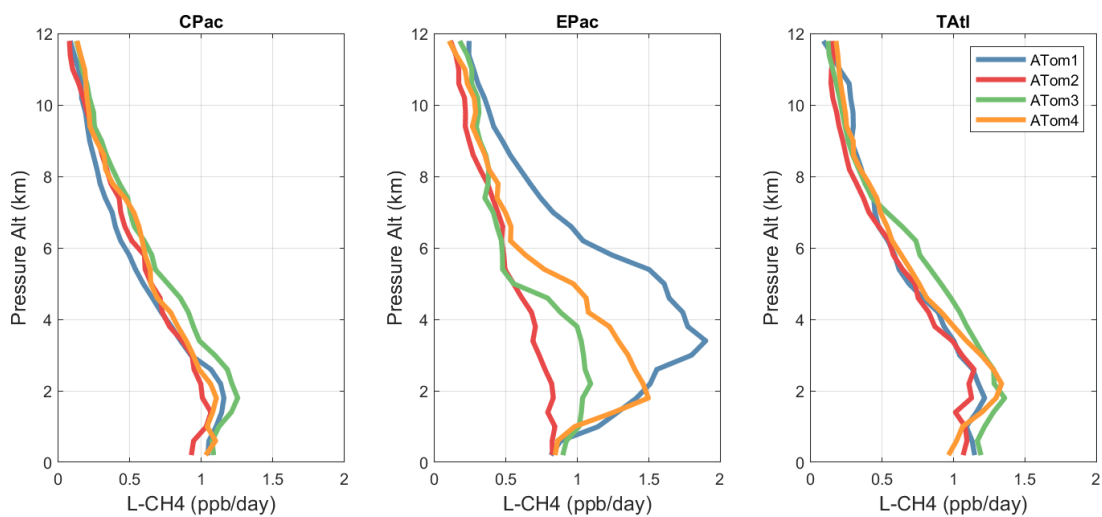


Figure 35. Mean altitude profile of L-CH<sub>4</sub> (ppb/day) over the 3 tropical basins for ATom-1234.

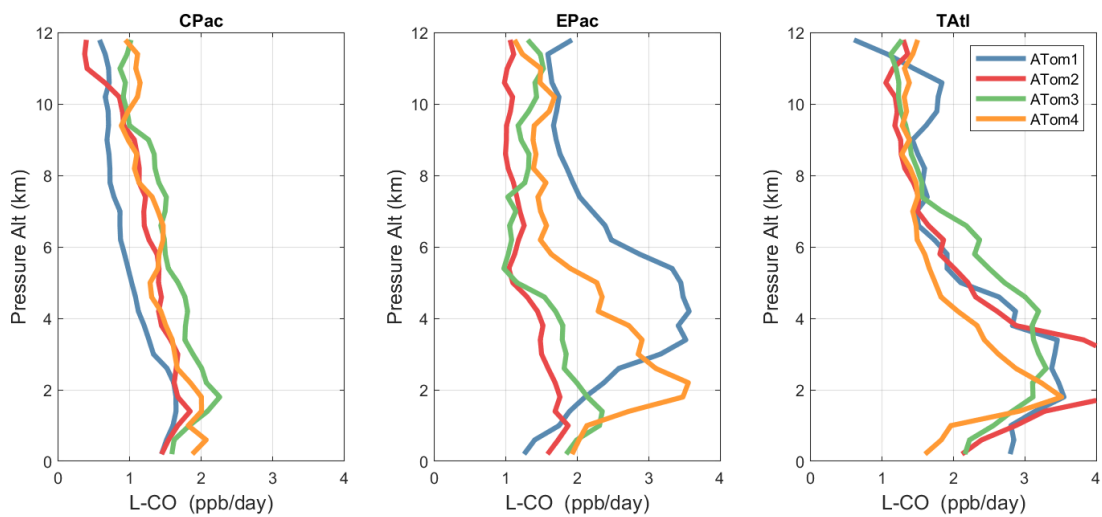
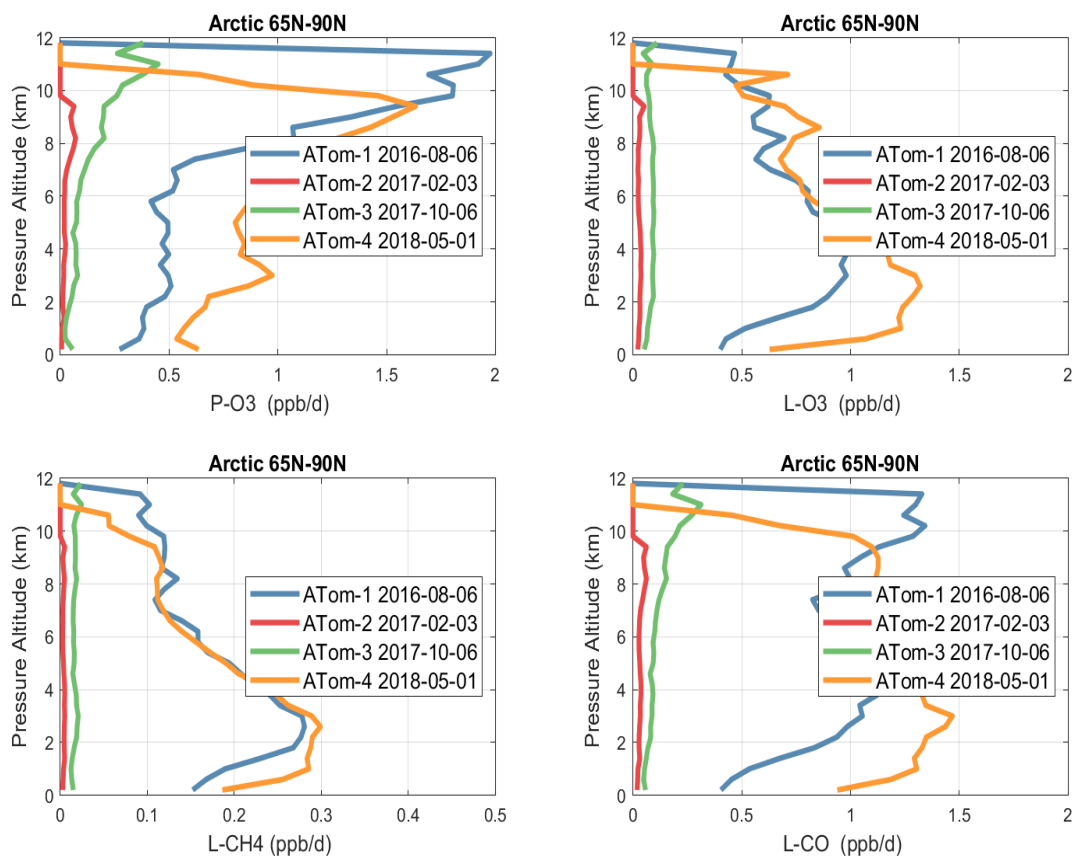
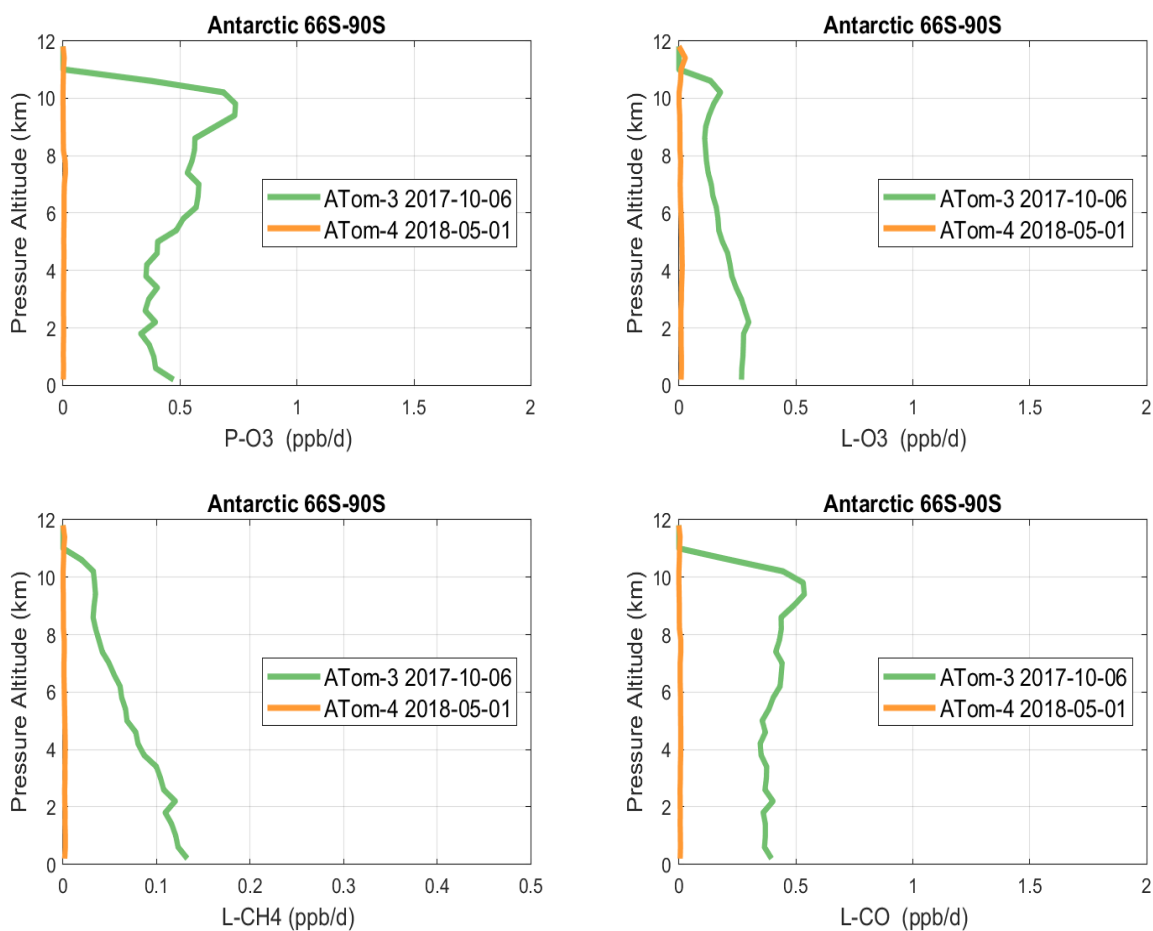


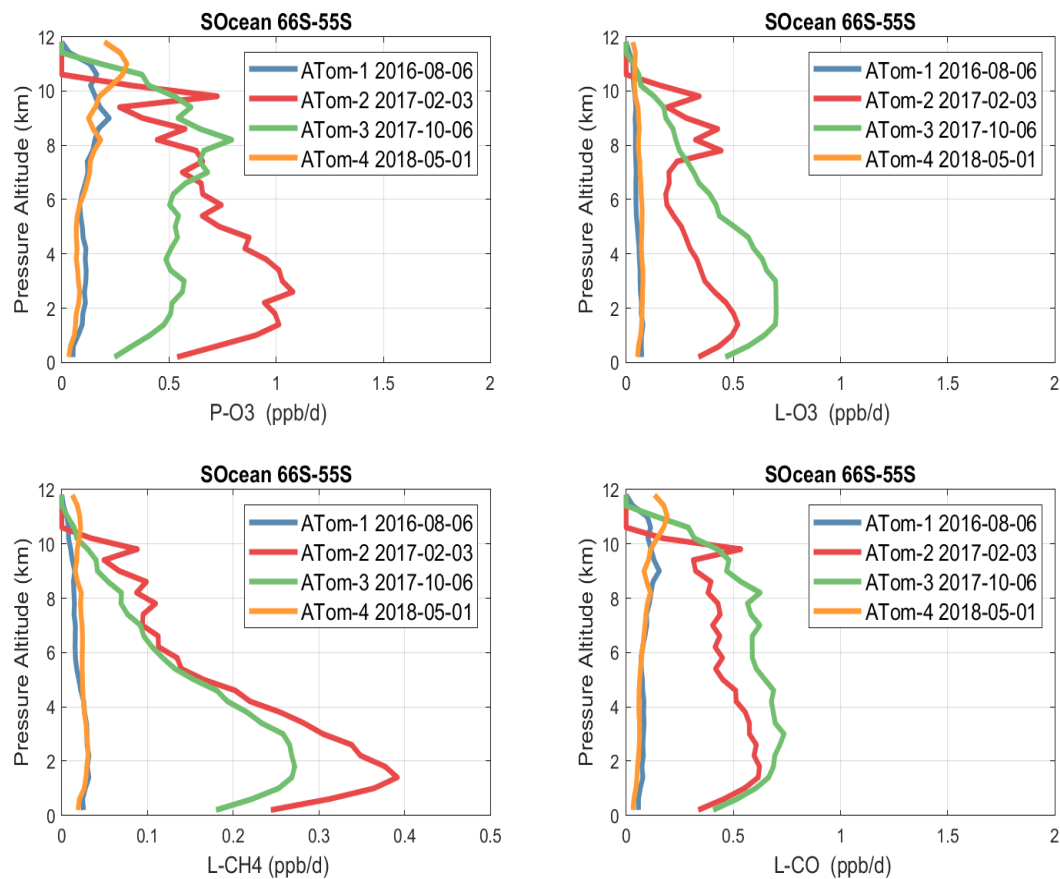
Figure 36. Mean altitude profile of L-CO (ppb/day) over the 3 tropical basins for ATom-1234.



420 **Figure 37.** Mean altitude profile of the 4 reactivities (P-O<sub>3</sub>, L-O<sub>3</sub>, L-CH<sub>4</sub>, L-CO, ppb/day) over the Arctic (66°N-90°N) for ATom-1234. All ATom 10s parcels are weighted by frequency of pressure sampling only. Troposphere-only parcels. Dates in the legend are the day of crossing the equator in the Pacific for each deployment



425 **Figure 38.** Mean altitude profile of the 4 reactivities (P-O<sub>3</sub>, L-O<sub>3</sub>, L-CH<sub>4</sub>, L-CO, ppb/day) over Antarctica on ATom-34. All ATom 10s parcels are weighted by frequency of pressure sampling only. Troposphere-only parcels. See Fig. 37.



430

**Figure 39.** Mean altitude profile of the 4 reactivities (P-O3, L-O3, L-CH4, L-CO, ppb/day) over the Southern Ocean (66°S-55°S) on ATom-1234. All ATom 10s parcels are weighted by frequency of pressure sampling only. Troposphere-only parcels. See Fig. 34.



435 **3.4 Probability densities of photochemical reactivities**

The probability densities (PDs) of the ATom reactivities have proven useful in testing model climatologies (see G2023) and are shown for the Pacific and Atlantic basins and the four reactivities in Fig. 40-43. All four deployments are shown in each panel. The relatively low P-O3 PD stands out for both Pacific and Atlantic. The L-CH4 PD peaks at the lowest value with a secondary peak above 1 ppb/d. The very low values of L-CH4 simply reflect the sampling of the upper troposphere where the OH+CH4 rate coefficient proportional to  $\exp(-1775/T)$  is very small. Thus, the L-CO PD, which is also proportional to OH peaks at higher values. Restricting our PDs to the three tropical regions (Fig. 44-47), we find some distinct deployments (e.g., low P-O3 in C. Pacific for ATom-1; high P-O3 in T. Atlantic for ATom-3; high L-CH4 in E. Pacific for ATom-1), but for the most part the reactivity PDs present similar patterns for each reactivity in each tropical basin. Thus, the ATom PDs provide a useful climatology for model comparisons.

445

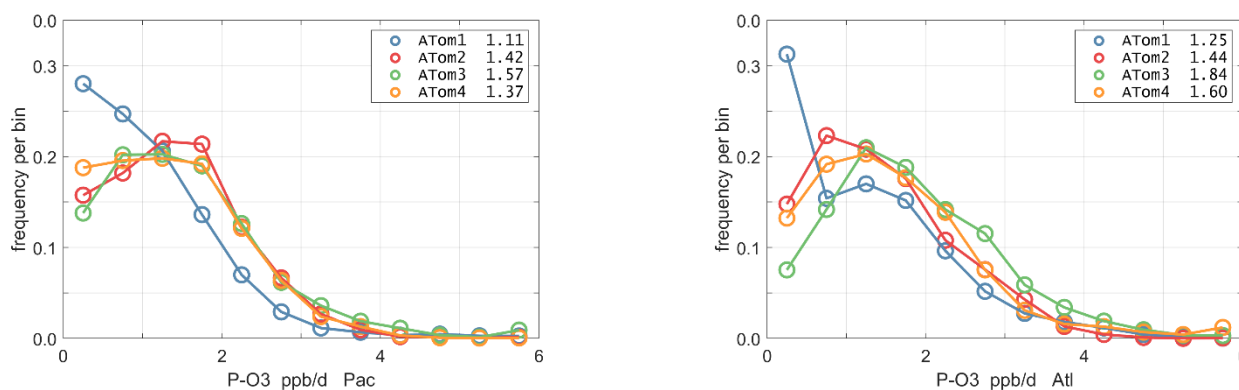


**Figure 40.** Probability Density of P-O3 (ppb/day) in Pacific and Atlantic basins (53°S-60°N) for ATom-1234. Values in the legend are the basin-wide weighted averages for each deployment. The frequency of parcels with reactivities greater than the maximum shown are added to the last point.

450

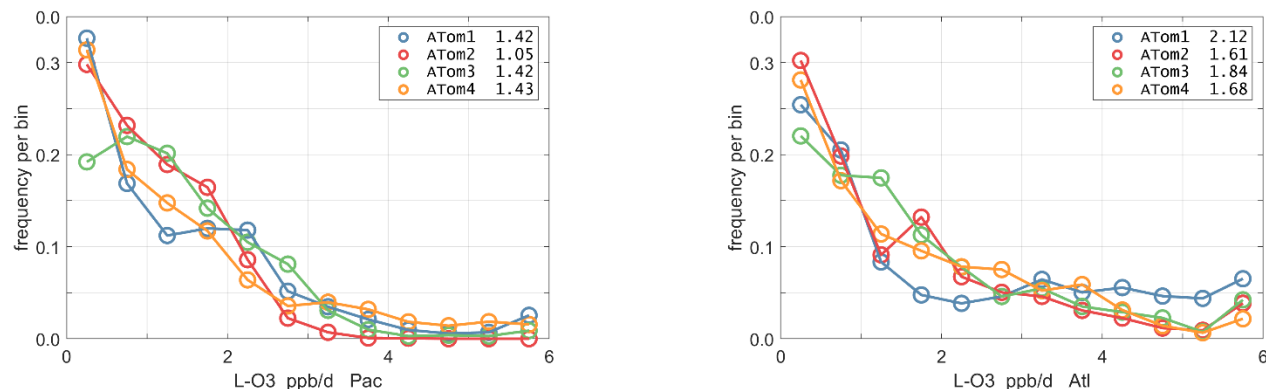


**Figure 41.** Probability Density of L-O3 (ppb/day) in Pacific and Atlantic basins for ATom-1234. See Fig. 40

455

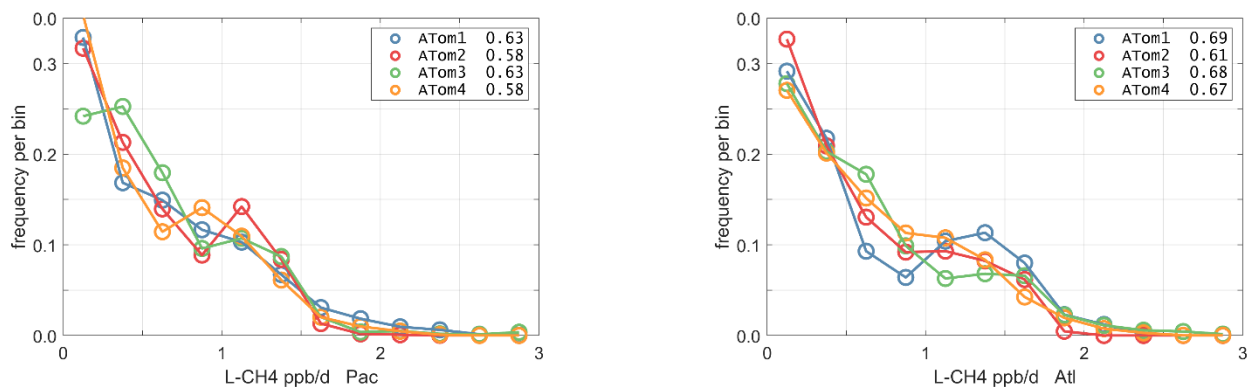


**Figure 42.** Probability Density of L-CH<sub>4</sub> (ppb/day) in Pacific and Atlantic basins for Atom-1234. See Fig. 40.

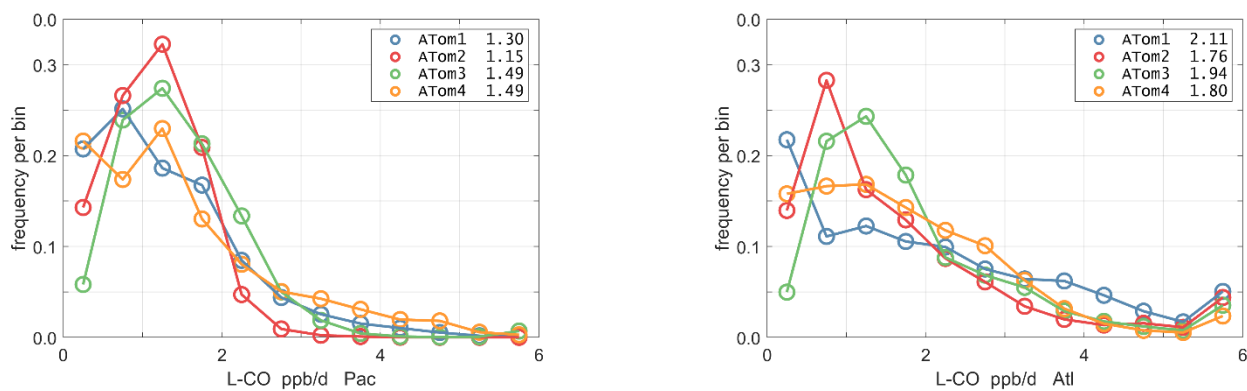


**Figure 43.** Probability Density of L-CO (ppb/day) in Pacific and Atlantic basins for Atom-1234. See Fig. 40.

460

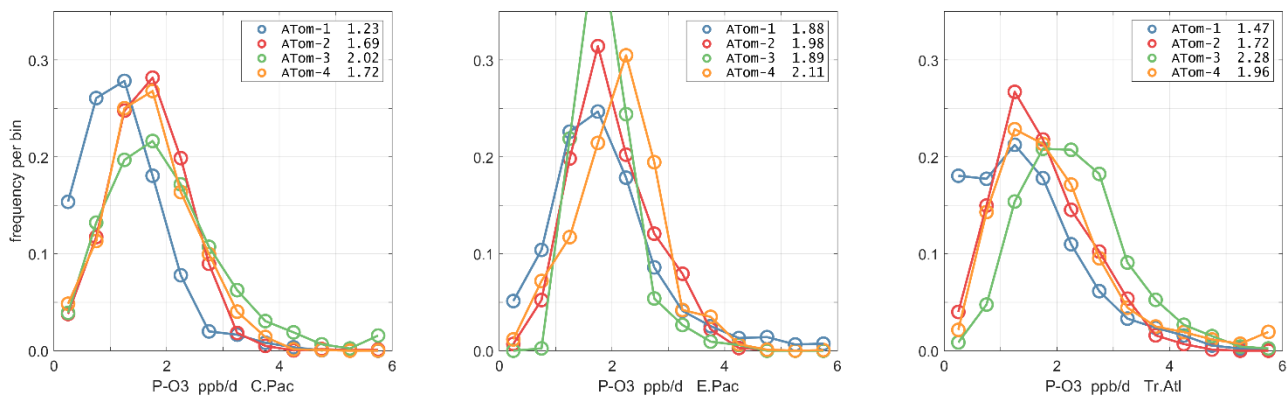


**Figure 44.** Probability Density of P-O<sub>3</sub> (ppb/day) in the 3 tropical basins (30°S-30°N) for Atom-1234. See Fig. 40.



465

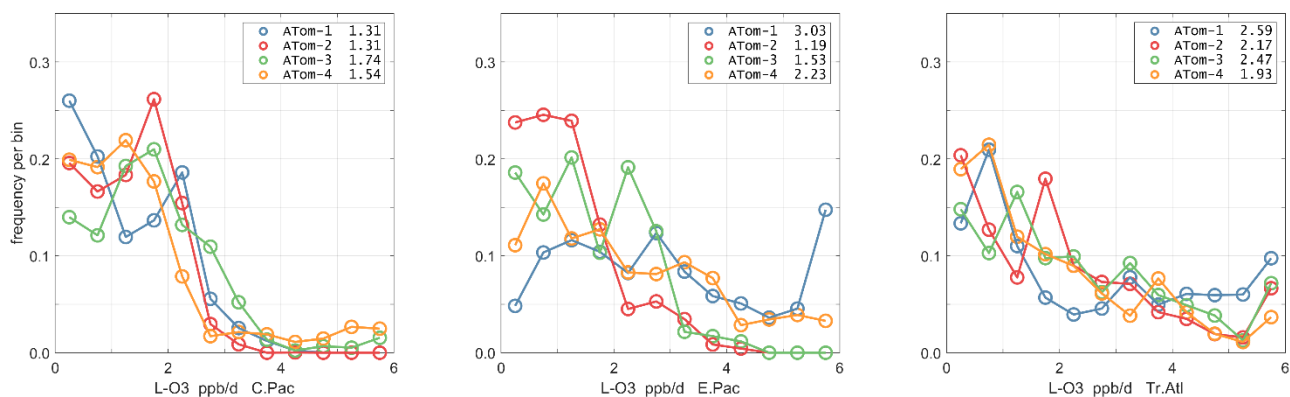


**Figure 45.** Probability Density of L-O<sub>3</sub> (ppb/day) in the 3 tropical basins for Atom-1234. See Fig. 40.

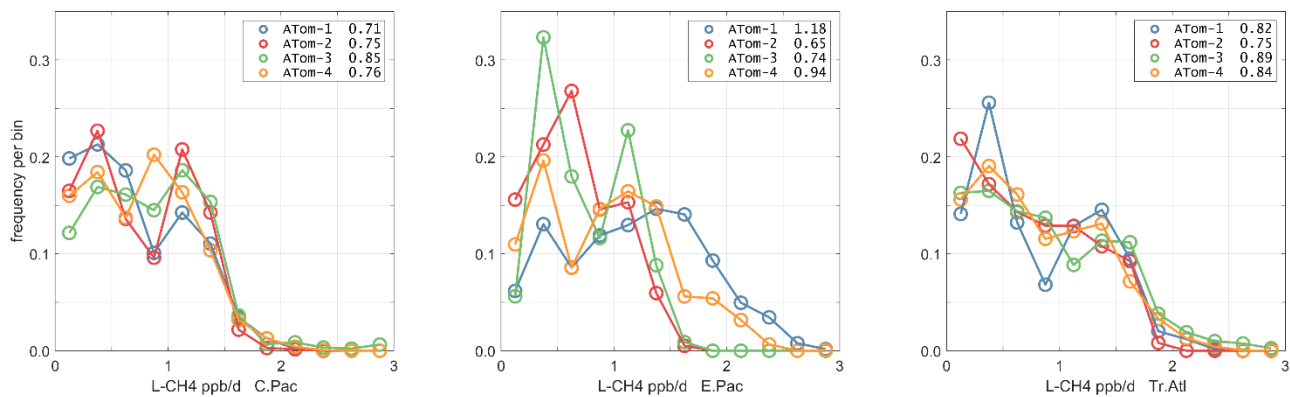


**Figure 46.** Probability Density of L-CH<sub>4</sub> (ppb/day) in the 3 tropical basins for Atom-1234. See Fig. 40.

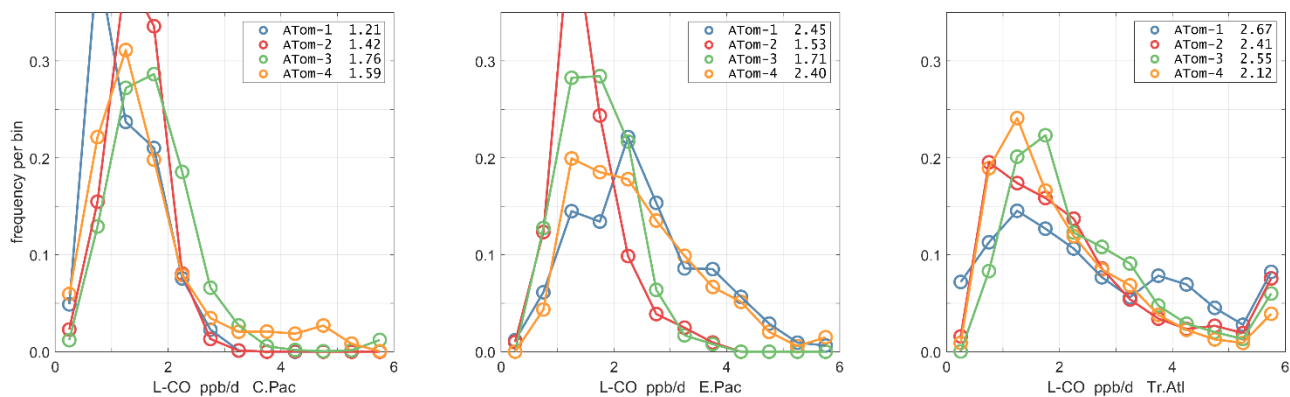


**Figure 47.** Probability Density of L-CO (ppb/day) in the 3 tropical basins for Atom-1234. See Fig. 40.



## 4 Chemical sensitivity analysis

### 4.1 First-order sensitivities

475 To identify the critical species controlling the tropospheric budgets of O<sub>3</sub> and CH<sub>4</sub>, we calculate the sensitivity of the  
weighted mean reactivity for the Pacific or Atlantic oceanic flights of ATom-1 (53°S to 60°N) with respect to the species  
measured by ATom. Sensitivity analyses are often calculated with CCMs to assess the factors controlling trends and  
variability in CH<sub>4</sub> lifetime (Holmes et al., 2013). With CCMs, the calculation includes emissions, scavenging, transport and  
chemistry, but here using ATom observations we are limited to a 24-hour snapshot with only chemical evolution of the  
480 parcels. We believe this limitation does not affect our goal of estimating the errors in the modeled budgets caused by errors  
in the modeled values of the critical species.

The sensitivity  $S$  of reactivity  $R$  to species  $X$  is calculated from the fractional change in  $R$  per fractional change in  $X$   
(dimensionless, e.g., % per %). We use  $\Delta = 10\%$ .

$$S \equiv d\{\ln(R)\} / d\{\ln(X)\} = \ln(R[X(1+\Delta)] / R[X]) / \ln(1+\Delta) \quad (1)$$

485 Results from 20 variables (19 chemical species plus T) for the four reactivities over the Pacific and Atlantic basins for  
ATom-1 are given in Table 2. The mean sensitivities are calculated using basin-wide averages and have only been  
calculated using one day's cloud fields (day 223), instead of the 5 days of different cloud fields (e.g., days 213, 218, 223,  
228, 233) used for the reactivities in Section 3. Basin-mean differences between two separated days (day 213 and 223) due  
to cloud fields and ozone column are evaluated and found to be small: <1 % of the value of  $S$ , or smaller than 0.002 in  
490 absolute. Thus evaluating  $S$  with one day is adequate.

Individual parcels show highly variable individual  $S$  values, see examples in Fig. 48. The scatter is particularly large  
because we have included all ATom-1 parcels, including continental data and very low sun angles. For comparison, the  
basin-mean values (large blue and red dots) are also plotted. Differences across basins and deployments are modest (not  
shown) and the Pacific-Atlantic comparison for ATom-1 covers this range, remembering that ATom-1 Pacific has unusually  
495 low P-O<sub>3</sub> values. Surprisingly, the initial value of many species has negligible or small impact on the reactivities. Species  
like alkanes and alkenes are unimportant because their average abundances are low over the oceans; and species like HCHO  
and HNO<sub>4</sub>, because their abundances are reset by the chemistry during the 24-hour integration.

The lessons from Table 2 are quite interesting. (i) T, H<sub>2</sub>O (Q) and O<sub>3</sub> are absolutely critical for all the chemical budgets; (ii)  
NO<sub>x</sub> is critical for P-O<sub>3</sub>, but less so for L-CH<sub>4</sub> and L-CO, and even less so for L-O<sub>3</sub>; (iii) CO as expected controls OH and  
500 L-CH<sub>4</sub>; (iv) CH<sub>4</sub> is like CO, but plays a bigger role in P-O<sub>3</sub> through HO<sub>x</sub> production via HCHO; (v) HOOH plays a modest  
role ( $S \sim 0.06$ ) in OH and thus L-CH<sub>4</sub> and L-CO; (vi) CH<sub>3</sub>OOH plays a surprisingly large role in P-O<sub>3</sub> because of the  
additional HO<sub>x</sub> release through HCHO; yet (vii) the initial HCHO plays a small role in P-O<sub>3</sub> because it is reset quickly by  
the chemistry in response to the other species listed here. PAN and HNO<sub>3</sub> contribute noticeably to P-O<sub>3</sub> through their slow  
decomposition to NO<sub>x</sub>. Acetaldehyde (CH<sub>3</sub>CHO) stands out in reducing P-O<sub>3</sub>, L-CH<sub>4</sub>, and L-CO, presumably from NO<sub>x</sub> to  
505 PAN conversion, with  $S$  ranging from -0.05 to -0.09.





One of the most interesting features of Table 2 is the impact of O<sub>3</sub> on it net P-O3 minus L-O3. With O<sub>3</sub> increases, the sum of reactions going into L-O3 increases almost linearly, while the P-O3 reactions decrease. Thus, the net sum decreases faster than linearly. The implications of this for the lifetime of O<sub>3</sub> perturbations is discussed with chemical feedbacks in Section 6.

**Table 2.** Sensitivities ( $S = d\ln[R]/d\ln[X]$ , dimensionless) for ATom-1

dln	Pacific				Atlantic			
	P-O3	L-O3	L-CH4	L-CO	P-O3	L-O3	L-CH4	L-CO
/dlnT/(10)	<b>0.715</b>	<b>0.292</b>	<b>0.753</b>	<b>0.775</b>	<b>0.628</b>	<b>0.279</b>	<b>0.751</b>	<b>0.771</b>
/dlnQ	<b>0.072</b>	<b>0.612</b>	<b>0.473</b>	<b>0.440</b>	<b>0.084</b>	<b>0.590</b>	<b>0.498</b>	<b>0.476</b>
/dlnO3	<b>-0.304</b>	<b>0.978</b>	<b>0.442</b>	<b>0.390</b>	<b>-0.407</b>	<b>1.007</b>	<b>0.483</b>	<b>0.444</b>
/dlnNOx	<b>0.734</b>	<b>0.055</b>	<b>0.188</b>	<b>0.209</b>	<b>0.724</b>	0.044	<b>0.156</b>	<b>0.172</b>
/dlnCO	0.017	0.009	<b>-0.337</b>	<b>0.637</b>	<b>0.060</b>	0.016	<b>-0.403</b>	<b>0.571</b>
/dlnCH4	<b>0.184</b>	-0.031	<b>0.764</b>	<b>-0.209</b>	<b>0.196</b>	-0.038	<b>0.799</b>	<b>-0.176</b>
/dlnHOOH	0.028	0.029	<b>0.066</b>	<b>0.072</b>	0.037	0.032	<b>0.062</b>	<b>0.063</b>
/dlnMeOOH	<b>0.085</b>	0.016	-0.047	-0.034	<b>0.076</b>	0.010	-0.041	-0.033
/dlnEtOOH	-0.006	-0.001	-0.008	-0.007	-0.008	-0.001	-0.007	-0.006
/dlnHCHO	0.019	0.013	-0.001	0.004	0.034	0.017	0.005	0.008
/dlnPAN	<b>0.066</b>	0.006	0.014	0.017	<b>0.062</b>	0.005	0.013	0.013
/dlnHNO3	<b>0.083</b>	0.008	0.019	0.019	<b>0.109</b>	0.008	0.021	0.024
/dlnHNO4	0.029	0.001	0.004	0.012	0.038	0.001	0.005	0.011
/dlnC2H6	0.000	-0.001	-0.003	-0.003	0.000	-0.001	-0.004	-0.004
/dlnAlkane	0.000	0.000	-0.001	-0.001	0.000	0.000	-0.001	-0.001
/dlnAlkene	0.000	0.000	0.000	0.000	-0.001	0.000	-0.001	-0.001
/dlnIsoprn	0.000	0.000	0.000	0.000	0.000	0.000	0.000	0.000
/dlnAcetone	-0.019	0.000	-0.009	-0.009	-0.026	-0.001	-0.011	-0.009
/dlnAcetAld	<b>-0.055</b>	-0.007	<b>-0.053</b>	-0.048	<b>-0.086</b>	-0.010	-0.045	-0.041
/dlnMeNO3	0.007	0.001	0.002	0.001	0.004	0.000	0.001	0.001

510

Table Notes: Sensitivities are calculated as  $S = d\ln[R]/d\ln[X]$ , in % per % with a 10% perturbation being applied to all 10 s parcels. Q is H<sub>2</sub>O and was perturbed 10% like all the chemical species. T is an exception with a 1% perturbation being used, and thus  $d\ln[R]/d\ln[T]$  should be multiplied by 10 to get % per %. Sensitivities that would round to  $|S| > 0.1$ , are shown in bold.

515 The average sensitivity over the basin is calculated here from (a) the single basin-wide average of R. Alternative but less desirable methods would average the individual parcel S values weighted by (b) frequency-of-occurrence and the R value or (c) just frequency of occurrence. Methods (a) and (b) are very close but not identical; while method (c) is clearly different. For any of the large S values ( $|S| > 0.1$ ), the difference between (a) and (b) are  $< 1\%$ , except for  $d\ln[P-O3]/d\ln[T]$ . As an example the (a)/(b)/(c) values in the Pacific are 0.715 / 0.694 / 0.811 for  $d\ln[P-O3]/d\ln[T]/(10)$ ; 0.764 / 0.764 / 0.796 for  $d\ln[L-CH4]/d\ln[CH4]$ ; and -0.304 / -0.305 / -0.311 for  $d\ln[P-O3]/d\ln[O3]$ .

520

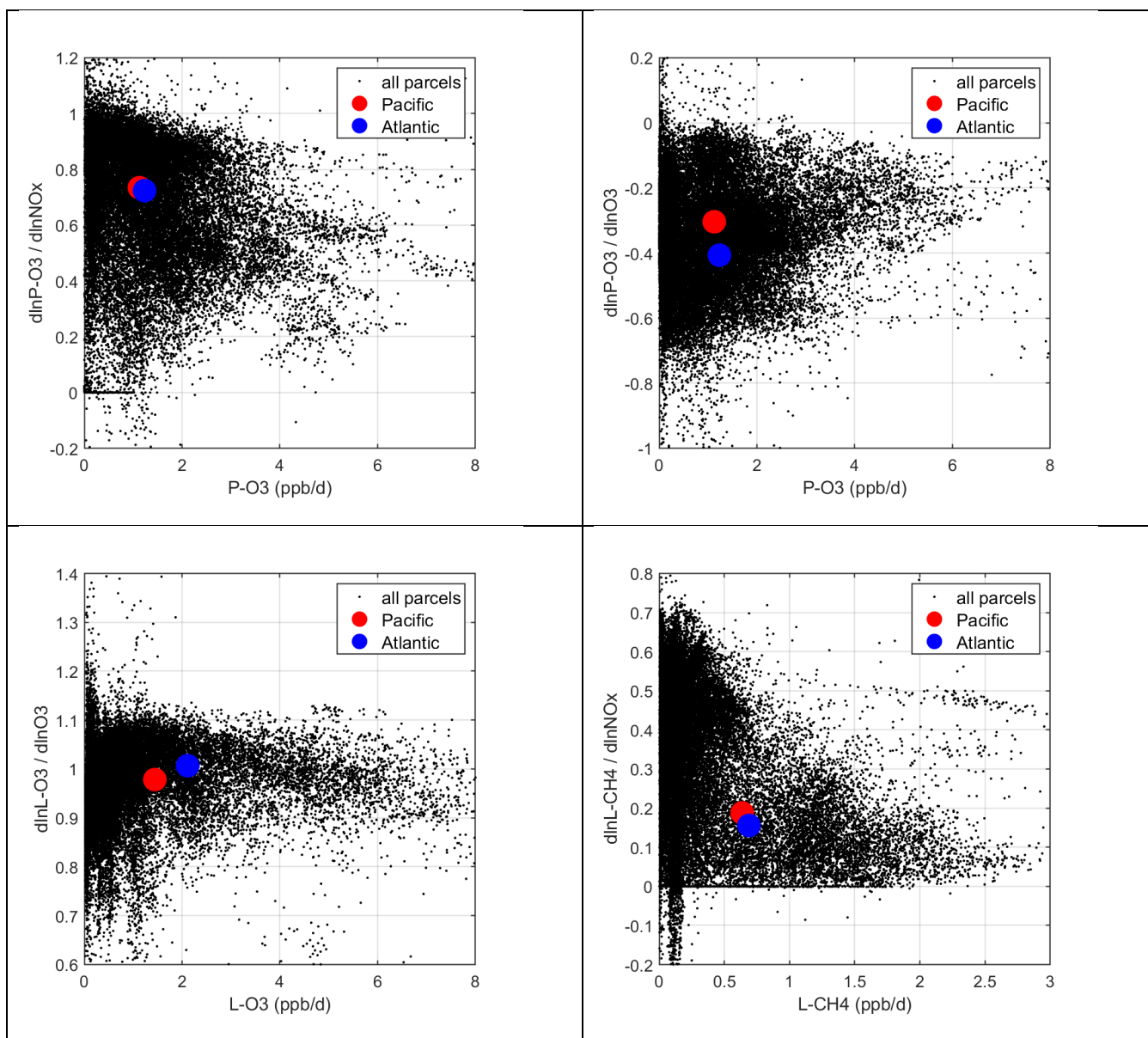


**Figure 48.** Sensitivity (% per %) plotted against reactivity (ppb/d) for ATom-1: (a)  $d\ln[P-O_3]/d\ln[NO_x]$ , (b)  $d\ln[P-O_3]/d\ln[O_3]$ , (c)  $d\ln[L-O_3]/d\ln[O_3]$ , and (d)  $d\ln[L-CH_4]/d\ln[NO_x]$ . All ATom-1 parcels, including continental data, are plotted as small black dots; the basin-mean values for the Pacific, as large red dots; and the Atlantic, as large blue dots.

525



## 4.2 Second-order terms

530 Considering that most chemical reactions are of the form  $R = k(T) X Y$  or  $k(T) X^2$ , we should evaluate the 2nd-order terms in the Taylor expansion. We first tested the quadratic nature of our  $S$  values by re-calculating with  $\Delta = 20\%$ , but the results hardly changed and so we are in a linear regime. The second-order cross-species terms are potentially more interesting. We calculate these from a coupled 10% perturbation of two different variables.

$$S_{XY} \equiv S(X+10\% \& Y+10\%) - S(X+10\%) - S(Y+10\%) \quad (2)$$

535 We calculated these cross terms only for  $X = O_3, NO_x, CO, CH_4, Q$  and  $T$ , using ATom-1 only as in Table 2. Table 3 shows the deviations from linearity ( $S_{XY}$ ) for each of the 15  $XY$ -pair combinations, listing the Pacific basin in the upper triangular part of the matrix, and the Atlantic basin in the lower triangular part. The diagonals simply give the mean first-order  $S_X$  values for Pacific plus Atlantic. These off-diagonal  $S_{XY}$  terms are clearly second-order in importance for the chemistry: e.g., the importance of the  $S_{XY}$  term in  $d^2 \ln(L-CO) / d \ln(O_3) d \ln(Q)$  for the Pacific is given as +0.017, which is a small fraction of the 1st order terms of +0.42 for  $d \ln(L-CO) / d \ln(O_3)$  and +0.46 for  $d \ln(L-CO) / d \ln(Q)$ . The near symmetry of the four matrices in Table 3 indicate that average  $S_{XY}$  sensitivities are similar for both basins. Hence we find no evidence that  
540 coupled perturbations must be considered when modelers explore the factors driving changes in the lifetime of  $CH_4$  (e.g., Holmes et al., 2013).

Although we have long known that  $H_2O$  and  $T$  are important factors (e.g., Table 2 of Holmes et al., 2013), these quantities have often been relegated to the physical climate system and not often thought of a major source of model error in the chemical system. Thus, when we are diagnosing the future tropospheric  $O_3$  or  $CH_4$  from the multi-model comparisons  
545 (Stevenson et al., 2013; Voulgarakis et al., 2013; Young et al., 2018; Griffiths et al., 2021), we need to document biases in  $T$  and  $H_2O$ . For example, from Thornhill et al., (2021a) we estimate an increase in  $CH_4$  loss frequency of about 4.5 %/K for the two consistent models. (The two other models in the Thornhill study each seem aberrant in their own way.) From Table 4, a +1 K change increases  $L-CH_4$  by 2.5%, and the Clausius-Clapeyron inferred 7% increase in  $Q$  adds 3.4% for a total of 5.9 %/K, a reasonable first-order result considering that other climate driven changes, such as  $O_3$ , are not included. For  
550 model evaluation, comparing  $T$  with mean profiles is straightforward, but  $H_2O$  is more difficult, even with profiles, because of the three orders of magnitude change over the troposphere. Thus, we recommend that relative humidity over liquid water (RHw, %) be used to detect bias. See statistics on critical species and RHw in the next section.



**Table 3.** Second-order cross-term sensitivities  $S_{XY}$  calculated as  $S(+dX+dY) - S(+dX) - S(+dY)$  for Pacific (upper triangular) and Atlantic (lower triangular) basins in ATom-1

<b>P-O3</b>						
	dO3	dNOx	dCO	dCH4	dQ	dT
dO3	<b>-0.36</b>	0.000	-0.001	0.004	0.004	0.003
dNOx	-0.005	<b>0.73</b>	0.004	0.001	-0.003	-0.016
dCO	-0.005	0.003	<b>0.04</b>	-0.005	0.000	0.002
dCH4	0.003	-0.001	-0.014	<b>0.19</b>	0.002	0.002
dQ	0.002	-0.006	-0.002	-0.005	<b>0.08</b>	0.004
dT	0.001	-0.023	-0.001	0.003	0.000	<b>0.67</b>
<b>L-O3</b>						
	dO3	dNOx	dCO	dCH4	dQ	dT
dO3	<b>0.99</b>	-0.004	0.001	-0.003	0.000	-0.002
dNOx	-0.003	<b>0.05</b>	-0.001	0.001	-0.002	0.002
dCO	0.001	-0.001	<b>0.01</b>	0.001	-0.001	0.000
dCH4	-0.003	0.001	0.000	<b>-0.03</b>	0.001	-0.001
dQ	0.000	-0.002	-0.002	0.001	<b>0.60</b>	-0.004
dT	-0.001	0.001	0.001	-0.001	-0.003	<b>0.29</b>
<b>L-CH4</b>						
	dO3	dNOx	dCO	dCH4	dQ	dT
dO3	<b>0.46</b>	-0.014	0.003	-0.002	0.016	-0.009
dNOx	-0.015	<b>0.17</b>	0.001	0.001	-0.008	0.003
dCO	0.002	0.001	<b>-0.37</b>	0.008	0.000	0.011
dCH4	-0.003	0.001	0.007	<b>0.78</b>	-0.002	-0.010
dQ	0.014	-0.008	-0.001	-0.003	<b>0.49</b>	-0.005
dT	-0.008	0.000	0.011	-0.008	-0.006	<b>0.75</b>
<b>L-CO</b>						
	dO3	dNOx	dCO	dCH4	dQ	dT
dO3	<b>0.42</b>	-0.015	0.004	-0.003	0.017	-0.009
dNOx	-0.016	<b>0.19</b>	0.001	0.002	-0.008	0.003
dCO	0.003	0.001	<b>-0.40</b>	0.008	0.001	0.011
dCH4	-0.004	0.001	0.006	<b>0.81</b>	-0.003	-0.009
dQ	0.015	-0.008	-0.001	-0.003	<b>0.46</b>	-0.005
dT	-0.009	0.000	0.011	-0.008	-0.006	<b>0.77</b>

555 Table Notes: T is temperature and was perturbed only 1%; Q is H<sub>2</sub>O and was perturbed 10% like all the chemical species. The diagonal elements are the average (Pacific and Atlantic) 1<sup>st</sup> order sensitivities  $S(+dX)$ , see Table 2. The upper triangular (Pacific) and lower triangular (Atlantic) matrices show the 2<sup>nd</sup> order sensitivities  $S_{XY} = S(+dX+dY) - S(+dX) - S(+dY)$ .



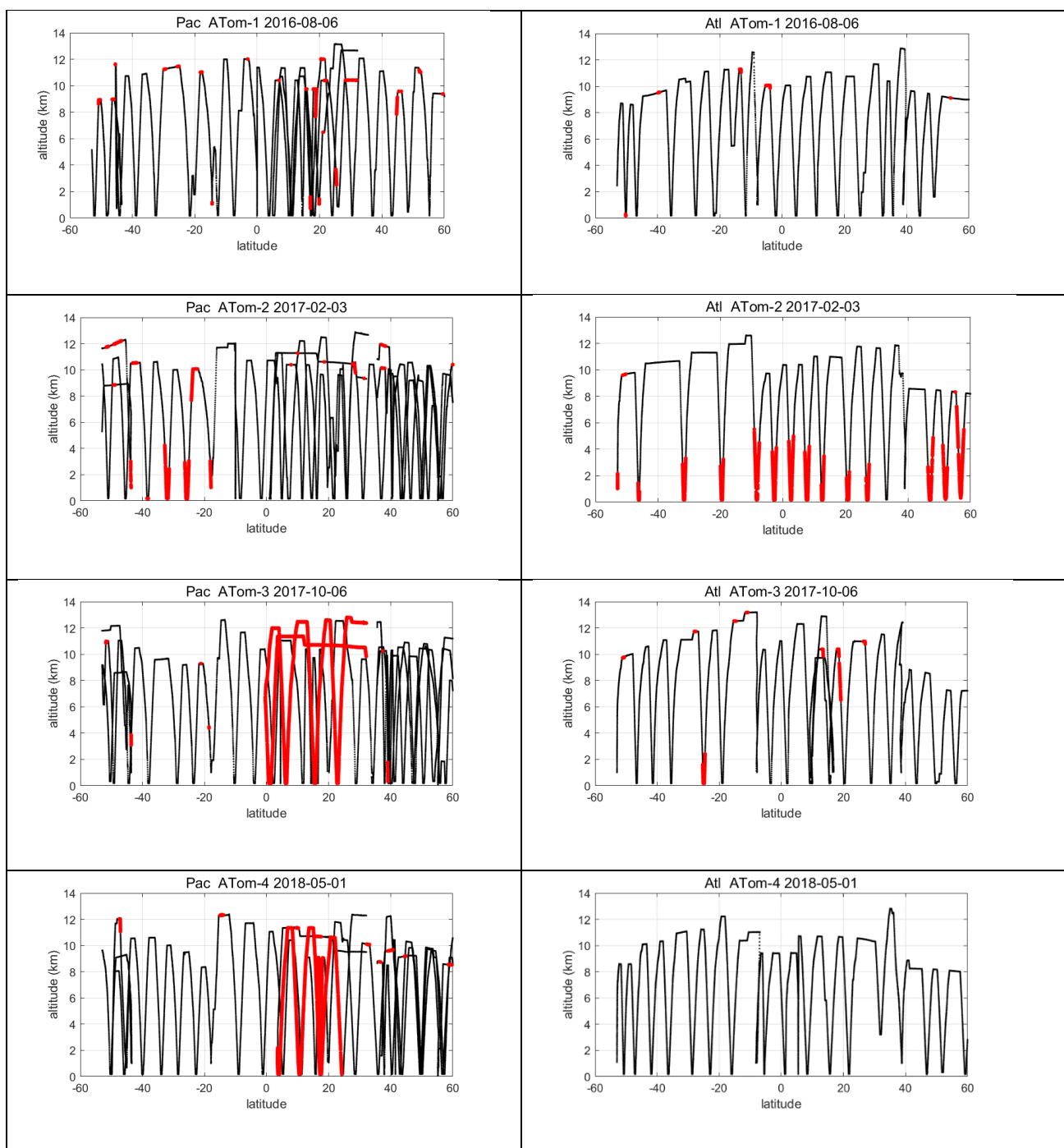
## 560 5 Key ATom species and NOx version 3

### 5.1 NOx version 3 and MDS flags

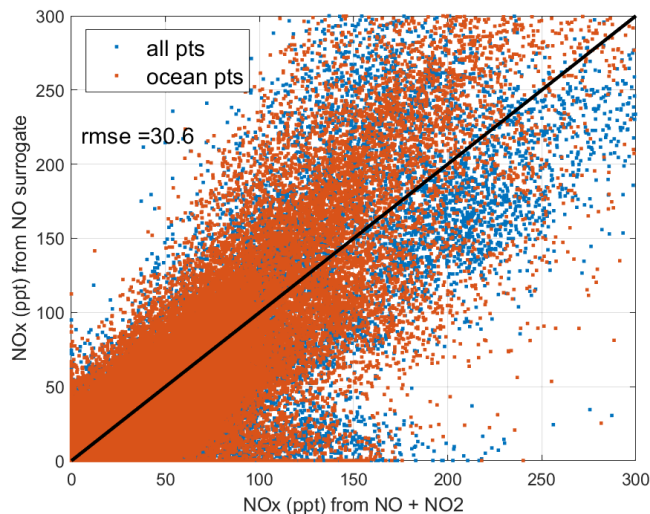
When completing this paper's analysis of the reactivities (Section 3) and re-examining the problems with NOx (NO<sub>2</sub> + NO) profiling that led to MDS version 2b (described in G2023), we re-examined the NOx long-gap interpolation. There were long stretches of these gaps (flag=4), as well as missing flight data (flag=5), that resulted in critical flight segments being filled with mean profile data. These gaps are caused by the lack of NO<sub>2</sub> rather than NO measurements as shown in Fig. 49 (4 ATom deployments x 2 ocean basins). The number of profiles with NO data but no NO<sub>2</sub> data (red dots) is extensive and covers some key regions (e.g., the lower troposphere in the Atlantic in ATom-2; the E. Pacific in ATom-34). Thus, we developed a secondary measurement of NOx (flag=2) based on the measured value of NO.

We look for a linear relationship between NOx and NO, i.e., [NOx<sup>fit</sup>] = A [NO], and use the Pacific and Atlantic Ocean basins to avoid continental pollution. Adding a multiplier of [O<sub>3</sub>] the right-hand side did not improve the fit. The ratio A does not depend noticeably on altitude. A linear fit of A minimizing the errors, NOx<sup>fit</sup> - NOx, for oceanic NOx values < 250 ppt gives A = 2.055. The unweighted mean value of NOx is 50 ppt; the one-sigma range of errors (16<sup>th</sup>-84<sup>th</sup> %) is ±22 ppt; and the rmse is 31 ppt. Figure 50 shows the oceanic NOx<sup>fit</sup> points (red) as well as all others (blue) plotted against NOx. The new 8400 NOx<sup>fit</sup> parcels are labeled with flag=2 and eliminate most of the long-gap parcels and all of the missing-flight parcels. The G2023 Table S4 percentage of flags = 0-1-2-3-4-5 for NOx changes from 0.8 - 80.8 - 0.0 - 8.3 - 7.6 - 2.5 % to 0.8 - 80.8 - 5.7 - 8.7 - 4.0 - 0.0 %. This new NOx<sup>fit</sup> is named 'NOxadd' in version 3 of the MDS (ATom\_MDS3.nc). In this paper the figures with the new version 3 NOx<sup>fit</sup> is labeled NOxx.

Caution should be taken when using the MDS data for observational statistics because of the gap filling needed to calculate the RDS. MDS data flagged with a 1 or 2 are reliable because they are based on primary or secondary instrument observations. Short-gap interpolation (flag =3) has been tested (G2023) and found to be reasonably accurate. Further, adding a short-gap, linearly interpolated flight segment (< 1 km in altitude) will have little effect on species statistics here because of the parcel weighting that is used to achieve equal sampling with altitude and latitude. Flags 4-5-6 are more worrisome as these long-gap or missing-flight methods cannot be evaluated for accuracy. In MDS v3, the chemical species with >10 % of parcels with flags 4-5-6 are HNO<sub>4</sub>, CH<sub>3</sub>OOH, C<sub>2</sub>H<sub>6</sub>, alkanes, C<sub>2</sub>H<sub>4</sub>, alkenes, C<sub>2</sub>H<sub>2</sub>, all alkyl nitrates, and SF<sub>6</sub>. Fortunately, the only one of these species that has a significant impact on the RDS (|S| ~ 0.1) is CH<sub>3</sub>OOH.



590 **Figure 49.** ATom-1234 profiling in Pacific and Atlantic basins showing parcels (large red dots) where  $\text{NO}_2$  observations are missing, where long-gap interpolation was used in MDS version 2b, and where shifting to  $\text{NO}_x^{\text{fit}}$  based on  $\text{NO}$  observations in MDS version 3 results in a change in  $\text{NO}_x$  of  $>1$  ppt.



595

**Figure 50.** Scatter plot of NO<sub>x</sub> using NO as a surrogate ( $\text{NO}_x = 2.055 \times \text{NO}$ , y-axis) and directly measured NO<sub>x</sub> (x-axis) for all ATom parcels where NO<sub>2</sub> is measured. The red points are all ocean basin parcels; and the blue points are all others. The 1:1 black line is for reference.

600

## 5.2 Updated version 3 reactivities

We did not have the resources to repeat all the calculations (5-day averages, sensitivities) with version 3 NO<sub>x</sub>, and so choose to redo all reactivity calculations with just the first day in each deployment (i.e., days 32, 121, 213, and 274). Comparisons of reactivities must then be done with the same single-day calculation with version 2b. Given the range in reactivities for ATom-1 Pacific and Atlantic, we also did not redo the sensitivities for MDS-3. Table 4 provides a summary of the changes in Pacific and Atlantic basin-mean and -median reactivities for ATom-1234 calculated using only the first day. Almost all the changes from v2b to v3 are negative. P-O3 has, as expected, the largest changes for ATom-3 Pacific and ATom-2 Atlantic. Here the median decrease (-13% and -16%, respectively) is twice as large as the mean, implying a large shift in the mid-level values of P-O3. The remaining changes in the mean reactivities are small, 0 to -3 %.

610 Vertical profiles of the four mean reactivities are shown in Figures 51-54, with separate panels for Pacific and Atlantic basins and ATom-1234 shown in each panel. The solid colored lines are calculated for one day with v3 NO<sub>x</sub><sup>fit</sup>; and the dashed colored lines, for v2b NO<sub>x</sub>. For P-O3, the difference is visible at different altitudes for ATom-234, but the profile shape is clearly changed for ATom-3 Pacific 10-12 km and ATom-2 Atlantic 0-2 km. Remembering that only NO<sub>x</sub> changes here with v3 and that P-O3 has highest sensitivity to NO<sub>x</sub>, we expect the other reactivities (L-O3, L-CH<sub>4</sub>, L-CO) to change little. That is the case except for L-CH<sub>4</sub> and L-CO for ATom-2 Atlantic 0-2 km.

620 The probability densities (PDs) for the reactivities in each ocean base are shown in the 8 panels of Figure 55. The weighted mean reactivities (ppb/d) in each basin are given for ATom-1234 in the figure legend with the v2b value followed by the v3 value. The PDs and mean values here are for one day only and thus differ slightly from the five-day averages analyzed in Section 3. Similar to the profiles, the PDs show detectable but insignificant changes from v2b to v3 and remain robust (i.e., compare with Fig. 40-43). For the most part, the mean reactivities change by < 0.01 ppb/d, with major exceptions for P-O3



in Pacific ATom-34 and Atlantic ATom-23, where the v3 value is 0.03 to 0.10 ppb/d smaller than the v2b value. The L-CO also shows some decreases with v3 of about 0.03 ppb/d (Pacific ATom-3, Atlantic ATom-2), and in a relative sense (~2%) this might be true for L-CH4, but it is not apparent with the precision shown given that L-CH4 is 2-3 times smaller than L-CO.

**Table 4.** Reactivity change (%) from MDS v2b to v3

625

	ATom1	ATom2	ATom3	ATom4	ATom1	ATom2	ATom3	ATom4
	Pacific mean				Pacific median			
P-O3	-1%	-1%	-6%	-3%	0%	-2%	-13%	-4%
L-O3	0%	0%	-1%	0%	0%	0%	-1%	0%
L-CH4	0%	0%	-2%	-2%	0%	2%	0%	0%
L-CO	0%	0%	-3%	-1%	0%	-2%	-4%	-1%
	Atlantic mean				Atlantic median			
P-O3	-1%	-8%	-2%	0%	0%	-16%	-2%	0%
L-O3	0%	-1%	-1%	0%	0%	-3%	0%	0%
L-CH4	0%	-2%	-1%	0%	0%	0%	0%	0%
L-CO	0%	-2%	-1%	0%	0%	-3%	-1%	0%

640

Table notes: Unweighted mean of all parcels. Calculated for day 1 only, not averaged over 5 separate days.

645





650

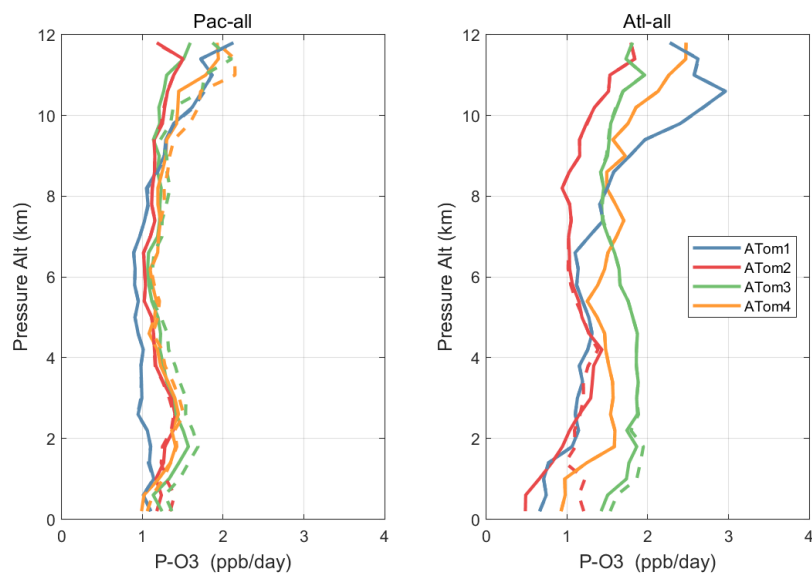
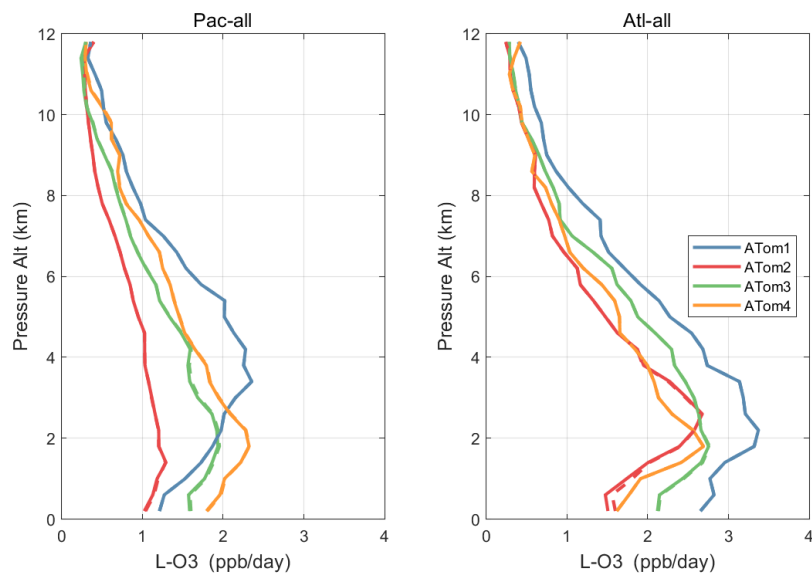


**Figure 51.** Altitude profiles of mean P-O3 (ppb/d) over Pacific and Atlantic basin for ATom-1234. Results are for one day only in each deployment (days 32, 121, 213, 274). Compare with Fig. 29. The solid lines are for version 3 NO<sub>x</sub> and the dashed for version 2b.



655

**Figure 52.** Altitude profiles of mean L-O3 (ppb/d) over Pacific and Atlantic basin for ATom-1234. See Fig. 51. Compare with Fig. 30. Solid lines are MDS-3, and dashed lines are MDS-2b.

660

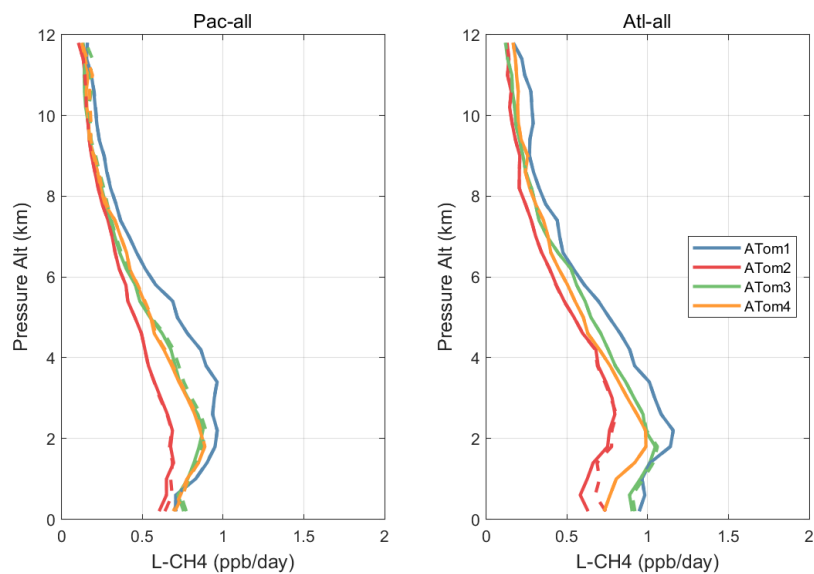


**Figure 53.** Altitude profiles of mean L-CH<sub>4</sub> (ppb/d) over Pacific and Atlantic basin for ATom-1234. See Fig. 51. Compare with Fig. 31. Solid lines are MDS-3, and dashed lines are MDS-2b.

665

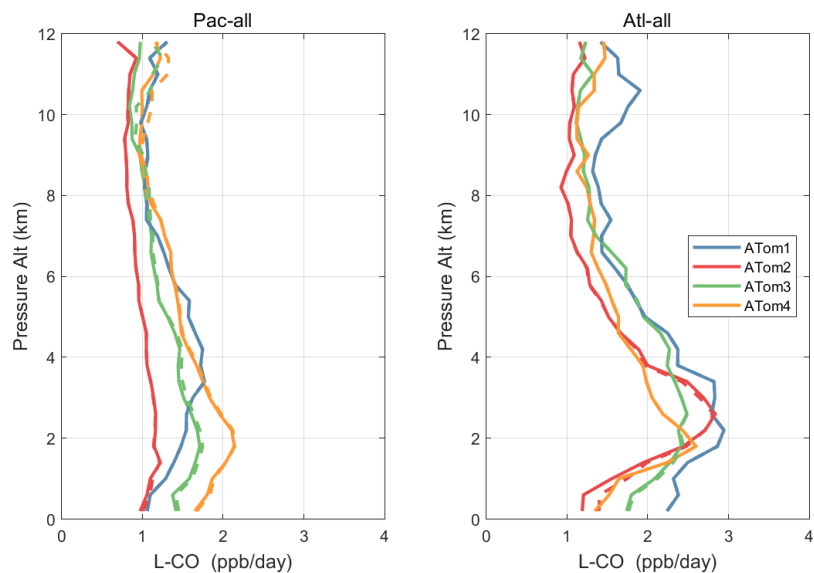
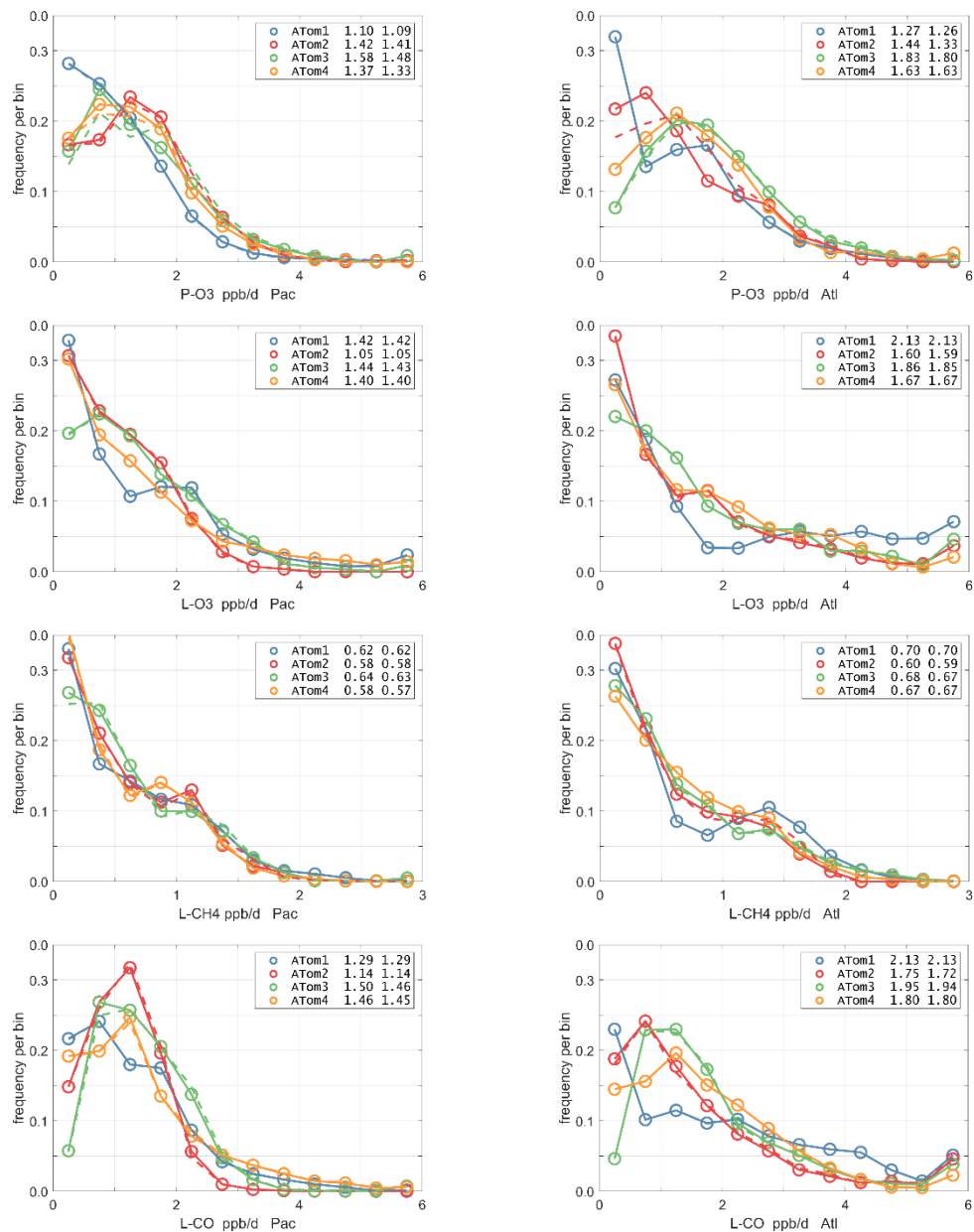


**Figure 54.** Altitude profiles of mean L-CO (ppb/d) over Pacific and Atlantic basin for ATom-1234. See Fig. 51. Compare with Fig. 32. Solid lines are MDS-3, and dashed lines are MDS-2b.



670



675

**Figure 55.** Probability Density of the 4 reactivities (P-O3, L-O3, L-CH4, L-CO, all in ppb/day) in (left) Pacific and (right) Atlantic basins (53°S-60°N). All 4 ATom deployments are shown in each panel. Only the first day of each deployment is shown (hence these are not identical to Figures 40-43). Values in the legend are the basin-wide averages for each deployment, given as v2b (dashed lines) and then v3 (solid lines). See Figure 40.

680



### 5.3 Distribution of key ATom species

We examine the distribution of key species over the Pacific and Atlantic ocean basins with mean profiles of NO<sub>x</sub> (v2b), NO<sub>x</sub><sup>fit</sup> (v3), and HOOH in Fig. 56. In the Pacific, the impact of v3 NO<sub>x</sub> (labeled NO<sub>xx</sub>) is to reduce some high values in ATom-34 and make ATom-234 almost identical in the Pacific. ATom-1 NO<sub>x</sub> remains much smaller than the other deployments. In the Atlantic, the v2b-v3 changes are not obvious, except for reducing the ATom-2 values below 3 km to look more like ATom-1. HOOH profiles often show a peak (500-1000 ppt) in the lower troposphere, 1-5 km, with the Atlantic usually being larger. For Pacific ATom-1, NO<sub>x</sub> (and P-O3) is particularly low, but HOOH (and L-O3) is particularly high.

Given the importance of the tropics, we replot these profiles of NO<sub>x</sub>(v2b), NO<sub>x</sub><sup>fit</sup>(v3), and HOOH for the three tropical regions in Fig. 57. The C. Pacific is not much affected by the v2b-v3 update, but the E. Pacific and T. Atlantic noticeably change. For Pacific HOOH, we find the 1-5 km peak is mostly in the E. Pacific, and thus relate high levels of HOOH and related HO<sub>x</sub> activity with outflow from continents.

The 2D curtain files for the Pacific and Atlantic basins show the level of heterogeneity in NO<sub>x</sub> for ATom-1234 in Fig. 58-59. These two figures compare NO<sub>x</sub>(v2b) with NO<sub>x</sub>(v3) in the Pacific and Atlantic, respectively. The biggest changes v2b to v3 in the Pacific occur for ATom-34 and are due to the E. Pacific flights as noted earlier. In these plots the E. Pacific profiles overlap with the C. Pacific profiles, and so some heterogeneity in this region is caused by longitudinally distant, not-along-flight parcels. Similarly, for ATom-234, the N. Pacific curtain plots here includes two separate flights: one in the E. Pacific from Palmdale to Anchorage and, a few days later, one in the C. Pacific from Anchorage to Kona. Overall, the NO<sub>x</sub> shows that high values (> 100 ppt) consistently but sporadically occur at the uppermost flight levels. These high-NO<sub>x</sub> parcels are probably due to lightning from deep convection, predominantly over continents, and they are the cause of high P-O3 values in the 10-12 km region of most ATom flights.

Figure 60 shows HOOH for both basins (8 panels). Unlike NO<sub>x</sub>, the HOOH patterns show extensive regions, 30° in latitude or wider, mostly tropical, with abundances >1000 ppt between 1 and 6 km. This pattern is expected with a large, somewhat homogeneous chemical source of HOOH that partly follows the sun with each ATom deployments. We often find high-NO<sub>x</sub> regions are separated from the high-HOOH ones. An unusual block of mid-tropospheric air was sampled in the southern Pacific (30°S-15°S) during ATom-3 (Figure 58). This air mass had uniformly high NO<sub>x</sub> values (60-100+ ppt), not typical of convective high-altitude NO<sub>x</sub>. These NO<sub>x</sub> values were directly measured and not affected by the v2b-v3 shift. The anti-correlation with HOOH (Figure 60) is surprising: high levels of HOOH surround the separate high-NO<sub>x</sub> air mass. Given the overall importance of high-NO<sub>x</sub> and (separately) high-HOOH regions to the chemical budgets, it would be valuable to check the CTM/CCM modeling of this feature to understand its cause.

Figures 61-64 show the probability densities (PDs) of CO (ppb), O<sub>3</sub> (ppb), relative humidity over water (RH<sub>w</sub>, %), and NO<sub>x</sub> (log(ppt)) for the tropical ocean regions (C. Pacific, E. Pacific, T. Atlantic). The PDs are calculated for lower troposphere (0-6 km) and the full ATom-sampled troposphere (0-12 km). For the first three quantities, the legend for each deployment lists the mean value, standard deviation, and skewness; while for NO<sub>x</sub> whose PD is uses log([NO<sub>x</sub>]), the legend lists just the mean value (ppt) and the mean log value (converted back to ppt).

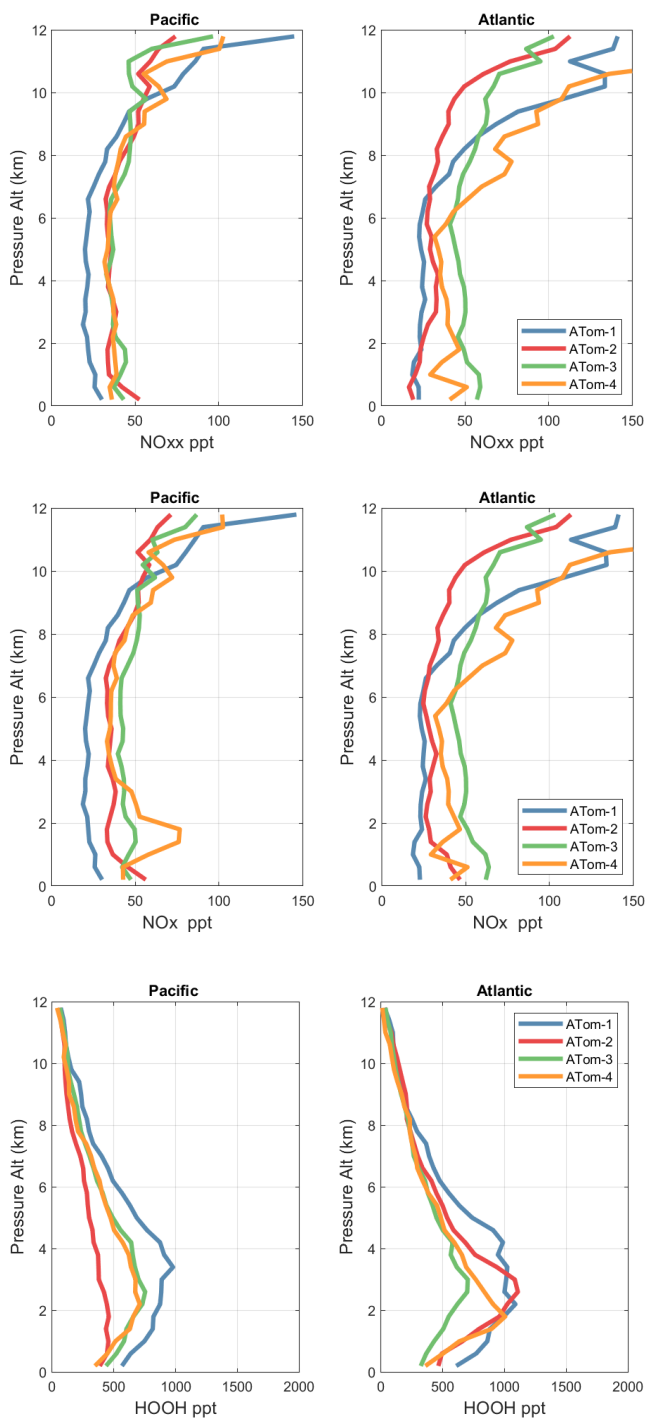
G2023 in their Figure 4 compared the ATom-1 PDs for NO<sub>x</sub>, HCHO, and HOOH with 6 CTM/CCM climatologies for August, and showed some clearly divergent model results. We believe these ATom PDs provide a valuable model metric



720 and can be used to track down model errors. Here we compare the ATom-1234 PDs for CO, O<sub>3</sub>, RHw, and NO<sub>x</sub> because  
these are critical species based on the sensitivities (Table 2). The NO<sub>x</sub> PDs are paired with v3 versus v2b panels; they show  
large shifts in the E. Pacific as expected from earlier comparisons. The T. Atlantic NO<sub>x</sub> PDs also show large shifts with  
version. Thus, the NO<sub>x</sub> PDs should be used with caution, although the C. Pacific PDs look similar across the four  
725 deployments and should provide a robust statistic on the NO<sub>x</sub> distributions in the 0-12 km altitude range. For CO, O<sub>3</sub>, and  
RHw, we find that the C. Pacific and T. Atlantic PDs are stable across deployments and should present an excellent  
observational climatology metric for the models. The E. Pacific PDs vary greatly with deployment and do not represent a  
stable climatology.

The RHw PDs are quite different from the chemical species. RHw has a bimodal distribution for the tropical regions with a  
narrow peak probability below 10% RHw and a broad maximum about 80% RHw. Thus, RHw clearly distinguishes  
730 between two types of tropical air masses reflecting the Hadley cell: a humid, generally upwelling tropical air mass, and a  
dry descending sub-tropical air mass. As for other species and reactivities, the E. Pacific RHw is highly variable with  
deployment, showing that ATom-14 (the more reactive periods) lack dry air with RHw < 20%, consistent with the sensitivity  
to H<sub>2</sub>O and the high reactivities noted above. For convenience in model comparisons, a tabulated version of the CO, O<sub>3</sub>, and  
RHw PDs, giving values for the 5<sup>th</sup>, 20<sup>th</sup>, 50<sup>th</sup>, 80<sup>th</sup>, and 95<sup>th</sup> percentiles for each basin and deployment, are provided in Table  
735 5.

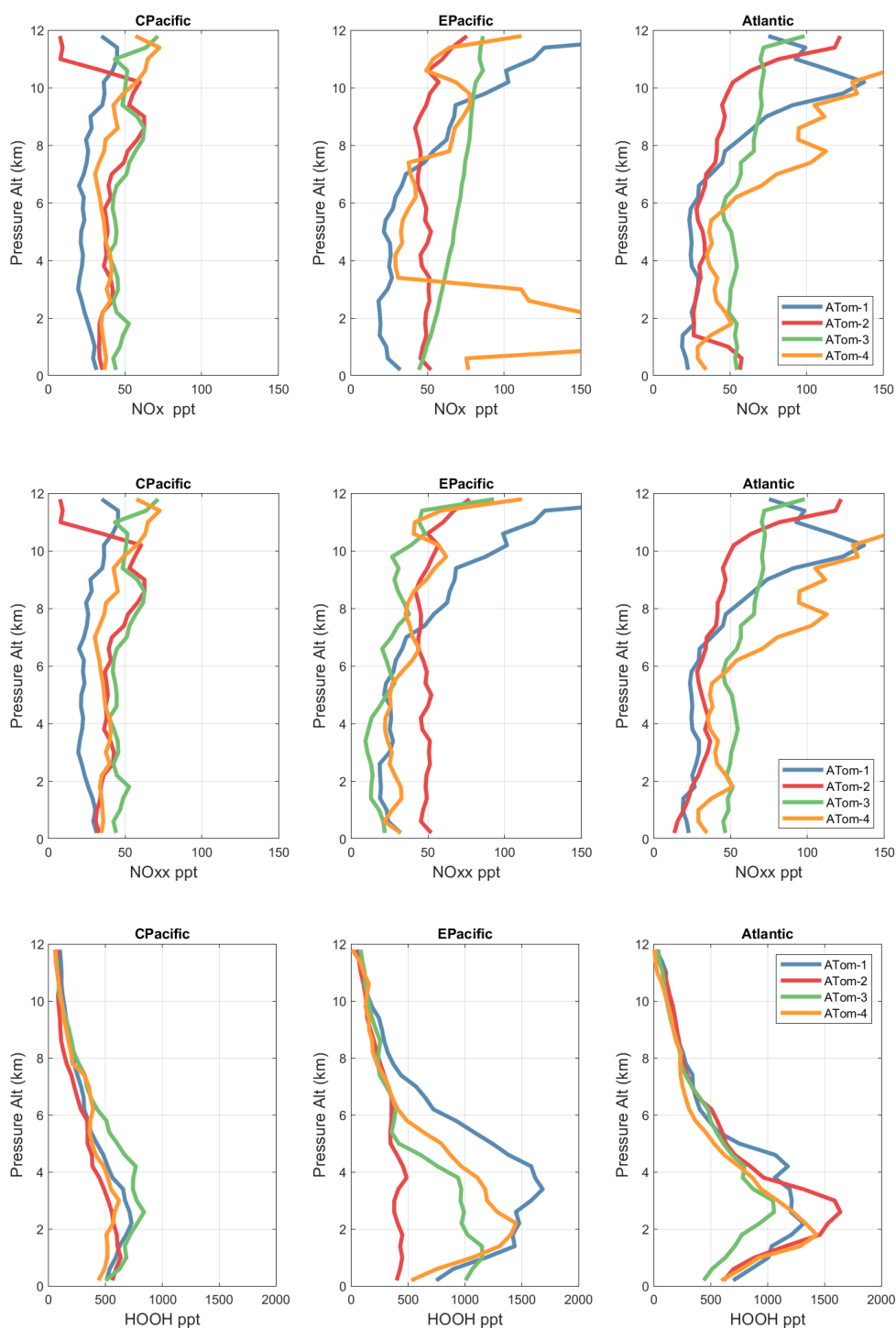
The use of two-dimensional PDs for species as a way of comparing models and measurements was investigated previously  
(P2017, P2018, and Fig. 7 of G2023). We do not pursue examples here, but recommend that these 2D PDs of critical species  
defined from the sensitivity analyses, including the fitted ellipses, be tested as model metrics.



740

745

**Figure 56.** Vertical mean profiles (ppt vs pressure altitude) of NOx (v2b), NOxx (=NOx v3) and HOOH over the Pacific and Atlantic basins. Standard weighting, see text.



750 **Figure 57.** Vertical mean profiles (ppt vs pressure altitude) of NOx (v2b), NOxx (=NOx v3), HOx (v2b) over the three tropical ocean regions (Central Pacific, Eastern Pacific, Atlantic). See Fig. 56.

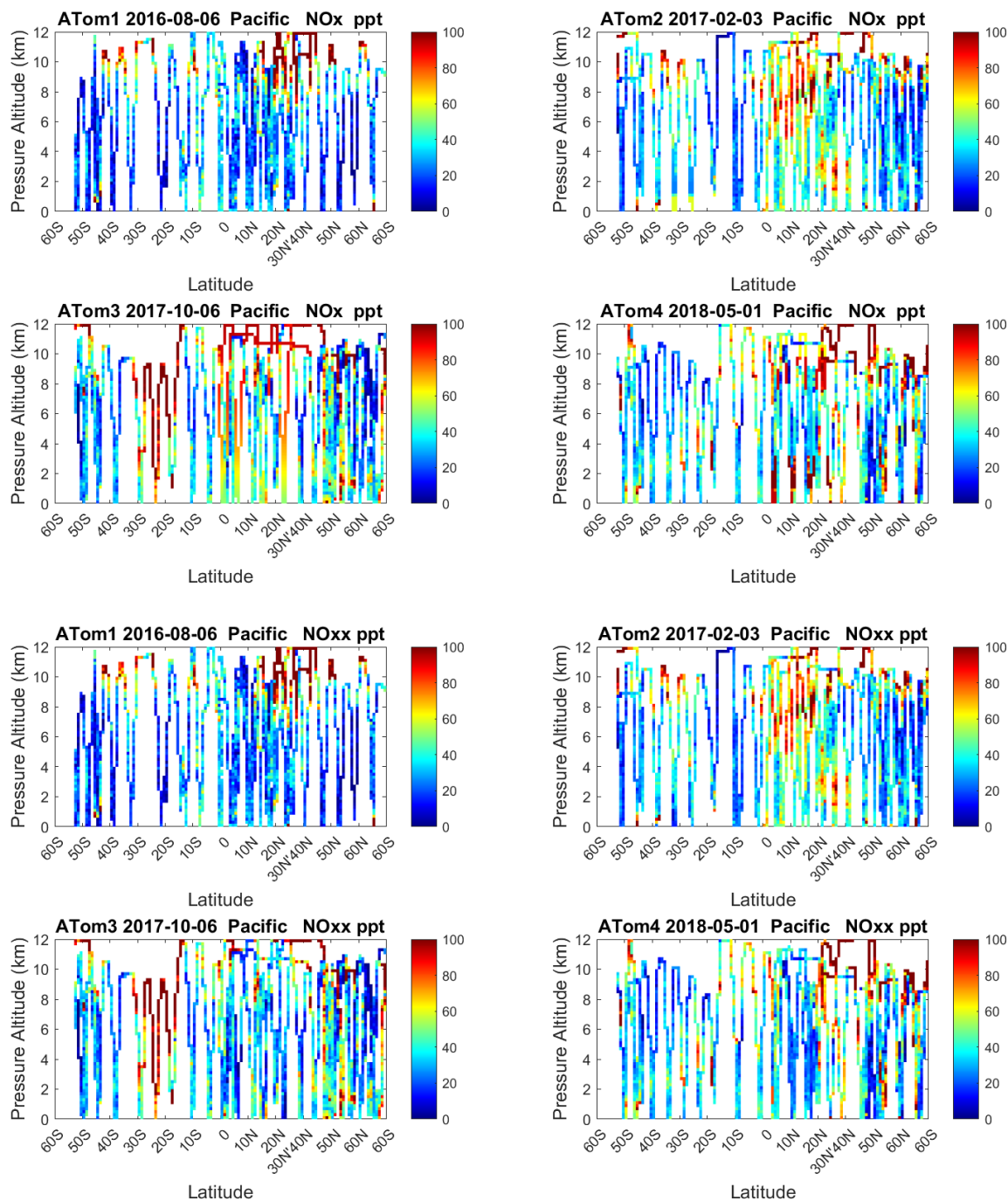
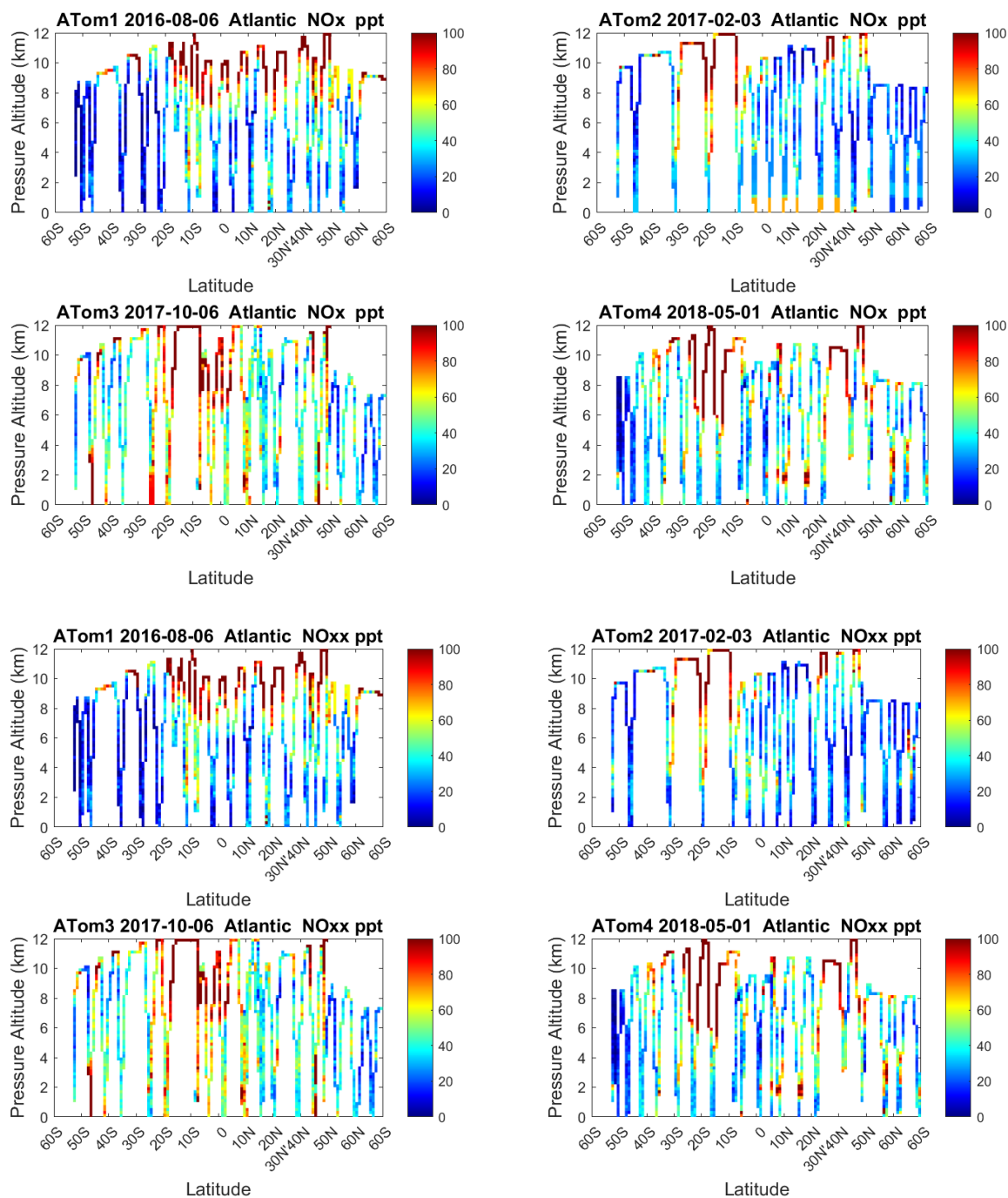
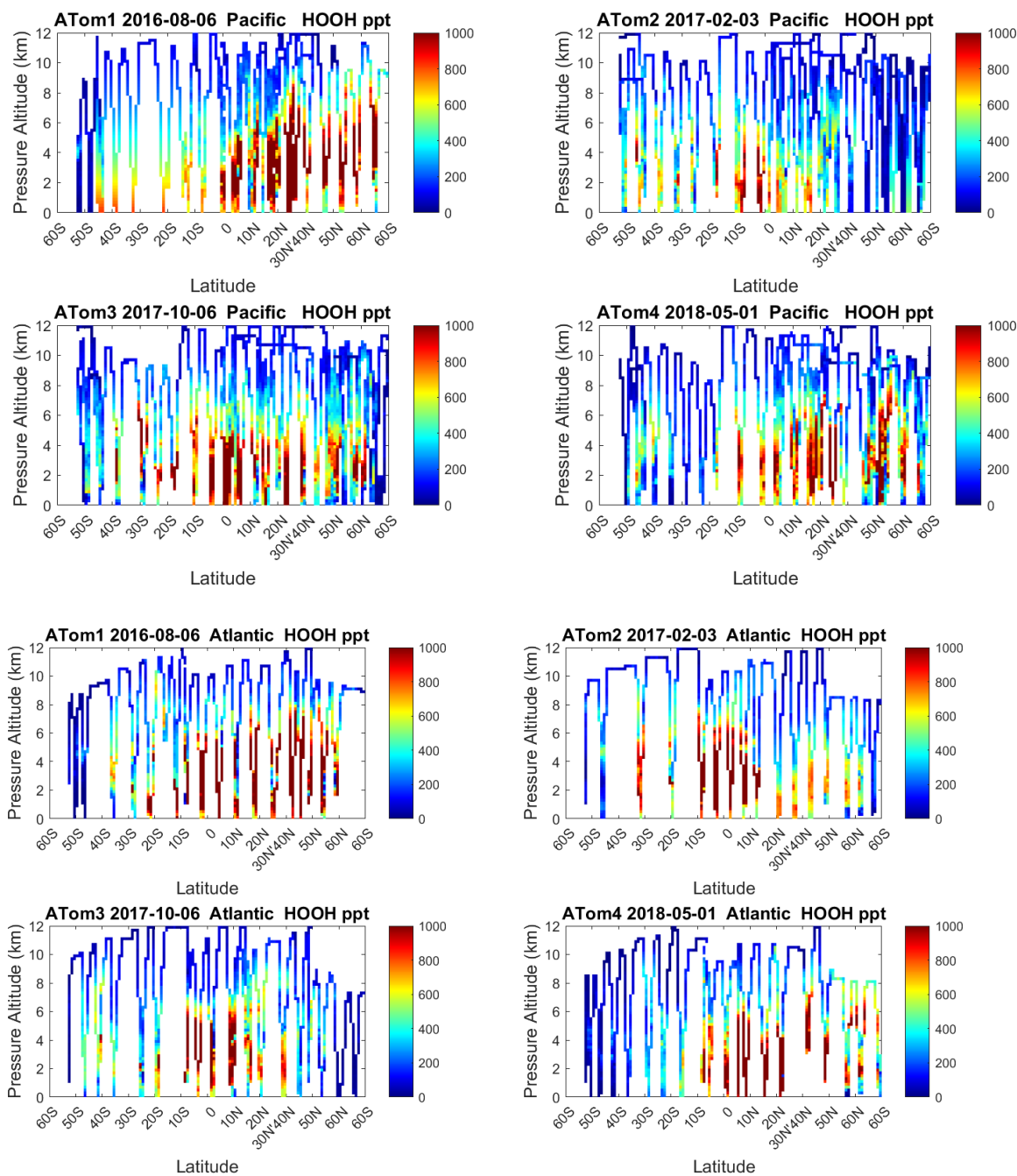


**Figure 58.** 2D Pacific curtain profiles for ATom-1234 of NO<sub>x</sub> (v2b) and NO<sub>xx</sub> (=NO<sub>x</sub> v3).



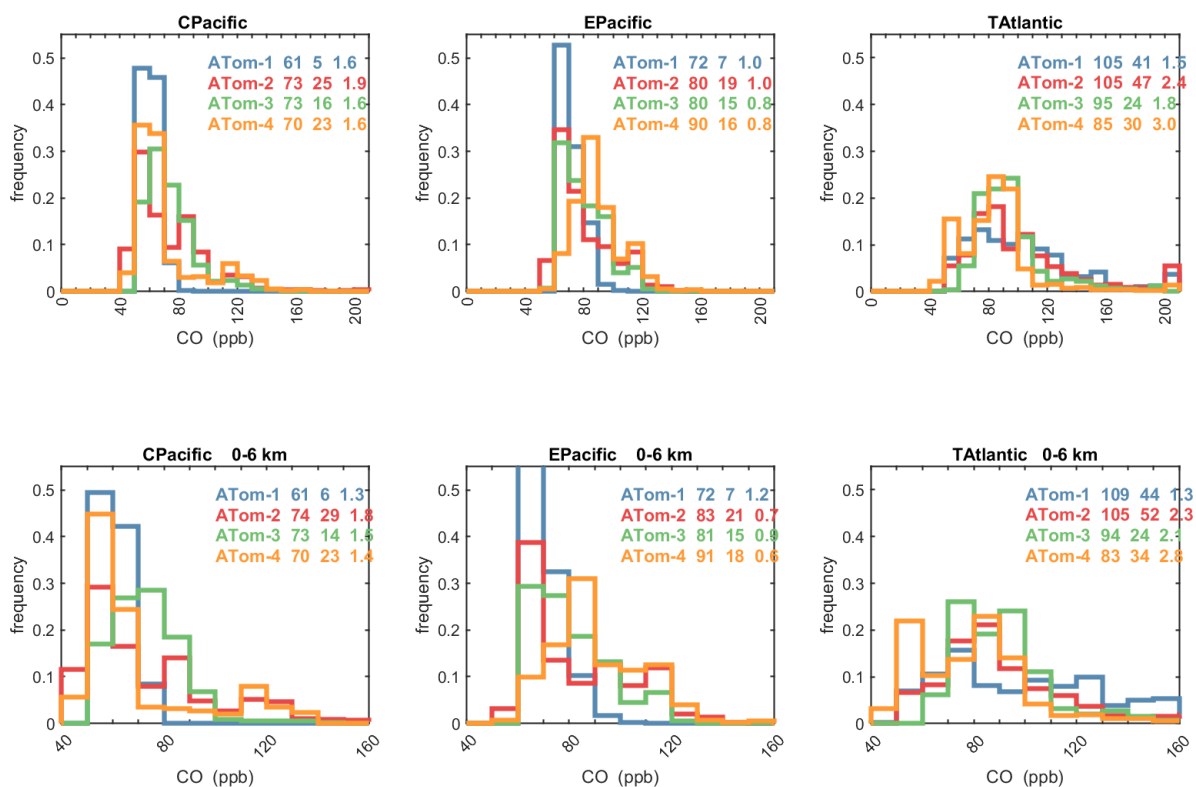


760 **Figure 59.** 2D Atlantic curtain profiles for ATom-1234 of NOx (v2b) and NOxx (=NOx v3).



765

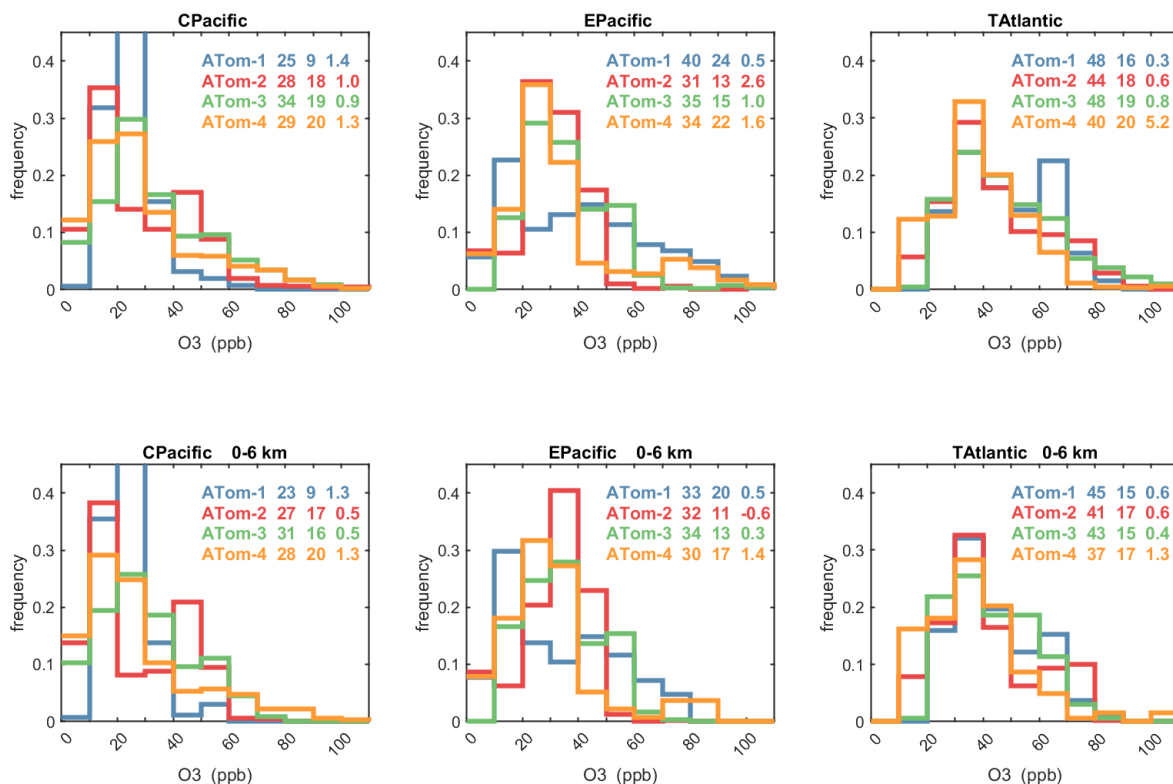
**Figure 60.** 2D Pacific and Atlantic curtain profiles for ATom-1234 of HOOH.



770

**Figure 61.** Probability Density of CO (ppb) in the 3 tropical basins (30°S-30°N) for Atom-1234. The standard weighting of ATom 10s air parcels is used. The lower panel shows 0-6 km pressure altitude where most of the chemical reactivity is located; while the upper panel shows the full troposphere, approximately 0-12 km. The color coding in the legend identifies the 4 ATom deployments. The numbers in the legend are, successively, the mean value, standard deviation, and skewness in ppb.

775



780

**Figure 62.** Probability Density of O<sub>3</sub> (ppb) in the 3 tropical basins (30°S-30°N) for Atom-1234. See Fig. 61. The numbers in the legend are, successively, the mean value, standard deviation, and skewness in ppb.

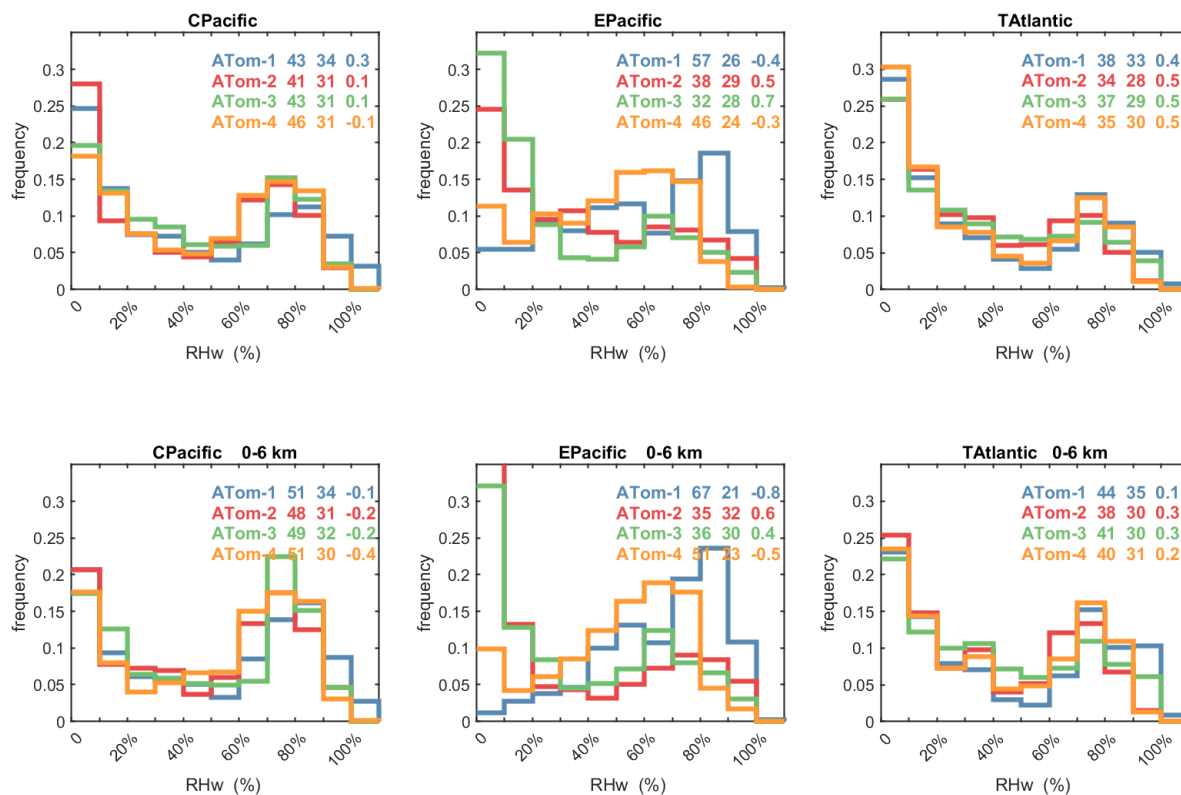


**Figure 63.** Probability Density of the relative humidity over liquid water (RHw, %) in the 3 tropical basins (30S-30N) for Atom-1234. See Fig. 61. The numbers in the legend are, successively, the mean value, standard deviation, and skewness in %.

785

790

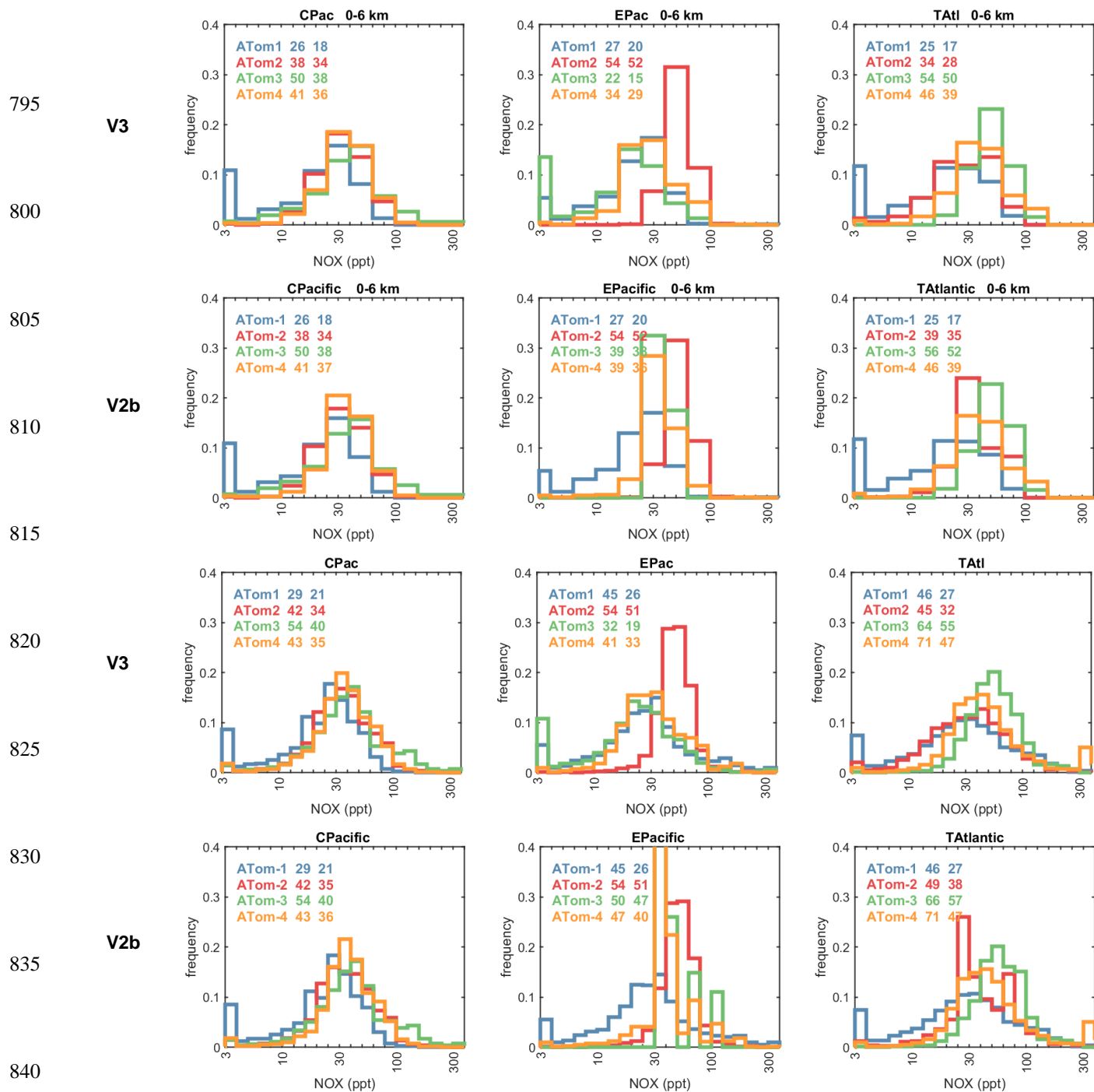


**Figure 64.** Probability Density of  $\log_{10}(\text{NO}_x, \text{ppt})$  in the 3 tropical basins ( $30^\circ\text{S}$ - $30^\circ\text{N}$ ) for Atom-1234, comparing MDS versions 3 and 2b. See Fig. 61. The numbers in the legend are, successively, the mean value of  $\text{NO}_x$  and the mean value of the  $\log_{10}(\text{NO}_x)$ , both in ppt. The 4 successive rows are: 0-6 km, MDS V3 and V2b; and 0-12 km, MDS V3 and V2b.

845



**Table 5.** Probability densities of three key quantities for the tropical oceans: (a) CO (ppb), (b) O<sub>3</sub> (ppb), (c) Relative humidity over water (%).

(a)	C.Pacific (30°S-30°N)				E.Pacific (0°-30°N)				T.Atlantic (30°S-30°N)			
	ATom1	ATom2	ATom3	ATom4	ATom1	ATom2	ATom3	ATom4	ATom1	ATom2	ATom3	ATom4
<b>CO 0-12 km (ppb)</b>												
mean	61.4	73.4	73.5	70.5	72.1	80.1	80.2	89.6	104.6	105.3	94.9	84.8
95%	72.4	122.2	108.1	125.9	85.1	118.5	111.4	119.4	187.8	202.3	145.5	127.9
80%	65.3	89.7	83.5	80.5	78.0	96.1	93.3	101.6	128.1	125.3	104.5	96.5
50%	60.2	64.5	70.3	62.7	69.7	74.5	77.3	87.5	97.9	92.7	90.8	84.4
20%	57.5	53.4	60.1	55.3	67.1	64.8	66.5	77.0	71.6	73.2	76.8	61.5
5%	54.9	48.1	57.7	50.1	63.5	58.9	63.0	67.0	57.9	56.0	69.5	51.1
<b>CO 0-6 km (ppb)</b>												
mean	61.2	74.5	73.2	69.6	71.5	82.8	81.0	91.0	108.9	104.9	94.0	83.0
95%	75.6	126.7	94.0	124.0	85.0	118.9	114.1	120.1	197.2	214.6	144.7	141.7
80%	65.1	91.7	83.4	86.2	76.6	103.1	92.4	108.7	140.3	123.1	101.4	98.4
50%	60.1	64.0	72.4	59.9	69.3	73.0	77.7	87.4	101.0	87.4	89.0	80.2
20%	56.8	52.7	60.4	53.8	66.5	64.2	66.7	76.5	72.0	70.6	75.8	55.6
5%	54.7	46.9	57.8	49.8	63.2	61.0	62.6	67.3	58.3	53.3	69.5	50.6

850

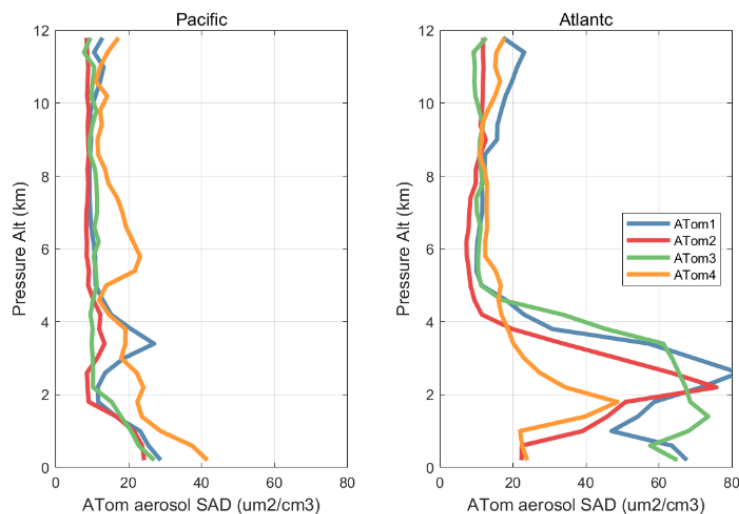
(b)	C.Pacific				E.Pacific				T.Atlantic			
	ATom1	ATom2	ATom3	ATom4	ATom1	ATom2	ATom3	ATom4	ATom1	ATom2	ATom3	ATom4
<b>O<sub>3</sub> 0-12 km (ppt)</b>												
mean	24.6	28.3	33.7	29.1	40.4	30.5	35.3	34.1	48.5	44.0	48.0	39.7
95%	41.1	57.2	73.0	71.4	84.2	46.0	58.7	81.3	73.0	77.3	84.5	64.3
80%	30.4	46.5	50.7	41.3	63.3	39.8	48.5	42.8	64.6	62.6	63.3	51.5
50%	23.2	22.5	28.7	23.9	37.5	30.1	32.7	27.6	46.7	39.8	44.2	37.5
20%	16.8	11.2	18.5	12.7	15.1	22.1	21.7	19.8	32.6	29.5	30.9	25.8
5%	13.4	8.9	7.8	6.7	9.7	7.9	14.9	8.1	26.0	17.7	23.2	15.8
<b>O<sub>3</sub> 0-6 km (ppt)</b>												
mean	23.4	26.7	30.5	27.9	33.2	31.7	33.8	29.8	44.7	40.9	43.1	37.4
95%	39.1	53.2	60.4	70.1	69.8	46.6	55.0	72.3	69.5	71.8	68.3	64.9
80%	29.1	46.8	47.3	41.3	51.0	41.6	46.0	37.2	60.4	58.1	56.9	47.8
50%	22.1	18.4	26.8	22.8	29.4	33.4	32.0	26.5	40.3	35.6	41.2	35.1
20%	15.4	10.7	16.2	11.3	12.9	23.4	21.1	16.8	30.9	28.2	29.6	21.7
5%	12.8	8.7	7.3	6.4	9.1	7.7	14.2	6.9	25.8	15.8	22.5	15.4

(c)	C.Pacific				E.Pacific				T.Atlantic			
	ATom1	ATom2	ATom3	ATom4	ATom1	ATom2	ATom3	ATom4	ATom1	ATom2	ATom3	ATom4
<b>RHw 0-12 km (%)</b>												
mean	43.4	41.5	43.1	46.2	57.0	37.6	31.7	46.3	38.1	34.5	36.9	34.6
95%	97.4	85.9	87.4	88.2	92.3	88.9	85.6	79.0	90.9	82.2	87.3	84.5
80%	81.1	74.7	77.2	77.7	82.7	68.8	64.7	68.5	76.7	66.2	69.3	72.1
50%	34.9	40.1	38.4	51.1	59.4	31.9	17.9	50.2	26.4	27.5	29.7	22.5
20%	7.6	6.0	10.1	11.0	29.6	7.8	6.8	22.1	5.7	6.1	7.7	6.3
5%	3.7	1.9	2.9	2.4	8.1	3.7	2.1	4.9	1.5	1.9	3.3	2.3
<b>RHw 0-6 km (%)</b>												
mean	50.7	47.9	48.6	50.9	66.9	34.8	36.4	50.9	44.3	37.8	40.8	40.5
95%	97.5	88.9	89.4	88.5	93.6	90.5	87.8	81.3	95.6	83.7	91.0	85.3
80%	84	78.3	79.7	79.8	84.6	72.7	68.9	73.7	80.9	71.2	74.9	74.7
50%	59.9	57.1	55.1	61.4	74.3	17.5	28.3	54.3	34.9	32.1	35.0	35.2
20%	9.2	9.2	11.1	11.1	48.0	6.2	8.2	29.8	4.8	5.3	8.8	8.4
5%	3.4	2.5	2.8	1.7	23.8	3.1	2.2	4.1	1.4	1.5	3.1	1.2



## 855 5.4 Heterogeneous Chemistry

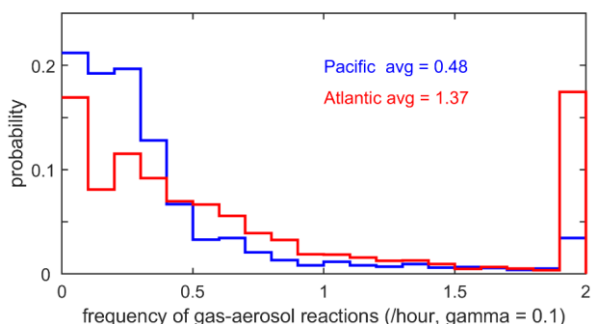
The potential role of heterogeneous (gas-aerosol) chemical reactions—which are not included in this study—is illustrated with the profiles of aerosol surface area density SAD ( $\mu\text{m}^2 \text{cm}^{-3}$ ) in Fig. 65. We calculate SAD as the sum of the four reported modes (nucleation, Aitken, accumulation, coarse) with most of the area coming from accumulation and coarse modes. In the Pacific, above the marine boundary layer, SAD is usually  $< 20 \mu\text{m}^2 \text{cm}^{-3}$ , while in the Atlantic SAD is much larger, 20-80  $\mu\text{m}^2 \text{cm}^{-3}$  everywhere below 4 km. This difference is extensive in all seasons and clearly due to low-altitude continental convection from, e.g., biomass burning. There is one example in these profiles where such convection delivers high aerosol loading near 6 km in the E. Pacific (ATom-4). We calculate the frequency distribution of reactions for all parcels in ATom-1 Pacific and Atlantic assuming a high reactivity coefficient  $\gamma = 0.10$  in Fig. 66. If we are looking for heterogeneous reactions to compete with radical chemistry rates (e.g., ROO, HO<sub>2</sub>), then we need a high  $\gamma$  and reaction frequency  $> 2$  per hour. For ATom-1 Pacific, that occurs in only 3% of the parcels, while for ATom-1 Atlantic, it is 17% of the parcels (as seen by the large SAD below 4 km). This evidence indicates that heterogeneous chemical reactions are not likely important in the reactivity statistics here, but a more thorough analysis considering the aerosol composition and realistic  $\gamma$ s is needed.



870 **Figure 65.** Vertical mean profiles of aerosol surface area density SAD ( $\mu\text{m}^2 \text{cm}^{-3}$ ), over the Pacific and Atlantic basins. Standard weighting, see text. SAD is the sum of the four reported modes (nucleation, Aitken, accumulation, coarse) with most of the area from accumulation and coarse modes.

875





880 **Figure 66.** Frequency distribution of gas-aerosol reactions (per hour) for ATom-1 Pacific (blue) and Atlantic (red) assuming a high reactivity coefficient  $\gamma = 0.10$ .

## 6. Chemical feedbacks

### 6.1 Timescale for $O_3$ perturbations

885 The sensitivities calculated for the parcels in ATom-1 allow us to estimate the timescale for an  $O_3$  perturbation. Most modeling studies make the simplistic assumption that the P-O3 and L-O3 derived from the rates defined above are the key terms in the continuity equation and, further, that P-O3 is constant while L-O3 is linear in  $[O_3]$ .

$$d[O_3]/dt = P-O3 - L-O3 = P^{\text{constant}} - [O_3]\{L-O3/[O_3]\} = P^{\text{constant}} - [O_3]/T^A \quad (3)$$

The approximate timescale,  $T^A = [O_3]/L-O3$ , is often called the  $O_3$  lifetime because the steady-state concentration is proportional to it:  $[O_3]^{\text{steady-state}} = P^{\text{constant}} T^A$ . This approximation is valid only if

890 
$$d\ln[L-O3] / d\ln[O_3] \equiv 1 \quad \text{and} \quad d\ln[P-O3] / d\ln[O_3] \equiv 0 \quad (4)$$

but instead from Table 4 we have for ATom-1 Atlantic

$$d\ln[L-O3] / d\ln[O_3] \equiv 1.01 \quad \text{and} \quad d\ln[P-O3] / d\ln[O_3] \equiv -0.41 \quad (5)$$

895 So, L-O3 is very close to linear in  $[O_3]$ , but P-O3 decreases as  $[O_3]$  increases, and thus the net P-minus-L (Eq 3) decreases faster, and an  $[O_3]$  increase decays faster than given by  $T^A$ . The true timescale  $T^T$  is given by the linearized  $O_3$  loss frequency.

$$1/T^T = d[-dO_3/dt] / d[O_3] \approx d[L-O3 - P-O3] / d[O_3] \quad (6)$$

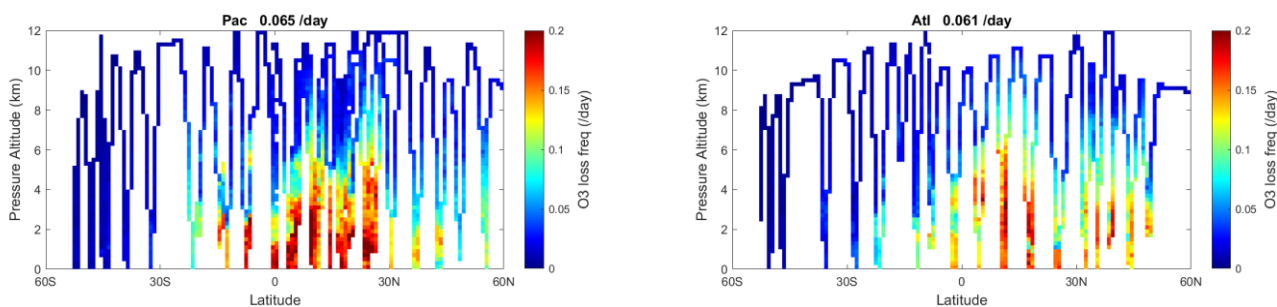
Figure 67 shows this linearized  $O_3$  loss frequency ( $1/T^T$ , units of per day) for the Pacific and Atlantic flight profiles of ATom-1. High values,  $> 0.15$  /d occur throughout the northern tropics below 5 km. In the upper troposphere, the timescale



900 for  $O_3$  is slow, 20 days or longer. Basin mean loss frequency is similar in both Pacific (0.065 /d) and Atlantic (0.061 /d) corresponding to a mean timescale  $T^T \sim 16$  days.

Profiles of the mean loss frequency, both  $1/T^T$  and  $1/T^A$ , are shown for Pacific and Atlantic basins in Fig. 68. Both basins show almost the same profiles, increasing from 0.01 /d at 12 km to  $\sim 0.1$  /d near the surface, with near constant differences,  $1/T^T - 1/T^A$ , of about +0.01 /d. Thus, the relative error in  $T^A$  decreases from 100% at 12 km to 10% at 0 km. The profiles of P-O3 and L-O3 in the basins in Fig. 68 indicate the shifting importance of the  $d[P-O_3]/d[O_3]$  term with altitude.

905 Our sensitivity calculations are made with 24-hour integrations, and over this time the HOx and NOx radicals readjust to the  $O_3$  increase, other species like HOOH partially respond, but for longer-lived key species such as CO (90 days) the adjustment is negligible. For  $O_3$ , the timescales for decay of the perturbation are 10-30 days, and thus we can ignore to first order any feedbacks on the chemistry caused by changes in CO or  $C_2H_6$  or  $CH_4$ . Other, longer-chain alkanes might readjust in 10-30 days to the new levels of  $O_3$ , but these species are not very important for the ATom oceanic flights. Thus, our 24-  
910 hour sensitivity calculations should be adequate for deriving the timescale for decay of an  $O_3$  perturbation.



915

**Figure 67.** 2D curtain plots of the linearized loss frequency for  $O_3$  ( $1/T^T$  in units of per day) for ATom-1 Pacific and Atlantic basins. The loss frequency is calculated from the sensitivity calculation  $d\ln(L-O_3 \text{ minus } P-O_3)/d\ln(O_3)$ .

920

925

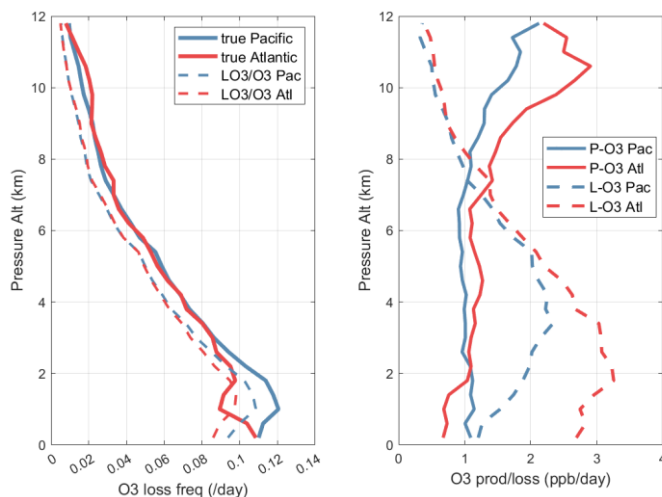


**Figure 68.** (left) O<sub>3</sub> loss frequency (/day) versus pressure altitude (km), averaged over Pacific (blue) and Atlantic (red) basins for ATom-1. True linearized loss frequency (1/T<sup>T</sup>, solid lines) is compared with the often-used approximation (1/T<sup>A</sup> = L-O<sub>3</sub>/O<sub>3</sub>, dashed lines).  
 930 (right) Altitude profiles for both ocean basins of P-O<sub>3</sub> (solid) and L-O<sub>3</sub> (dashed), both in ppb/d.

## 6.2 CH<sub>4</sub> lifetime feedback

A positive perturbation to the CH<sub>4</sub> abundance reduces tropospheric OH and thus increases the timescale of the perturbation relative to its steady-state lifetime (Prather 1994, 1996). A measure of this chemical feedback is the sensitivity, dln[L-CH<sub>4</sub>]/dln[CH<sub>4</sub>] (% per %), calculated here. These sensitivities, for all ATom-1 10 s parcels including continental data, are plotted versus L-CH<sub>4</sub> as small black dots in Fig. 69. The basin-mean values are shown for Pacific (large red dot, 0.76 % per %) and Atlantic (large blue dot, 0.80 % per %). The number we want from these calculations is the sensitivity of the OH weighted by the CH<sub>4</sub> loss (i.e., including the temperature factor in the rate coefficient, exp(-1775/T)).  
 935

$$s_{OH} = dln[L-CH_4]/dln[CH_4] - 1 \quad (7)$$

The values of  $s_{OH}$  for the ATom-1 parcels are plotted for the Pacific and Atlantic flight profiles in Fig. 70 (top panels), and the mean values are -0.24 and -0.20, respectively. The value of  $s_{OH}$  is most negative, about -0.3 in the lower troposphere, where CH<sub>4</sub> dominates the chemistry and controls much of the OH loss. The value of  $s_{OH}$  drops to below -0.1 in the upper troposphere where cold temperatures make the OH+CH<sub>4</sub> reaction very slow compared with the OH+CO reaction. The CH<sub>4</sub> feedback factor describes the increase in the timescale for a CH<sub>4</sub> perturbation relative to the OH lifetime in steady state (i.e., OH lifetime = atmospheric burden divided by loss to OH reactions).  
 945

$$ff_{CH_4} = 1 / (1 + s_{OH}) \quad (8)$$

The values of  $ff_{CH_4}$  along the flights tracks vary from about 1.2 to 1.6, see Fig. 70 (bottom panels). Averaging the two basins for  $s_{OH}$ , we calculate a mean  $ff_{CH_4} \sim 1.28$ .



This 24-hour calculation, however, does not include the adjustment to other key species that will occur in response to the  
950 decadal decay of a CH<sub>4</sub> perturbation. The correct way to model this is to run CTM/CCM perturbation+control sequences for  
several years with different CH<sub>4</sub> lower boundary conditions (e.g., Holmes, 2018). During this time other species, specifically  
CO, which is the other major sink of OH radicals, will adjust to the CH<sub>4</sub>-driven changes in OH. The CO change, an increase,  
will then further reduce OH and amplify the ff<sub>CH<sub>4</sub></sub>.

We can make a simple, first-order estimate of this CO adjustment to a 10% CH<sub>4</sub> increase. The s<sub>OH</sub> directly from the CH<sub>4</sub>  
955 change averages -0.22 (Table 2, average of Pacific & Atlantic), or -2.2% change in the loss frequency of CH<sub>4</sub>. The change in  
L-CO from the 10% CH<sub>4</sub> increase is -1.9% (Table 2, average of Pacific & Atlantic). If CO is in balance between sources and  
L-CO, then CO will increase by 1.9%. The two-basin average sensitivity of L-CH<sub>4</sub> to CO is -0.37, so the CO increase will  
decrease L-CH<sub>4</sub> by a further -0.7% to -2.9%. The updated s<sub>OH</sub>\* = -0.29, a 30% increase in magnitude, and the ff<sub>CH<sub>4</sub></sub>\* = 1.41.  
This CO amplification may be an overestimate as some of the CO source, from CH<sub>4</sub> specifically, will be reduced with OH.  
960 Another correction is that the feedback factor used to calculate the perturbation time for a CH<sub>4</sub> pulse must be derived from  
the total CH<sub>4</sub> lifetime that includes losses in the stratosphere and to soils where the loss frequencies do not respond to a CH<sub>4</sub>  
perturbation (e.g., Holmes, 2018). This full budget calculation gives a reduced s<sub>TOTAL</sub> = -0.25 and ff = 1.34, quite in line  
with recent global model results (1.30±0.07, Thornhill et al., 2021b). We do not support the use ATom-like chemical  
climatologies as a comparable result relative to the CTM/CCMs, but it does provide a measurement check point and estimate  
965 of first-order responses of tropospheric chemistry to global change.

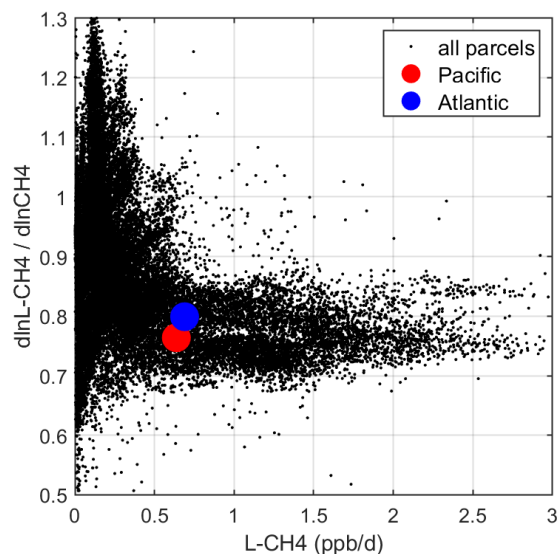
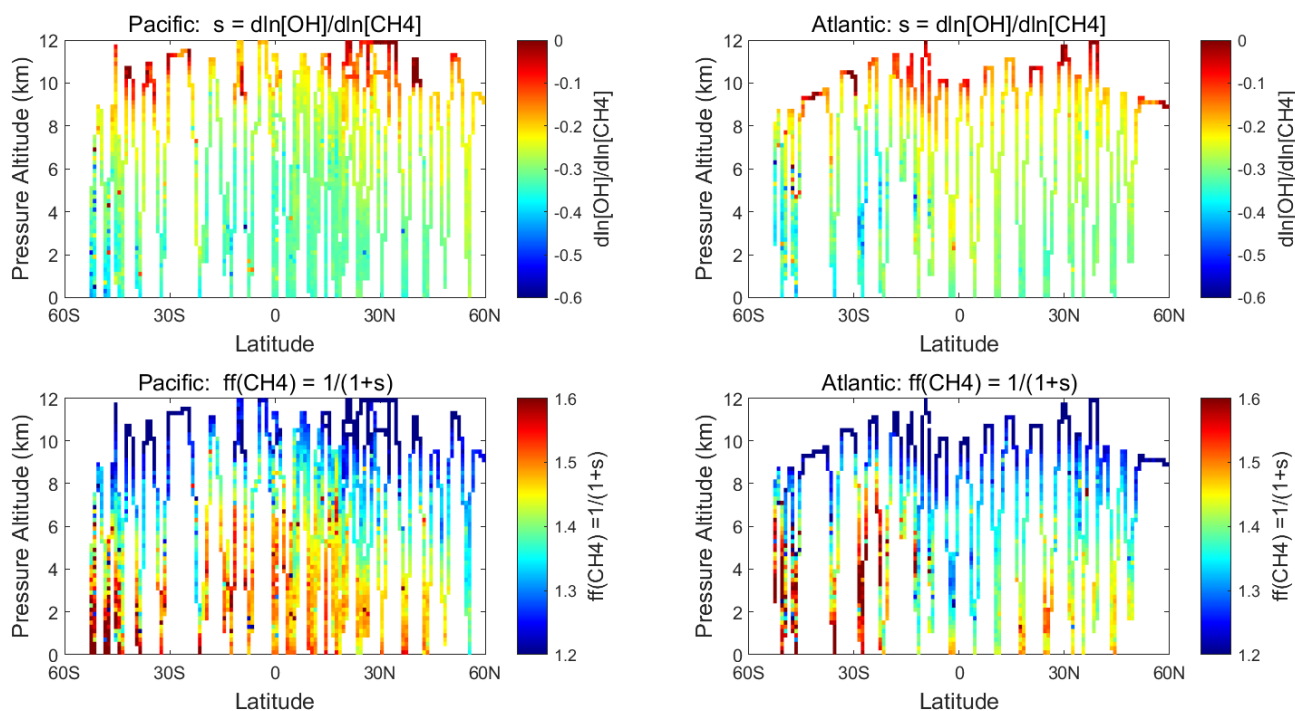


**Figure 69.** Sensitivity of CH<sub>4</sub> loss with respect to its abundance (dln[L-CH<sub>4</sub>]/dln[CH<sub>4</sub>], in % per %) versus loss rate (L-CH<sub>4</sub>, in ppb/d) for  
970 parcels in ATom-1. All ATom-1 10 s parcels, including continental data, are plotted (small black dots) as well as the basin-mean values for  
Pacific (red dot) and Atlantic (blue dot).



975 **Figure 70.** 2D curtain plots from ATom-1 of (top) the OH sensitivity to CH<sub>4</sub>,  $s_{\text{OH}} = \text{dln}[\text{OH}]/\text{dln}[\text{CH}_4] = \text{dln}[\text{L-CH}_4]/\text{dln}[\text{CH}_4] - 1$ , for Pacific and Atlantic basins, and (bottom) the CH<sub>4</sub> lifetime feedback factor,  $\text{ff}_{\text{CH}_4} = 1/(1+s_{\text{OH}})$  for the same.

## 7. Conclusions and Perspective

This manuscript completes the presentation and analysis of the ATom observations focusing on reactive, gas-phase chemistry affecting the tropospheric budgets of CH<sub>4</sub> and O<sub>3</sub>. For the four seasonal deployments of ATom-1234 (August, February, October and May, respectively), we use the profiling curtains to identify large-scale regions of the troposphere that drive the budgets, particularly in the lower troposphere for loss of O<sub>3</sub> and CH<sub>4</sub>, as well as the smaller heterogeneities, particularly in the upper troposphere for NO<sub>x</sub>-driven hot spots of O<sub>3</sub> production. These results are the first near-global views of the remote troposphere, primarily the middle of the Pacific and Atlantic Ocean basins, from the perspective of their net chemical reactivities based on observations at 200 m scales. Statistics are also accumulated for the Southern Ocean and Arctic basin, but as expected from global chemistry models, these regions contribute little to the global O<sub>3</sub> and CH<sub>4</sub> budgets.

ATom's regular profiling of the ocean basins allows for weighted averages to build probability densities for key species and reactivities. Although the individual curtain plots for each ocean transect show clear meteorological variability for each deployment, these probability densities are quite similar and provide a robust test for the modeled distribution of species and reaction rates. For example, the 30°S-30°N tropical distributions of O<sub>3</sub>, CO and relative humidity are distinct between the



990 Pacific and Atlantic (higher values of both) but similar for each deployment in each basin. On the other hand, the Eastern  
Pacific transect (0°-30°N, 121°W) is very different for each deployment. The compelling statistics built up from the ATom  
deployments are a metric that should be used to evaluate our current global chemistry models.

The Modeling Data Stream (MDS) developed for ATom (G2023 plus this publication) relies on gap-filling for sporadic  
measurements or missing data and is essential if reactivities for the 10 s air parcels are to be calculated without losing most  
995 of the parcels. The MDS concept was a reasonable and necessary step for the Reactivity Data Stream (RDS); however, as  
we have seen with the successive MDS versions, there is a painful learning curve for what to do with missing data and no  
truly optimal method yet identified. The MDS/RDS approach defined in the pre-ATom deployment papers (P2017; P2018)  
is still the best method for calculation diel-averaged rates. The ATom-method of inserting the observed chemical  
composition of 10 s parcels in global chemistry models to calculate reaction rates (RDS) remains a compromise: integrating  
1000 without sources or sinks means that NO<sub>x</sub> and alkanes decrease over 24 hours while HOOH and CH<sub>3</sub>OOH increases. We  
cannot identify a method of including these that does not also prejudice the results and that remains easy to implement in  
most global models. One improvement might be to use satellite derived photolysis rates for the day of observation (e.g.,  
Holmes, 2016) rather than just having the models pick 5 days from their own meteorology fields to average over.

The calculation of reactivities (R) with the RDS protocol allows us to step further and derive the sensitivity factors ( $S =$   
1005  $\ln(R)/\ln(X)$ ) relative to the chemical species (X). From these sensitivities, we can identify the critical species where  
model error in their atmospheric simulation will cause large errors in the budgets. This information is useful in directing  
model-measurement comparisons. From the sensitivities, we have also derived correctly linearized lifetimes and even the  
CH<sub>4</sub> chemical feedback. Admittedly these are only first-order estimates and do not include the full set of feedbacks in a  
flux-driven, free-running global chemistry model. Nevertheless, it does provide an independent estimate based primarily on  
1010 observations.

The ATom measurements can provide a substantial contribution to understanding model differences and even identifying  
model errors in global tropospheric chemistry. What is clear from this measurement-model analysis since P2017 is that most  
of the model difference is caused by models calculating different climatologies for the key species such as O<sub>3</sub>, CO, H<sub>2</sub>O,  
NO<sub>x</sub>, CH<sub>4</sub> plus T. When models use the same distribution of key species, they calculate nearly the same reactivities even  
1015 though their chemical models have a wide range of species and complexity.

There remain uncertainties in kinetic rates and cross sections, yet models tend to use the same values (e.g., Burkholder et al.,  
2020). Using fixed MDS chemical composition, the model differences are due mostly to variability in photolysis rates  
driven by clouds (Hall et al., 2018). For example, the model-model root-mean-square differences in reactivities adopting the  
same chemical composition are ~10% using the same model but different years (hence different cloud fields); they are ~20%  
1020 for different models that come close to matching one another; they reach 50% if those models use different H<sub>2</sub>O and T; and  
they exceed 100% for some models that are known to be aberrant in other diagnostics. Thus, the most important model  
metric to develop from the ATom measurements would be standard probability densities of the key species in those regions  
where reactivities are largest: the lower tropics for loss of O<sub>3</sub> and CH<sub>4</sub>, the upper tropics for production of O<sub>3</sub>. These could  
include co-variation patterns (2D probability densities, in G2023). Sensitivity analysis of the 24-hour reactivities provides  
1025 some core data that we feel should become a standard part of CCM evaluations and inter-comparisons.



1030 The other ATom information that is important to understand for tropospheric chemistry but is not readily a metric, are the unusual large-scale air masses (20° in latitude) of high reactivity that are clearly transient events, most likely of continental origin: ATom-3 south Tropical Atlantic large mass of high-NO<sub>x</sub>, high P-O<sub>3</sub> surrounded by high L-O<sub>3</sub>; ATom-14 Eastern Pacific huge air masses of very high L-O<sub>3</sub>. Overall, the ATom data set based on 10 s (2 km) air parcels, has allowed us to partially deconstruct the spatial scales and variability that defines tropospheric chemistry from composition to reactivity.

1035 **Data/Code Availability.** The full raw ATom data set is first posted short-term on the NASA ESPO ATom website (<https://espo.nasa.gov/atom/content/ATom>). The final archive for ATom data and merged data sets will be at Oak Ridge National Laboratory (ORNL), see [https://daac.ornl.gov/ATOM/guides/ATom\\_merge.html](https://daac.ornl.gov/ATOM/guides/ATom_merge.html), and Wofsy et al., 2021. The MDS and RDS data sets as well as the MATLAB codes and some intermediate data used in this analysis are posted on Dryad (<https://doi.org/10.7280/D1B12H>, see Prather et al., 2023). Earlier versions, primarily for Atom-1 based on Guo et al. (2021; 2023), are posted on Dryad (<https://doi.org/10.7280/D1Q699> and link to [https://zenodo.org/record/5905662#.ZBS1Kx\\_MIIw](https://zenodo.org/record/5905662#.ZBS1Kx_MIIw), see Guo, 2022).

**Author contribution.** MJP designed the analysis, developed the MDS, and wrote the manuscript. HG and XZ performed most of the RDS calculations. HG worked on the MDS design and co-wrote the manuscript.

1040 **Competing interests.** The authors declare that they have no conflict of interest.

**Acknowledgements.** The authors are indebted to the entire ATom Science Team including the managers, pilots and crew, who made this mission possible. We thank the instrument teams who were co-authors on the first paper (Guo et al., 2023) for this valuable data set. Primary funding of the preparation of this paper at UC Irvine was through NASA grants NNX15AG57A and 80NSSC21K1454.

## 1045 **References**

- Allen, H. M., Crouse, J. D., Kim, M. J., Teng, A. P., Ray, E. A., McKain, K., Ray E.A., Sweeney, C., and Wennberg, P.O.: H<sub>2</sub>O<sub>2</sub> and CH<sub>3</sub>OOH (MHP) in the remote atmosphere: 1. Global distribution and regional influences. *Journal of Geophysical Research: Atmospheres*, 127, e2021JD035701. <https://doi.org/10.1029/2021JD035701>, 2022.
- 1050 Anderson, D. C., B. N. Duncan, A. M. Fiore, C. B. Baublitz, M. B. Follette-Cook, J. M. Nicely, and G. M. Wolfe (2021), Spatial and temporal variability in the hydroxyl (OH) radical: understanding the role of large-scale climate features and their influence on OH through its dynamical and photochemical drivers, *Atmos Chem Phys*, 21(8), 6481-6508, 10.5194/acp-21-6481-2021, 2021.
- 1055 Brock, C. A., Froyd, K. D., Dollner, M., Williamson, C. J., Schill, G., Murphy, D. M., Wagner, N. J., Kupc, A., Jimenez, J. L., Campuzano-Jost, P., Nault, B. A., Schroder, J. C., Day, D. A., Price, D. J., Weinzierl, B., Schwarz, J. P., Katich, J. M., Wang, S. Y., Zeng, L. H., Weber, R., Dibb, J., Scheuer, E., Diskin, G. S., DiGangi, J. P., Bui, T., Dean-Day, J. M., Thompson, C. R., Peischl, J., Ryerson, T. B., Bourgeois, I., Daube, B. C., Commane, R., and Wofsy, S. C. (2021) Ambient aerosol properties in the remote atmosphere from global-scale in situ measurements, *Atmos Chem Phys*, 21(19), 15023-15063, 10.5194/acp-21-15023-2021, 2021.



- 1060 Brune, W. H., Miller, D. O., Thames, A. B., Allen, H. M., Apel, E. C., Blake, D. R., Bui, T. P., Commane, R., Crouse, J. D., Daube, B. C., Diskin, G. S., DiGangi, J. P., Elkins, J. W., Hall, S. R., Hanisco, T. F., Hannun, R. A., Hints, E. J., Hornbrook, R. S., Kim, M. J., McKain, K., Moore, F. L., Neuman, J. A., Nicely, J. M., Peischl, J., Ryerson, T. B., St Clair, J. M., Sweeney, C., Teng, A. P., Thompson, C., Ullmann, K., Veres, P. R., Wennberg, P. O., and Wolfe, G. M. (2020): Exploring Oxidation in the Remote Free Troposphere: Insights From Atmospheric Tomography (ATom), *J Geophys Res-Atmos*, 125, ARTN e2019JD031685, 10.1029/2019JD031685, 2020.
- 1065 Burkholder, J.B.; Sander, S.P.; Abbatt, J.P.D.; Barker, J.R.; Cappa, C.; Crouse, J.D.; Dibble, T.S.; Huie, R.E.; Kolb, C.E.; Kurylo, M.J.; Orkin, V.L.; Percival, C.J.; Wilmouth, D.M.; Wine, P.H. (2020) "Chemical Kinetics and Photochemical Data for Use in Atmospheric Studies, Evaluation No. 19," JPL Publication 19-5, Jet Propulsion Laboratory, Pasadena, May 2020, <http://jpldataeval.jpl.nasa.gov>, 2020.
- 1070 Griffiths, P. T., Murray, L. T., Zeng, G., Shin, Y. M., Abraham, N. L., Archibald, A. T., Deushi, M., Emmons, L. K., Galbally, I. E., Hassler, B., Horowitz, L. W., Keeble, J., Liu, J., Moeini, O., Naik, V., O'Connor, F. M., Oshima, N., Tarasick, D., Tilmes, S., Turnock, S. T., Wild, O., Young, P. J., and Zanis, P. (2021) Tropospheric ozone in CMIP6 simulations, *Atmos Chem Phys*, 21, 4187-4218, 10.5194/acp-21-4187-2021, 2021.
- Guo, Hao (2022), Heterogeneity and chemical reactivity of the remote Troposphere defined by aircraft measurements, Dryad, Dataset, <https://doi.org/10.7280/D1Q699>, 2022.
- 1075 Guo, H., Flynn, C. M., Prather, M. J., Strode, S. A., Steenrod, S. D., Emmons, L., Lacey, F., Lamarque, J.-F., Fiore, A. M., Correa, G., Murray, L. T., Wolfe, G. M., St. Clair, J. M., Kim, M., Crouse, J., Diskin, G., DiGangi, J., Daube, B. C., Commane, R., McKain, K., Peischl, J., Ryerson, T. B., Thompson, C., Hanisco, T. F., Blake, D., Blake, N. J., Apel, E. C., Hornbrook, R. S., Elkins, J. W., Hints, E. J., Moore, F. L., and Wofsy, S.: Heterogeneity and Chemical Reactivity of the Remote Troposphere defined by Aircraft Measurements, *Atmos. Chem. Phys.*, 21, 13729–13746,
- 1080 <https://doi.org/10.5194/acp-21-13729-2021>, 2021, see Guo et al., 2023.
- 1085 Guo, H., Flynn, C. M., Prather, M. J., Strode, S. A., Steenrod, S. D., Emmons, L., Lacey, F., Lamarque, J.-F., Fiore, A. M., Correa, G., Murray, L. T., Wolfe, G. M., St. Clair, J. M., Kim, M., Crouse, J., Diskin, G., DiGangi, J., Daube, B. C., Commane, R., McKain, K., Peischl, J., Ryerson, T. B., Thompson, C., Hanisco, T. F., Blake, D., Blake, N. J., Apel, E. C., Hornbrook, R. S., Elkins, J. W., Hints, E. J., Moore, F. L., and Wofsy, S., (2023). Heterogeneity and Chemical Reactivity of the Remote Troposphere defined by Aircraft Measurements - CORRECTED, *Atmos. Chem. Phys.*, 23, 99-117, 10.5194/acp-23-99-2023, 2023.
- 1090 Hall, Samuel R., Kirk Ullmann, Michael J. Prather, Clare M. Flynn, Lee T. Murray, Arlene M. Fiore, Gustavo Correa, Sarah A. Strode, Stephen D. Steenrod, Jean-Francois Lamarque, Jonathon Guth, Béatrice Josse, Johannes Flemming, Vincent Huijnen, N. Luke Abraham, and Alex T. Archibald (2018) Cloud impacts on photochemistry: a new climatology of photolysis rates from the Atmospheric Tomography mission, *Atmos. Chem. Phys.*, 18, 16809–16828, doi: 10.5194/acp-18-16809-2018, 2018.





- Holmes, C.D. (2016) Sat-J: a satellite-derived dataset of global atmospheric photolysis rates, AGU Fall Meeting Abstracts, 2016, abstract #A33A-0189. <https://agu.confex.com/agu/fm16/meetingapp.cgi/Paper/182189>, 2016.
- Holmes, C. D. (2018). Methane feedback on atmospheric chemistry: Methods, models, and mechanisms. *Journal of Advances in Modeling Earth Systems*, 10, 1087–1099. doi: 10.1002/2017MS001196, 2018.
- Holmes, C. D., M. J. Prather, O. A. Sovde, and G. Myhre (2013), Future methane, hydroxyl, and their uncertainties: key climate and emission parameters for future predictions, *Atmos Chem Phys*, 13(1), 285-302, 10.5194/acp-13-285-2013, 2013.
- Prather, M.J. (1994) Lifetimes and eigenstates in atmospheric chemistry, *Geophys.Res.Lett.*, 21, 801-804, 1994.
- Prather, M.J. (1996) Natural modes and time scales in atmospheric chemistry: theory, GWPs for CH<sub>4</sub> and CO, and runaway growth, *Geophys.Res.Lett.*, 23, 2597-2600, 1996.
- Prather, M. J. (2009), Tropospheric O<sub>3</sub> from photolysis of O<sub>2</sub>, *Geophys. Res. Lett.*, 36, L03811, 10.1029/2008GL036851, 2009.
- Prather, M.J., Flynn, C.M., Zhu, X., Steenrod, S.D., Strode, S.A., Fiore, A.M., Correa, G., Murray, L.T. and Lamarque, J.F., (2018). How well can global chemistry models calculate the reactivity of short-lived greenhouse gases in the remote troposphere, knowing the chemical composition. *Atmospheric Measurement Techniques*, 11(5), 2653-2668, <https://doi.org/10.5194/amt-11-2653-2018>, 2018.
- Prather, M.J., Zhu, X., Flynn, C.M., Strode, S.A., Rodriguez, J.M., Steenrod, S.D., Liu, J., Lamarque, J.F., Fiore, A.M., Horowitz, L.W. and Mao, J., (2017). Global atmospheric chemistry—which air matters. *Atmospheric Chemistry and Physics*, 17(14), 9081-9102, 10.5194/acp-17-9081-2017, 2017.
- Prather, M. J., Guo, H., Flynn, C. M., Strode, S. A., Steenrod, S. D., Emmons, L., Lacey, F., Lamarque, J.-F., Fiore, A. M., Correa, G., Murray, L. T., Wolfe, G. M., St. Clair, J. M., Kim, M., Crouse, J., Diskin, G., DiGangi, J., Daube, B. C., Commane, R., McKain, K., Peischl, J., Ryerson, T. B., Thompson, C., Hanisco, T. F., Blake, D., Blake, N. J., Apel, E. C., Hornbrook, R. S., Elkins, J. W., Hints, E. J., Moore, F. L., and Wofsy, S., (2023), Heterogeneity and chemical reactivity of the remote troposphere defined by the NASA ATom Mission aircraft measurements – the Modeling and Reactivity Data Streams (MDS & RDS), Dryad, Dataset, <https://doi.org/10.7280/D1B12H>, 2023.
- Schill, G. P., Froyd, K. D., Bian, H., Kupc, A., Williamson, C., Brock, C. A., Ray, E., Hornbrook, R. S., Hills, A. J., Apel, E. C., Chin, M., Colarco, P. R., and Murphy, D. M. (2020), Widespread biomass burning smoke throughout the remote troposphere, *Nat Geosci*, 13, 422-425, 10.1038/s41561-020-0586-1, 2020.
- Stevenson, D. S., Young, P. J., Naik, V., Lamarque, J. F., Shindell, D. T., Voulgarakis, A., Skeie, R. B., Dalsoren, S. B., Myhre, G., Berntsen, T. K., Folberth, G. A., Rumbold, S. T., Collins, W. J., MacKenzie, I. A., Doherty, R. M., Zeng, G., van Noije, T. P. C., Strunk, A., Bergmann, D., Cameron-Smith, P., Plummer, D. A., Strode, S. A., Horowitz, L., Lee, Y. H., Szopa, S., Sudo, K., Nagashima, T., Josse, B., Cionni, I., Righi, M., Eyring, V., Conley, A., Bowman, K. W., Wild, O., and



- 1125 Archibald, A., (2013), Tropospheric ozone changes, radiative forcing and attribution to emissions in the Atmospheric Chemistry and Climate Model Intercomparison Project (ACCMIP), *Atmos Chem Phys*, 13, 3063-3085, 10.5194/acp-13-3063-2013, 2013.
- Strode, S. A., J. H. Liu, L. Lait, R. Commane, B. Daube, S. Wofsy, A. Conaty, P. Newman, and M. Prather (2018), Forecasting carbon monoxide on a global scale for the ATom-1 aircraft mission: insights from airborne and satellite observations and modeling, *Atmos Chem Phys*, 18(15), 10955-10971, 10.5194/acp-18-10955-2018, 2018.
- 1130 Thompson, C. R., Wofsy, S. C., Prather, M. J., Newman, P. A., Hanisco, T. F., Ryerson, T. B., Fahey, D. W., Apel, E. C., Brock, C. A., Brune, W. H., Froyd, K., Katich, J. M., Nicely, J. M., Peischl, J., Ray, E., Veres, P. R., Wang, S., Allen, H. M., Asher, E., Bian, H., Blake, D., Bourgeois, I., Budney, J., Bui, T. P., Butler, A., Campuzano-Jost, P., Chang, C., Chin, M., Commane, R., Correa, G., Crouse, J. D., Daube, B., Dibb, J. E., Digangi, J. P., Diskin, G. S., Dollner, M., Elkins, J. W., Fiore, A. M., Flynn, C. M., Guo, H., Hall, S. R., Hannun, R. A., Hills, A., Hints, E. J., Hodzic, A., Hornbrook, R. S., Huey, L. G., Jimenez, J. L., Keeling, R. F., Kim, M. J., Kupc, A., Lacey, F., Lait, L. R., Lamarque, J., Liu, J., Mckain, K., 1135 Meinardi, S., Miller, D. O., Montzka, S. A., Moore, F. L., Morgan, E. J., Murphy, D. M., Murray, L. T., Nault, B. A., Neuman, J. A., Nguyen, L., Gonzalez, Y., Rollins, A., Rosenlof, K., Sargent, M., Schill, G., Schwarz, J. P., St. Clair, J. M., Steenrod, S. D., Stephens, B. B., Strahan, S. E., Strode, S. A., Sweeney, C., Thames, A. B., Ullmann, K., Wagner, N., Weber, R., Weinzierl, B., Wennberg, P. O., Williamson, C. J., Wolfe, G. M., & Zeng, L., (2021), The NASA Atmospheric Tomography (ATom) Mission: Imaging the Chemistry of the Global Atmosphere, *Bulletin of the American Meteorological Society*, on-line release, 10.1175/bams-d-20-0315.1, 2021.
- 1140 Thornhill, G., Collins, W., Olivié, D., Skeie, R. B., Archibald, A., Bauer, S., Checa-Garcia, R., Fiedler, S., Folberth, G., Gjermundsen, A., Horowitz, L., Lamarque, J.-F., Michou, M., Mulcahy, J., Nabat, P., Naik, V., O'Connor, F. M., Paulot, F., Schulz, M., Scott, C. E., Séférian, R., Smith, C., Takemura, T., Tilmes, S., Tsigaridis, K., and Weber, J.: Climate-driven chemistry and aerosol feedbacks in CMIP6 Earth system models, *Atmos. Chem. Phys.*, 21, 1105–1126, 1145 <https://doi.org/10.5194/acp-21-1105-2021>, 2021a.
- Thornhill, G. D., Collins, W. J., Kramer, R. J., Olivié, D., Skeie, R. B., O'Connor, F. M., Abraham, N. L., Checa-Garcia, R., Bauer, S. E., Deushi, M., Emmons, L. K., Forster, P. M., Horowitz, L. W., Johnson, B., Keeble, J., Lamarque, J.-F., Michou, M., Mills, M. J., Mulcahy, J. P., Myhre, G., Nabat, P., Naik, V., Oshima, N., Schulz, M., Smith, C. J., Takemura, T., Tilmes, S., Wu, T., Zeng, G., and Zhang, J.: Effective radiative forcing from emissions of reactive gases and aerosols – a multi- 1150 model comparison, *Atmos. Chem. Phys.*, 21, 853–874, <https://doi.org/10.5194/acp-21-853-2021>, 2021b.
- Travis, K. R., Heald, C. L., Allen, H. M., Apel, E. C., Arnold, S. R., Blake, D. R., Brune, W. H., Chen, X., Commane, R., Crouse, J. D., Daube, B. C., Diskin, G. S., Elkins, J. W., Evans, M. J., Hall, S. R., Hints, E. J., Hornbrook, R. S., Kasibhatla, P. S., Kim, M. J., Luo, G., McKain, K., Millet, D. B., Moore, F. L., Peischl, J., Ryerson, T. B., Sherwen, T., Thames, A. B., Ullmann, K., Wang, X., Wennberg, P. O., Wolfe, G. M., and Yu, F. Q. (2020), Constraining remote 1155 oxidation capacity with ATom observations, *Atmos Chem Phys*, 20, 7753-7781, 10.5194/acp-20-7753-2020, 2020.
- Veres, P. R., Neuman, J. A., Bertram, T. H., Assaf, E., Wolfe, G. M., Williamson, C. J., Weinzierl, B., Tilmes, S., Thompson, C. R., Thames, A. B., Schroder, J. C., Saiz-Lopez, A., Rollins, A. W., Roberts, J. M., Price, D., Peischl, J., Nault,



- B. A., Moller, K. H., Miller, D. O., Meinardi, S., Li, Q. Y., Lamarque, J. F., Kupc, A., Kjaergaard, H. G., Kinnison, D., Jimenez, J. L., Jernigan, C. M., Hornbrook, R. S., Hills, A., Dollner, M., Day, D. A., Cuevas, C. A., Campuzano-Jost, P.,  
1160 Burkholder, J., Bui, T. P., Brune, W. H., Brown, S. S., Brock, C. A., Bourgeois, I., Blake, D. R., Apel, E. C., and Ryerson, T. B. (2020), Global airborne sampling reveals a previously unobserved dimethyl sulfide oxidation mechanism in the marine atmosphere, *P Natl Acad Sci USA*, 117, 4505-4510, 10.1073/pnas.1919344117, 2020.
- Voulgarakis, A., Naik, V., Lamarque, J. F., Shindell, D. T., Young, P. J., Prather, M. J., Wild, O., Field, R. D., Bergmann, D., Cameron-Smith, P., Cionni, I., Collins, W. J., Dalsoren, S. B., Doherty, R. M., Eyring, V., Faluvegi, G., Folberth, G. A.,  
1165 Horowitz, L. W., Josse, B., MacKenzie, I. A., Nagashima, T., Plummer, D. A., Righi, M., Rumbold, S. T., Stevenson, D. S., Strode, S. A., Sudo, K., Szopa, S., and Zeng, G., (2013), Analysis of present day and future OH and methane lifetime in the ACCMIP simulations, *Atmos Chem Phys*, 13, 2563-2587, 10.5194/acp-13-2563-2013, 2013.
- Williamson, C. J., Kupc, A., Rollins, A., Kazil, J., Froyd, K. D., Ray, E. A., Murphy, D. M., Schill, G. P., Peischl, J., Thompson, C., Bourgeois, I., Thomas, B. R. A., Diskin, G. S., DiGangi, J. P., Blake, D. R., Bui, T. P. V., Dollner, M.,  
1170 Weinzierl, B., and Brock, C. A. (2021), Large hemispheric difference in nucleation mode aerosol concentrations in the lowermost stratosphere at mid- and high latitudes, *Atmos Chem Phys*, 21, 9065-9088, 10.5194/acp-21-9065-2021, 2021.
- Wofsy, S.C., S. Afshar, H.M. Allen, E.C. Apel, E.C. Asher, B. Barletta, J. Bent, H. Bian, B.C. Biggs, D.R. Blake, N. Blake, I. Bourgeois, C.A. Brock, W.H. Brune, J.W. Budney, T.P. Bui, A. Butler, P. Campuzano-Jost, C.S. Chang, M. Chin, R. Commane, G. Correa, J.D. Crouse, P. D. Cullis, B.C. Daube, D.A. Day, J.M. Dean-Day, J.E. Dibb, J.P. DiGangi, G.S.  
1175 Diskin, M. Dollner, J.W. Elkins, F. Erdesz, A.M. Fiore, C.M. Flynn, K.D. Froyd, D.W. Gesler, S.R. Hall, T.F. Hanisco, R.A. Hannun, A.J. Hills, E.J. Hints, A. Hoffman, R.S. Hornbrook, L.G. Huey, S. Hughes, J.L. Jimenez, B.J. Johnson, J.M. Katich, R.F. Keeling, M.J. Kim, A. Kupc, L.R. Lait, K. McKain, R.J. Mclaughlin, S. Meinardi, D.O. Miller, S.A. Montzka, F.L. Moore, E.J. Morgan, D.M. Murphy, L.T. Murray, B.A. Nault, J.A. Neuman, P.A. Newman, J.M. Nicely, X. Pan, W. Paplawsky, J. Peischl, M.J. Prather, D.J. Price, E.A. Ray, J.M. Reeves, M. Richardson, A.W. Rollins, K.H. Rosenlof, T.B.  
1180 Ryerson, E. Scheuer, G.P. Schill, J.C. Schroder, J.P. Schwarz, J.M. St.Clair, S.D. Steenrod, B.B. Stephens, S.A. Strode, C. Sweeney, D. Tanner, A.P. Teng, A.B. Thames, C.R. Thompson, K. Ullmann, P.R. Veres, N.L. Wagner, A. Watt, R. Weber, B.B. Weinzierl, P.O. Wennberg, C.J. Williamson, J.C. Wilson, G.M. Wolfe, C.T. Woods, L.H. Zeng, and N. Vieznor (2021). ATom: Merged Atmospheric Chemistry, Trace Gases, and Aerosols, Version 2. ORNL DAAC, Oak Ridge, Tennessee, USA. <https://doi.org/10.3334/ORNLDAAC/1925>, 2021.
- 1185 Wolfe, G. M., Nicely, J. M., Clair, J. M. S., Hanisco, T. F., Liao, J., Oman, L. D., Brune, W. B., Miller, D., Thames, A., Abad, G. G., Ryerson, T. B., Thompson, C. R., Peischl, J., McCain, K., Sweeney, C., Wennberg, P. O., Kim, M., Crouse, J. D., Hall, S. R., Ullmann, K., Diskin, G., Bui, P., Chang, C., and Dean-Day, J. (2019), Mapping hydroxyl variability throughout the global remote troposphere via synthesis of airborne and satellite formaldehyde observations, *P Natl Acad Sci USA*, 116, 11171-11180, 10.1073/pnas.1821661116, 2019.
- 1190 Young, P. J., Naik, V., Fiore, A. M., Gaudel, A., Guo, J., Lin, M. Y., Neu, J. L., Parrish, D. D., Rieder, H. E., Schnell, J. L., Tilmes, S., Wild, O., Zhang, L., Ziemke, J., Brandt, J., Delcloo, A., Doherty, R. M., Geels, C., Hegglin, M. I., Hu, L., Im, U., Kumar, R., Luhar, A., Murray, L., Plummer, D., Rodriguez, J., Saiz-Lopez, A., Schultz, M. G., Woodhouse, M. T., and



Zeng, G., (2018) Tropospheric Ozone Assessment Report: Assessment of global-scale model performance for global and regional ozone distributions, variability, and trends, *Elementa-Science of the Anthropocene*, 6, 10.1525/elementa.265, 2018.